JGERI
Journal of Green Energy Research and Innovation
ISSN: 3041-9018

Journal of Green Energy Research and Innovation

Volume 2, Issue 3, Summer 2025

PUBLISHER
Arak University

Journal of Green Energy Research and Innovation (JGERI)

Publisher: **Arak University**

Director-in-Charge: **Dr. Ali Asghar Ghadimi**

Editor-in-Chief: **Prof. Gevork B. Gharehpetian**

Deputy Editor: **Dr. Abolghasem Daeichian**

Managing and Executive Editor**: Dr. Mahyar Abasi**

Coverage area: **International**

Journal Type: **Scientific and technical**

Scientific Rank (Iran MSRT): **B**

Language: **English**

Frequency: **Quarterly**

Review Time: **4-8 Weeks**

Publication Type: **Electronic**

Open Access: **Yes**

Policy: **Peer-Reviewed**

DOI**: 10.61186/jgeri**

E-mails: **jgeri@araku.ac.ir**

Website: **https://jgeri.araku.ac.ir/**

Address: **Department of Electrical Engineering, Faculty of Engineering, Arak University, Arak, Iran.**

P.O. Box: **38156-8-8349**

Tel: **086-32625099**

Editorial Board

About Journal

JGERI is an international, open-access, and free-of-charge journal in the field of green and renewable energies, published quarterly, only electronically, in cooperation with the Renewable Energy Research Institute (**RERI**) of Arak University and Iranian Association of Electrical and Electronics Engineers (**IAEEE**). Articles accepted and published by **JGERI** are in three formats: research articles, review articles, and applied articles. **JGERI** accepts manuscripts that provide results of scientific achievements in a very wide scope of fundamental, engineering, and industrial research focusing on green energy.

The following articles are acceptable:

- **Research articles** are expected to present innovative solutions, new concepts, or creative ideas that can help solve existing or emerging technical challenges in the field of green and renewable energy.
- **Review articles** are expected to provide enlightening and specialized reviews, trainings, or case studies on an important topic, timely and widely in the field of green and renewable energies.
- **Applied articles** are expected to share the results of the industry's valuable experiences in dealing with challenging technical issues, developing/adopting new standards, applying new technologies or solving complex problems in the field of green and renewable energies. These articles can have a significant impact on the strategic plans of the industry in the coming years.

Aims and Scope

JGERI is interested on the qualified international multidisciplinary research results related to all aspects of green energy. The scope of **JGERI** is very broad, and welcomes original, novel fundamental and engineering research. We also publish reviews and industrial reports of green energy and its impact on the eco-environment.

We welcome research papers that focus on, but are not limited to, the following areas:

- Policies and Strategies for Green Energy Systems
- Fundamental And Industrial Applications for Green Energy Systems
- Energy Conversion, Control Techniques, and Grid Interactive Systems for Green Energy Systems
- Environmental Impacts of Energy Technologies and Pollution Control
- Materials And Catalysis for Green Energy Systems
- Green Energy Consumption
- Artificial Intelligence, Machine Learning, and Computational Methods in Green Energy Systems
- Public Awareness and Education for Green Energy Systems
- Solar Energy and Photovoltaic
- Wind Energy
- Hydrogen Energy and Energy Storage
- Biofuel and Bioenergy
- Utilization of Green Energies in the Structure of Power Systems
- Development of Manufacturing Technology for Green Energy Production Tools
- Electricity Market in the Presence of Green Energies
- The Effects of Green Energy Production on Power Quality of the Power System
- Impact of Expansion Planning of Power Systems on the Development of Green Energy Generation
- Operation of Green Energy-Based Microgrids
- Control and Protection of Power Systems in Networks Equipped with Green and Renewable Generation
- Energy Management in Networks Consisting of Green Energies
- Studies on the Technology of Hybrid Vehicles Based on Green Energy Fuels
- The Future Perspective of the Electricity Industry in the Presence of Production-Based Technologies and Green Energy-Based Consumers
- Green Energy Storage Technologies
- Communication Infrastructures and Protocols and Internet in Green Energy-Based Power Systems
- Cyber Security and Defense Activities in the Field of Green Energy Management

Each manuscript will go through a rigors peer-review process. you can visit our Guide for Authors page for information on preparing your manuscript.

Guide for Authors

1. Important points and rules for manuscript submission and publication

-Submitting a manuscript to a journal means that the manuscript is not under review or has not been published anywhere in any other language before.
-The submission of the manuscript for publication by the author, implicitly or explicitly, implies the approval of the organization or body where the author works and has used its affiliation.
-By submitting the manuscript, all authors officially declare their agreement to grant the copyright of the manuscript in case of acceptance to Arak University and **JGERI**. However, the authors are responsible for all the contents published in the manuscript, and the journal is only a reviewer and publisher.
- All authors are required to declare any actual or potential conflicts of interest, including financial, personal, or relationships with individuals or organizations that could affect their work.
- Each of the authors must declare their contribution and role in the manuscript on the Title Page to the journal. The statement of approval of all authors and their role in the manuscript is the responsibility of the corresponding author.
- Authors should note that all manuscripts sent to **JGERI** are checked with Authenticate's CrossCheck software to analyze the authenticity of the content. In this analysis, the overlap and similar texts presented in the submitted manuscripts will be determined.
- **JGERI** makes its manuscripts open to access after publication and there is no charge (APC) for reviewing and publication of manuscripts, and readers can download and use the articles for free.
- All authors, if they had financial support in conducting research related to this manuscript, should briefly state their role. If financial source(s) have no role in the results of the research published by the article, this should also be mentioned by the authors.
- Acknowledgments to individuals and institutions can be mentioned in a separate section at the end of the manuscript before References, and they must not be included as footnotes or in any other form. In this section, it is recommended to mention the names of those who have collaborated during the research (such as those helping in the language correctness aspect of the manuscript, assisting in writing the manuscript or proofreading it, and other cases).
- Non-commercial use of the manuscript will be governed by the Creative Commons Attribution-NonCommercial 4.0 International License, which is currently available at the link (https://creativecommons.org/licenses/by-nc/4.0/). This certificate allows others to use the authors' work in a non-commercial way and utilize it in their research work, although in the new work, they need to acknowledge the authors and mention its non-commercial nature.

2. Initial submission of the manuscript

Submission to this journal is online and you will be accompanied in all the steps of creating a user account and uploading files. All correspondence, including notification of the editor's decision and request for revision, will be made via email. To submit your manuscript, just click on the **Submit Manuscript** option on the journal page. Then, click on **Register** to create an author account. A message will be sent to your email containing your username and password. Then, log in to the manuscript submission system on the Users login page, where you need to enter the username and password and submit your new manuscript. Once you are logged in, you can change your password by clicking on My Home in the top menu. For the next time, just log in to your account. Please include the names, addresses, and email addresses of at least three potential academic reviewers with the paper. Please include reviewers' names and their academic rank, affiliation, and contact information (mail address is mandatory). However, only the editor has the right to decide on the use of suggested reviewers. All the submitted manuscripts undergo the process of plagiarism check with IThenticate software and the review process begins. According to the journal policy, there is a difference between the requirements for initial and revised submission files. Required files for initial submission include three files: **JGERI_Main_Manuscript**, **JGERI_Form_for _Copyright_Transfer_Statement and Conflict_ of_ Interest_ Disclosure** and **JGERI_Cover_Letter**, all three of which must be sent to the journal in PDF format. You can use the links below to download the requirements and suggestions files of these three files.

- JGERI_Guideline_for_Main_Manuscript
- JGERI_Guideline_for_Cover_Letter
- JGERI_Form_for_Copyright_Transfer_Statement and Conflict_ of_ Interest_ Disclosure

3. Submission of the revised manuscript

If the submitted manuscript, after going through the initial review process, is evaluated by the officials and reviewers of the journal and a decision is made to make corrections and revisions in the form of minor or major, the authors are obliged to make the corrections and prepare the response letter to the reviewers within the time specified by the journal. Three files must be sent to the journal at this stage: WORD and PDF files of the revised manuscript (changes should be highlighted), PDF file of the response to the reviewers (including the comments and responses of each of the reviewers separately), Title Page and Authorship file in WORD format (containing two main forms: Title Page and Authorship). The link to download the necessary files along with their requirements and instructions is given below. Points raised in the file **JGERI_Revised_Manuscript** must be followed for compiling the revised manuscript. The authors are obliged to submit the revised file in PDF and WORD format to the

journal. Also, different parts of the file **JGERI_Form_for_Title_Page_ and_ Authorship** needs to be completed and signed by the corresponding author, but **JGERI_Response_to_the_Reviewers_Comments** is suggested by the journal and it is not necessary to follow all the points of that file. It should be noted that all the stages of page layout and editing in the form of final publication are the responsibility of the journal. In the completion stages of this process, the cooperation of the authors is needed, and we will inform you at each stage. Thus, the minimum requirements for file compilation are provided in the template file.

- JGERI_Guideline_for_Revised_Manuscript
- JGERI_Form_for_Title_Page_ and_ Authorship
- JGERI_Guideline_for_Response_to_the_Reviewers_Comments

4. **After the final acceptance of the manuscript**

After announcing the final acceptance of the manuscript (reviews may happen several times), the files **JGERI_Revised_Manuscript** and **JGERI_Form_for_ Title_Page_ and_ Authorship** will be sent to the paging unit for page layout and final editing. After the final acceptance announcement, the authors will be asked to send a graphic abstract included in a single file. Then, the process of compilation of the manuscript will be completed by the journal and finally, the proof version of the manuscript will be sent to the authors. The authors are obliged to check the proof file completely and report to the journal if they find any ambiguity or error in the final file. In some cases, along with the final proof file of the manuscript, there may be a series of errors and ambiguities in the manuscript, which are sent to the author in the form of comments along with the proof version of the manuscript. The corresponding author is obliged to clarify and resolve these problems and ambiguities in the specified time.

5. **After publication on the journal's website**

After announcing the initial acceptance, the information of the article without its content will be indexed in the Articles in the Press section of the website. After including the article in the issue selected by the journal, the desired article will be indexed in the Current Issue unit along with Vol., No., and pp. Also, the electronic file of the article can be introduced in all scientific references through the DOI link. The important point is that, after acceptance and indexing, the names of the authors cannot be changed, that is, it will not be possible to add, delete, or change the order of the names of the authors and their organizational affiliations.

Cooperative Publication Organization

Renewable Energy Research Institute of Arak University
http://araku.ac.ir/web/riren

Iranian Association of Electrical and Electronics Engineers
https://iaeee.ir/

Iranian Wind Energy Association
https://www.irwea.org/fa/

Indexing Databases and Social Networks

Iran MSRT: https://journals.msrt.ir/home/detail/21538/

Magiran: https://www.magiran.com/magazine/8484

Google Scholar: https://scholar.google.com/citations?user=47bsJFoAAAAJ&hl=en

Linkedin: https://www.linkedin.com/in/jgeri-arak-university-0818872b9

Academia:https://independent.academia.edu/JournalofGreenEnergyResearchandInnovationJGERI

MyScineceWork: https://www.mysciencework.com/profile/j.green.energy.res.innov.jgeri

Contents

Journal of Green Energy Research and Innovation

An Analysis of Heating and Cooling Energy Consumption in High-Rise Versus Low-Rise Buildings with Reference to The Predicted Mean Vote (pmv) Comfort Index: A Case Study

Hamed Safikhani, Mohammad Farahani, Kimia Rezaei, Asgar Minaei

Highlights

- **The energy consumption for the cooling and heating across eight different building scenarios was compared.**
- **The three climate scenarios represented the cities of Yazd (hot), Arak (moderate), and Shahr-e Kord (cold) were modelled.**
- **buildings without common walls (single floors) could have 58.9% and 67.1% more load and energy consumption in heating and cooling, respectively.**
- **The difference between the energy consumption of the building with the highest and lowest number of shared walls was observed to be about 60% on average.**

Graphical Abstract

Use your device to scan and read the article online

Citation

H. Safikhani, M. Farahani, K. Rezaei, and A. Minaei," An Analysis of Heating and Cooling Energy Consumption in High-Rise Versus Low-Rise Buildings with Reference to The Predicted Mean Vote (pmv) Comfort Index: A Case Study," *Journal of Green Energy Research and Innovation*, vol. 2, no. 3, pp. 1-13, 2025.

https://doi.org/10.61882/jgeri.2.3.1

Journal of Green Energy Research and Innovation 2.3 (2025) 1-13

Online ISSN: 3041-9018

Journal of Green Energy Research and Innovation

Journal Homepage: www.jgeri.araku.ac.ir

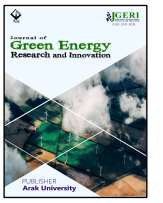

An Analysis of Heating and Cooling Energy Consumption in High-Rise Versus Low-Rise Buildings with Reference to The Predicted Mean Vote (pmv) Comfort Index: A Case Study

Hamed Safikhani [1,*], Mohammad Farahani [2], Kimia Rezaei [3], Asgar Minaei [4,*]

[1] *Department of Mechanical Engineering, Faculty of Engineering, Arak University, Arak, Iran.*

[2] *School of Mechanical Engineering, Arak University of Technology, Arak, Iran.*

[3] *Department of Mechanical Engineering, Faculty of Engineering, Eastern Mediterranean University, Famagusta, North Cyprus via Mersin, Türkiye.*

[4] *Department of Mechanical Engineering, Faculty of Engineering, University of Mohaghegh Ardabili, Ardabil, Iran.*

A R T I C L E I N F O

Keywords:
Energy Optimization,
Residential Buildings,
High-Rise and Mid-Rise Buildings,
Fanger comfort index.

Article History:
Received: 23 February 2025;
Revised: 27 April 2025;
Accepted: 02 May 2025.

Article type:
Research Article

* ***Corresponding authors***
E-mail address
h-safikhani@araku.ac.ir (H. Safikhani)
a.minaei@uma.ac.ir (A. Minaei)

A B S T R A C T

The choice between residing in tall buildings and in few-story or detached dwellings has been the subject of considerable debate, with each approach attracting its own proponents and critics. This study investigates and compares the heating and cooling energy consumption of multi-story and low-elevation buildings, incorporating the Fanger comfort index as a measure of thermal comfort. Energy performance is evaluated on eight building configurations with varying numbers of floors, under three distinct climatic conditions, using the Predicted Mean Vote (PMV) index as the primary comfort criterion. The building scenarios range from single-story detached houses to 50-story high-rise structures. The climatic cases—representing hot (Yazd), moderate (Arak), and cold (Shahr-e Kord) environments—are simulated and analyzed using DesignBuilder software. The results section presents detailed analyses of heating and cooling loads, comfort index values, and electricity and gas demand for each building–climate combination, with monthly and annual performance trends. The findings reveal that the number of shared walls exerts a greater influence on energy consumption than the number of floors. Specifically, detached single-story buildings, which lack shared walls, exhibit up to 58.9% higher heating demand and 67.1% higher cooling demand compared to their counterparts with shared walls.

1. Introduction

In recent years, the debate between vertical residential developments (high-rise buildings) and horizontal, independent housing has intensified, with both approaches attracting strong proponents and critics. High-rise buildings are common in densely populated areas where horizontal expansion is limited, while detached, low-rise dwellings are preferred in regions where families seek greater privacy, exclusive ownership, and larger living spaces. Each of these residential forms has distinct implications for energy consumption, energy efficiency, occupant comfort, and environmental sustainability. Escalating global concerns over energy scarcity and supply instability have intensified the demand for energy-efficient residential solutions. With the growing emphasis on sustainable urban development and the evolution of architectural practices, the accurate modeling and optimization of buildings' energy performance have become increasingly vital. This issue is especially pronounced in the Middle East, where accelerated population growth and mounting energy consumption underscore the pressing need to reconcile resource preservation with the provision of thermal comfort for occupants. In recent decades, two dominant paradigms of residential development—vertical expansion through high-rise buildings and horizontal expansion through low-rise, detached dwellings—have been the focus of considerable scholarly and professional debate. Each approach is underpinned by distinct socio-economic, cultural, and environmental drivers, and both have their respective advocates and critics.

High-rise developments are increasingly adopted in densely populated urban centers, where limited land availability, rapid urbanization, and the need to optimize infrastructure necessitate vertical growth. By contrast, low-rise and independent housing typologies remain prevalent in areas where land is more accessible and where residents prioritize privacy, individual ownership, outdoor spaces, and a stronger connection with the surrounding environment.

The implications of these two development strategies extend well beyond architectural form and urban density. They have profound consequences for building energy consumption, operational efficiency, and occupant well-being, as well as for broader environmental sustainability. High-rise buildings, while often associated with economies of scale and shared infrastructure, may face challenges related to increased cooling and heating loads due to higher exposure of façades, complex HVAC requirements, and greater reliance on artificial ventilation and lighting. Conversely, low-rise dwellings typically benefit from simpler design and operation, greater adaptability to passive design strategies, and reduced dependence on mechanical systems, but they may contribute to urban sprawl, higher land consumption, and increased transportation-related energy use. Understanding the trade-offs between these residential typologies is therefore crucial for architects, urban planners, and policymakers seeking to balance energy efficiency, occupant comfort, and sustainable urban growth.

Worldwide, escalating concerns regarding energy deficits and imbalances between supply and demand have emerged as critical challenges, underscoring the urgent need for the adoption of energy-efficient residential strategies. Concurrently, the global transition toward sustainability-driven urban development, combined with rapid innovations in architectural design and building technologies, has heightened the importance of accurately modeling and optimizing the energy performance of residential buildings. These challenges are particularly pronounced in the Middle East, where rapid population growth, urbanization, and rising energy consumption converge to create a multifaceted problem: achieving an optimal balance between resource conservation, environmental sustainability, and the comfort and well-being of building occupants. In this context, the development of integrated design and simulation approaches is essential for supporting evidence-based decisions that enhance energy efficiency while maintaining high standards of thermal comfort and livability.

At the urban scale, Urban Building Energy Modeling (UBEM) has emerged as a valuable framework for analyzing and optimizing energy consumption [1]. Unlike top-down models that rely on aggregated time-series data, UBEM adopts a bottom-up methodology, enabling more detailed evaluations of technological performance at the building level, as noted by Reinhardt and Cerezo Davila [2]. Energy simulation platforms such as Design Builder, EnergyPlus, and TRNSYS further support this process by allowing scholars to investigate specific building typologies and their environmental implications [3,4]. According to Hong et al. [5], multi-story buildings are typically associated with greater cooling demands due to elevated solar exposure, whereas low-rise buildings often exhibit higher heating requirements because of their extensive envelope area. Moreover, building geometry plays a critical role in shaping energy efficiency. Kim et al. [6] demonstrated that variations in architectural form can substantially influence energy demand, while Chen et al. [7] underscored the importance of localized climatic variables—such as temperature, solar radiation, and humidity—in determining the design of region-specific HVAC strategies.

The optimization of Heating, Ventilation, and Air Conditioning (HVAC) systems plays a pivotal role in reducing energy consumption and enhancing overall building performance. Kimura et al. [8] demonstrated that tailoring HVAC configurations to specific climatic conditions can yield significant operational benefits. Their study indicated that gas-based heating systems outperform electric alternatives in cold climates, while evaporative cooling technologies achieve higher efficiency in hot, arid regions. These findings underscore the potential for substantial annual energy savings in residential buildings and highlight the critical importance of implementing climate-responsive HVAC design strategies.

Moreover, the effectiveness of HVAC optimization is closely linked to building typology. High-rise buildings, with their extensive façade exposure and complex internal layouts, often require sophisticated HVAC strategies to maintain uniform thermal comfort across multiple floors, whereas low-rise, detached dwellings can more readily exploit passive heating and cooling techniques alongside simpler HVAC configurations. Advanced energy modeling tools, such as DesignBuilder, EnergyPlus, and similar simulation platforms, provide the ability to assess the interaction between building design, local climate, and HVAC performance, enabling designers and engineers to identify the most efficient and comfortable system configurations for each context. Integrating such modeling approaches with climate-sensitive HVAC strategies is therefore essential for achieving both energy efficiency and optimal occupant comfort in diverse residential typologies.

Yu et al. [9] demonstrated that Variable Air Volume (VAV) systems outperform Constant Air Volume (CAV) systems in terms of energy efficiency, particularly in mixed-use urban buildings where fluctuating occupancy patterns and diverse functional requirements necessitate flexible climate control. VAV systems adjust the airflow rate based on real-time thermal demand, thereby reducing unnecessary energy consumption and enhancing occupant comfort compared to the fixed-flow operation of CAV systems. In addition to HVAC system optimization, material selection and façade design play a crucial role in improving building performance. The use of high-performance insulation materials, low-emissivity glazing, and adaptive façade technologies can significantly reduce heat transfer, optimize natural lighting, and minimize cooling and heating loads. Collectively, these design strategies highlight the importance of integrating mechanical system efficiency with passive architectural features to achieve substantial improvements in overall building energy performance. According to Gong et al. [10], the use of materials with high solar reflectance and low thermal emittance can effectively reduce cooling loads in warm climates by minimizing heat absorption. Building envelope characteristics, particularly the window-to-wall ratio (WWR) and glazing specifications, also have a pronounced impact on energy efficiency. Wang et al. [11] observed that larger WWRs are advantageous in colder climates, whereas smaller ratios are more suitable in warmer regions. Comfort considerations further extend to adaptive models; Page et al. [12] emphasized that incorporating occupant-specific comfort variations allows for greater flexibility in designing energy-efficient indoor environments.

Building-Integrated Photovoltaics (BIPVs) represent another significant strategy for enhancing building efficiency, especially in solar-abundant areas. Yalcin and Selcuk [13] demonstrated that integrating BIPVs with cooling strategies can substantially reduce

dependence on conventional grid power. The rise of smart technologies, including Internet of Things (IoT)-enabled systems, has also transformed energy management practices. Wang et al. [14] demonstrated that the integration of real-time monitoring systems with big data analytics significantly enhances the calibration of building energy models, thereby reducing the discrepancies between simulated predictions and actual operational performance. This advancement not only increases the reliability of energy modeling but also provides a more accurate basis for decision-making in building design and energy management. Similarly, Dong et al. [15] reported that the deployment of smart technologies such as occupancy sensors and intelligent thermostats facilitates dynamic control of HVAC systems. By adapting heating, cooling, and ventilation schedules in response to real-time occupancy patterns, these technologies have been shown to reduce residential energy consumption by more than 25%. Such findings underscore the transformative role of digitalization and smart control strategies in bridging the performance gap, optimizing energy use, and advancing the development of resilient, energy-efficient buildings.

Policy frameworks play an equally important role in driving efficiency improvements. Yan et al. [16] highlighted the effectiveness of rigorous energy-efficient construction standards in promoting sustainable practices. Comparative analyses of high-rise and low-rise housing also inform urban planning strategies; Buffat et al. [17] demonstrated that GIS-based modelling facilitates optimized urban energy planning. Moreover, urban heat island phenomena significantly influence energy demand. Xu et al. [18] argued that integrating microclimatic conditions—such as localized temperature variations, wind patterns, solar radiation intensity, and humidity levels—into building energy simulation models substantially improves predictive accuracy. By accounting for these site-specific factors, simulation outcomes more closely align with real-world energy performance, thereby reducing the uncertainties commonly associated with generalized climate assumptions. Furthermore, the inclusion of microclimatic variables enables the development of more effective optimization strategies for building design and operation, particularly in urban contexts where factors like shading from surrounding structures, urban heat islands, and localized airflow can significantly influence thermal comfort and energy demand. This approach ultimately supports the design of context-sensitive, energy-efficient buildings that are better adapted to their immediate environmental conditions.

To address the increasing complexity of urban energy systems, new modelling frameworks have been developed. Remmen et al. [19] introduced TEASER, an open-source platform for urban energy modelling of building stocks, capable of integrating heterogeneous datasets for scalable assessments. Complementarily, Ferrando et al. [20] reviewed bottom-up, physics-based UBEM approaches, outlining emerging trends and identifying key opportunities for advancing energy-efficient building design.

Advancements in geospatial data integration have significantly improved the accuracy of urban heat demand modeling. Nouvel et al. [21] highlighted the critical role of data quality, showing that 3D city models with high-resolution geospatial datasets yield more precise energy demand predictions. Furthermore, Nouvel et al. [22] demonstrated that coupling GIS-based statistical and engineering approaches provides a robust framework for multi-scale policy support in urban energy planning, effectively linking neighborhood-level analyses with broader city-scale assessments. Recent studies have also employed advanced simulation tools, particularly Design Builder, to model energy performance across diverse building typologies and case studies [23-27].

Several studies have investigated the impact of building geometry on energy performance, highlighting that high-rise buildings with more shared walls tend to exhibit reduced heat loss and energy demand compared to low-rise or detached structures due to minimized exposed surfaces [28,29]. While the Fanger PMV model is widely used for assessing thermal comfort, it has been criticized for its limitations in residential and naturally ventilated settings, as it does not account for adaptive behaviors such as clothing adjustment or window operation [30]. Recent advancements propose adaptive comfort models that better reflect real occupant responses, particularly in diverse climate zones, often resulting in 15–20% energy savings compared to PMV-based systems [31,32]. Moreover, enhanced modeling approaches now incorporate vertical temperature gradients or artificial intelligence (AI)-based HVAC optimization to improve both comfort prediction and energy efficiency [33,34].

To address existing knowledge gaps in residential building performance, this study conducts a comprehensive evaluation of eight building scenarios in combination with three distinct HVAC system configurations, spanning a wide spectrum of building types—from single-unit villas to 50-story high-rise structures. The primary focus of the analysis is the application of the Predicted Mean Vote (PMV) comfort index, which serves as a quantitative measure of thermal comfort for building occupants. Simulations are carried out using DesignBuilder software, incorporating detailed modeling of building geometry, material properties, occupancy patterns, and HVAC operational strategies.

The study is performed across three representative Iranian cities—Yazd, Arak, and Shahr-e Kord—each representing unique climatic conditions, including hot-arid, moderate, and cold climates, respectively. By examining the interaction between building design, HVAC systems, and local climate, the research aims to identify key factors that influence energy consumption, thermal comfort, and overall building performance.

The insights gained from this study are intended to provide practical guidance for architects, engineers, urban planners, and policymakers in designing and implementing high-performance residential developments. In particular, the findings may inform decisions related to building typology, HVAC selection, and climate-responsive design strategies, ultimately supporting the development of energy-efficient, comfortable, and sustainable urban housing solutions. The anticipated findings are expected to contribute to the broader discourse on climate-responsive architecture and sustainable energy management within the context of urban development, offering both design-oriented and policy-relevant implications.

2. Different Building Scenarios

Due to spatial constraints—particularly in major economic, political, and social centers—high-rise construction has emerged as a prevalent solution in urban areas worldwide. Figure 1 illustrates several notable examples of high-rise buildings, highlighting the global trend toward vertical residential development. In contrast, recent years have seen an increasing preference for low-rise, independent housing, driven by residents' desire for greater autonomy, privacy, and comfort, as well as the rise of residential communities structured around such typologies. Figure 2 depicts the newly developed Amirkabir city near Arak, Iran, which predominantly comprises flat housing units.

In the present study, eight building scenarios with varying block configurations and floor counts, as detailed in Figure 3 and Table 1, are systematically modeled and compared to evaluate their energy demand. The analysis considers both heating and cooling requirements, incorporating factors such as building geometry, climatic conditions, and HVAC system performance, in order to provide a comprehensive understanding of how different residential typologies influence energy efficiency and thermal comfort.

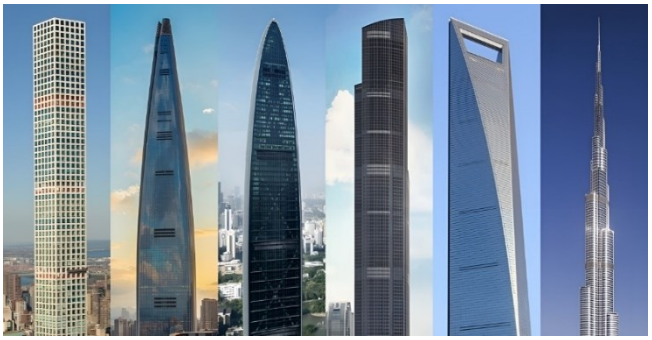

Figure 1. Notable high-rise buildings around the world, illustrating global trends in tall building construction.

Figure 2. Comparison of high-rise developments and low-rise housing in Amirkabir New Town near Arak, Iran, illustrating alternative urban residential typologies.

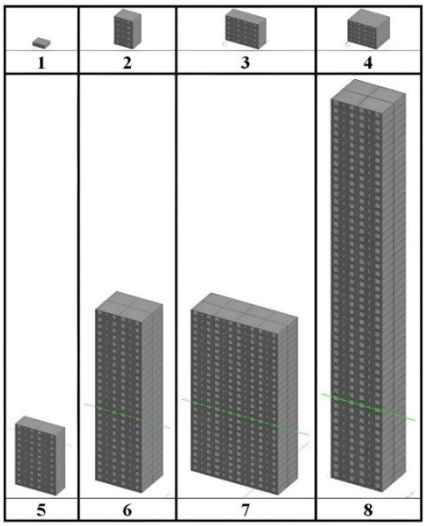

Figure 3. Schematic representation of the eight building scenarios considered in this study, illustrating variations in the number of floors and block configurations (Details are described in Table 1).

Table 1. Specifications of the eight modeled scenarios, including building names, number of floors, and block configurations, employed in this study.

Scenario No.	Name	No. of blocks	No. of floors	No. of units/floor	No. of common walls
1	200×1×1	200	1	1	0
2	40×5×1	40	5	1	2
3	20×5×2	20	5	2	3
4	10×5×4	10	5	4	4
5	10×10×2	10	10	2	3
6	2×25×4	2	25	4	4
7	1×25×8	1	25	8	5
8	1×50×4	1	50	4	4

In all scenarios, a standardized building with a floor area of approximately 100 m^2 was modeled, the layout of which is presented in Figure 4.

3. Different Climate Scenarios

The building scenarios described previously were simulated and systematically analyzed under three contrasting climatic conditions, represented by the Iranian cities of Yazd (hot), Arak (moderate), and Shahr-e Kord (cold). This approach enables a comprehensive assessment of the influence of climate variability on both building energy performance and occupant thermal comfort. Table 2 provides the recent average temperature and humidity data for these locations, serving as key inputs for the simulation models and ensuring that the analysis accurately reflects local environmental conditions. By incorporating these climatic parameters, the study captures the interaction between building design, HVAC system performance, and local weather, facilitating a nuanced evaluation of energy demand and comfort outcomes across diverse residential typologies.

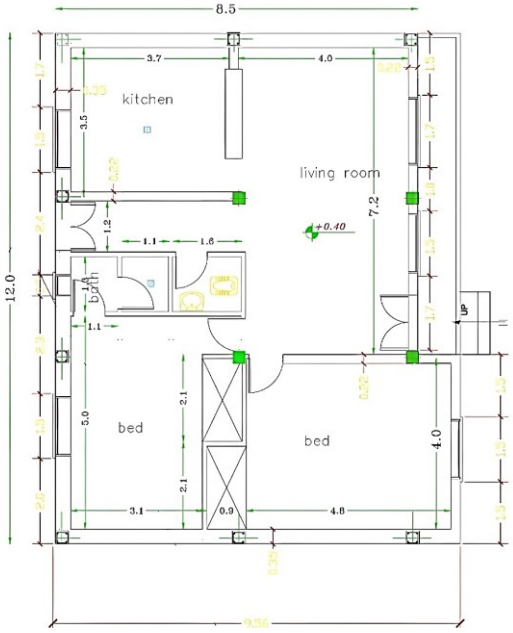

Figure 4. Layout of a standardized 100 m^2 building used in all scenarios.

Table 2. Key climatic parameters of Arak, Shahr-e Kord, and Yazd across different seasons.

Climatic properties		Arak	Shar-e Kord	Yazd
Height above mean sea level (m)		1742	2045	1212
Summer conditions at 15:00	DB (°C)	35	33	40
	WB (°C)	16	18	18
	RH %	17	23	12
Summer conditions at 6:00	DB (°C)	-12	-14	-5
	RH %	79	81	71

4. Numerical Modeling

4.1. Equations

This study investigates energy consumption in eight distinct building scenarios, under conditions that maintain comparable levels of thermal comfort. The assessment of thermal comfort is conducted using the Fanger method as in Equation (1).

$$PMV = 0.303 \times e^{-0.0208}\{M - W - 3.05 \times 10^{-3} \times [5733 - 6.99(M - W) - P_a] \quad (1)$$
$$-0 \cdot 42\left[(M - W) - 58 \cdot 15\right] - 1 \cdot 7 \times 10^{-5} \times \left(5867 - p_a\right) - 0 \cdot 0014M \times (34 - t_a) - 3 \cdot 96 \times 10^{-8}$$
$$\times f_{cl}[(t_{cl} + 273)^4 - (t_{mrt} + 273)^4] - f_{cl}h_c(t_{cl} - t_a)\}$$

where M is the metabolic rate (W/m^2), W is the effective mechanical power (W/m^2); p_a is the water vapor partial pressure (Pa); fcl is the clothing surface area factor; ta is the air temperature (°C) and Icl is the clothing insulation (m^2 K/W). The mentioned parameters are calculated as follows:

Here, M denotes the metabolic rate (W/m^2), W represents the effective mechanical power (W/m^2), p_a is the water vapor partial pressure (Pa), f_{cl} refers to the clothing surface area factor, t_{at} indicates the air temperature (°C), and I_{cl} denotes the clothing insulation (m^2·K/W). These parameters are determined as follows in Equations (2) to (6):

$$t_{cl} = 35.7 - 0.028(M - W) - R_{cl}\{39.6 \times 10^{-9} f_{cl}[(t_{cl} + 273)^4 - (t_{mrt} + 273)^4] + f_{cl}h_c(t_{cl} - t_a) \quad (2)$$

$$h_c = 2 \cdot 38(t_{cl} - t_a)^{0 \cdot 25}, \quad h_c = 12 \cdot 1\sqrt{v} \quad (3)$$

$$f_{cl} = 1 + 0 \cdot 2I_{cl} \quad I_{cl} \prec 0 \cdot 5clo \quad (4)$$

$$f_{cl} = 1 \cdot 05 + 0 \cdot 1I_{cl} \quad I_{cl} \succ 0 \cdot 5clo \quad (5)$$

$$M = \left(2 \cdot 06 \times 10^4\right) \times \dot{V}\left(F_{oi} - F_{oe}\right) \quad (6)$$

In this study, t_r indicates the mean radiant temperature (°C), var signifies the relative air velocity (m/s), and t_{cl} denotes the clothing surface temperature (°C), all of which influence occupant thermal comfort. Based on these parameters, the level of occupant dissatisfaction in each building is determined using the Apple index, offering a comprehensive evaluation of indoor comfort conditions. The Apple index is calculated as follows in Equation (7):

$$PPD = 100 - 95\exp\left[-\left(0 \cdot 03353PMV^4 + 0 \cdot 2179PMV^2\right)\right] \quad (7)$$

4.2. HVAC and modelling of the details

Conducting energy simulations for the proposed building scenarios and estimating both cooling and heating loads necessitate the specification of a comprehensive set of input parameters within DesignBuilder software. These inputs encompass building geometry, construction materials, occupancy patterns, internal heat gains, and HVAC system specifications, all of which significantly affect simulation accuracy and the reliability of energy performance predictions. The key parameters employed in this modeling process are summarized in Table 3, providing a detailed overview of the data used to generate precise and robust simulation outcomes.

The importance of these inputs becomes particularly evident when comparing high-rise and low-rise residential typologies. High-rise buildings, with their greater façade exposure, complex floor layouts, and vertical stacking of units, require careful specification of thermal properties, shading, and HVAC system performance to accurately capture energy demand and thermal comfort. In contrast, low-rise, detached dwellings benefit from simpler geometries and more uniform environmental conditions, allowing passive design strategies to have a more pronounced effect on reducing energy consumption. By integrating these detailed inputs into the simulation models, the study is able to evaluate the interplay between building design, climatic conditions, and system configurations, thereby informing strategies to optimize energy efficiency and enhance occupant comfort across diverse residential forms.

Table 3. Key parameters and inputs employed in the energy modeling of buildings in this study.

Parameter	Value
Occupancy (People/m^2)	0.11
Winter clothing (Clo)	1
Summer clothing (Clo)	0.5
Heating set point (°C)	22
Cooling set point (°C)	24
Glazing Type	Double 6mm/6mm Arg
Lighting power density (W/m^2-100 lux)	5
ACH	5
HVAC type	Fan coil unit
Heating	Natural gas
Cooling	Electricity
DHW	Same as HVAC

5. Results And Discussion

This section presents the simulation outcomes for the eight building scenarios, differentiated by floor numbers and block configurations, as illustrated in Figure 3 and summarized in Table 1. The results are evaluated under three distinct climatic conditions to examine the combined effects of building geometry, HVAC systems, and local climate on both energy consumption and occupant thermal comfort. Key performance indicators, including cooling and heating loads, Predicted Mean Vote (PMV), and the Apple index, are analyzed to provide a comprehensive understanding of how design variations impact overall building efficiency and indoor comfort levels.

The heating and cooling loads for the selected cities and building typologies are presented in Figures 5 and 6, respectively. The results reveal that Yazd experiences the highest cooling demands, whereas Shahr-e Kord exhibits the greatest heating requirements across all scenarios. Among the eight examined building scenarios, Scenario 1 consistently demonstrates the highest combined heating and cooling loads, while Scenario 7 records the lowest energy demand. Table 4 summarizes the percentage increase in heating and cooling loads relative to Scenario 7, showing that energy consumption may rise by up to 67.1% for cooling and 58.9% for heating.

These results highlight the critical role of building typology and configuration in shaping energy performance. High-rise buildings, with their extensive façade exposure, vertical stacking of units, and more complex internal layouts, generally exhibit higher heating and cooling demands compared to low-rise, detached dwellings, which benefit from simpler geometries and greater potential for passive design strategies. Furthermore, the variations in energy loads directly affect occupant thermal comfort, as buildings with higher loads may require more intensive HVAC operation to maintain desirable indoor conditions. Consequently, optimizing building design, floor arrangements, and HVAC systems is essential not only for reducing energy consumption but also for enhancing overall occupant comfort across diverse climatic contexts.

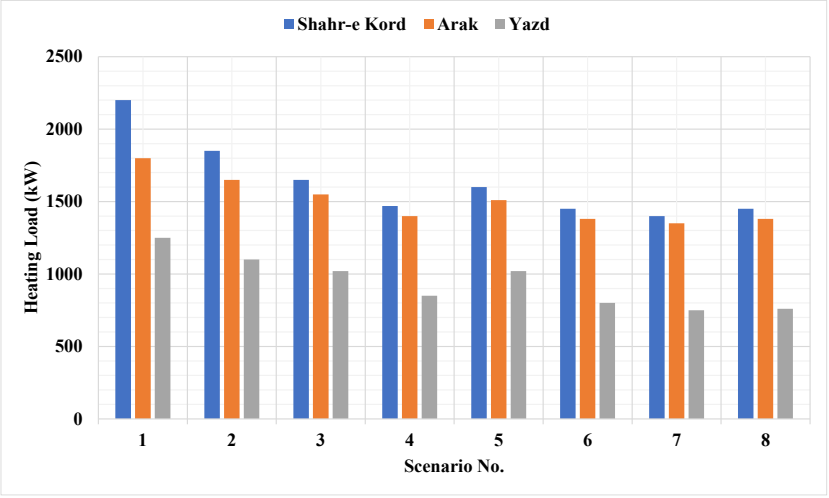

Figure4. Comparison of heating loads across the eight building scenarios in the three cities: Shahr-e Kord, Arak, and Yazd.

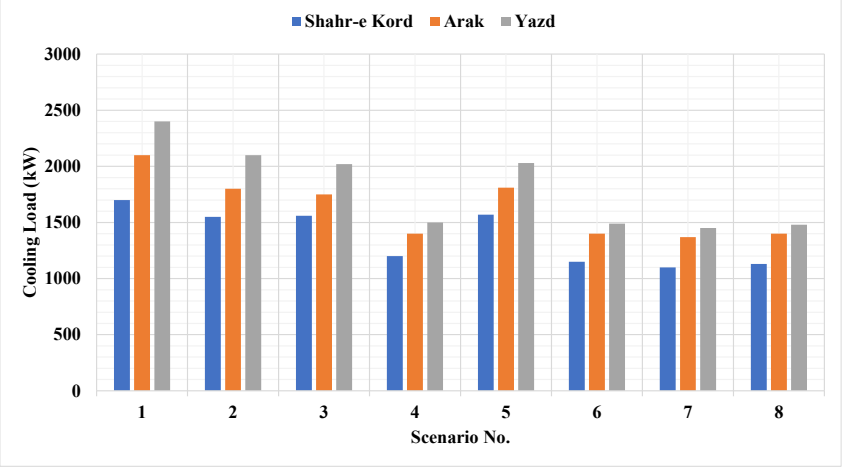

Figure 5. Cooling load in different cities across the eight scenarios.

Table 4. Details of name, number of floors and blocks of 8 different scenarios used in this paper.

Scenario No.	No. of common walls	Percentage of load difference (%)	
		Heating	Cooling
1	0	58.9	67.1
2	2	39.6	47.4
3	3	28.5	45.1
4	4	8.8	6.5
5	3	27.2	49.2
6	4	5.6	5.7
7	5	0	0
8	4	5.3	4.9

One of the most influential factors affecting heating and cooling loads across all scenarios is the number of common walls shared with adjacent units. Figure 7 illustrates the relationship between the number of shared walls and the resulting energy demand in Arak, showing that increased wall sharing reduces both heating and cooling loads by enhancing thermal insulation and minimizing the exposed surface area of the building envelope. The results demonstrate a clear inverse relationship: as the number of shared walls increases, energy consumption decreases. Specifically, Scenario 7, which incorporates the highest number of shared walls (five), exhibits the lowest overall load, whereas Scenario 1, with no shared walls, records the highest.

These findings have important implications for different building typologies. High-rise buildings, which often feature stacked units with multiple shared walls, can benefit from reduced energy demand due to increased thermal coupling between units, whereas low-rise, detached dwellings with minimal or no shared walls tend to experience higher heating and cooling requirements. Furthermore, variations in energy loads directly influence occupant thermal comfort, as buildings with higher loads require more intensive HVAC operation to maintain desirable indoor conditions. Consequently, careful consideration of unit configuration and wall-sharing strategies is critical in designing energy-efficient, comfortable, and sustainable residential developments across diverse climatic contexts.

Furthermore, calculating the comfort index provides valuable insight into the distribution of cooling and heating loads across the different scenarios with enhanced accuracy. Figure 8 illustrates the annual variation of the Fanger comfort index for all eight building scenarios. Although the index demonstrates broadly similar seasonal trends across scenarios, subtle variations between individual cases are evident, reflecting differences in building geometry, floor number, and block configuration. These variations align closely with the cooling and heating loads presented in Figures 4 and 5, highlighting the strong correlation between energy demand and occupant comfort. The results emphasize the importance of integrating thermal comfort analysis into the design process, offering guidance for architects and engineers to optimize building layouts, envelope design, and HVAC system performance to achieve both energy efficiency and high occupant comfort.

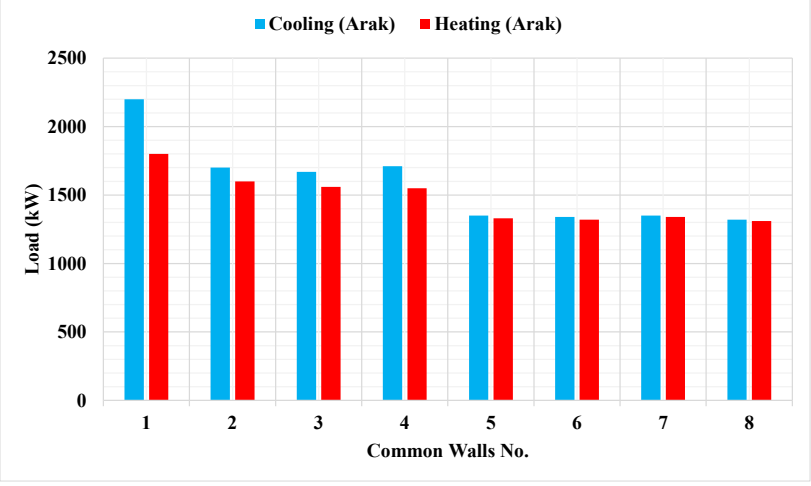

Figure 6. Variation of cooling and heating loads in Arak with respect to the number of walls shared between adjacent units.

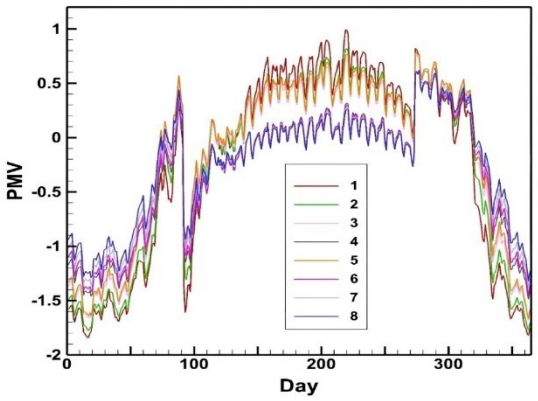

Figure 7. Comfort index (PMV) for all eight scenarios throughout 365 days of the year.

A central question in evaluating building energy performance is identifying which components contribute most significantly to heat loss under different scenarios. As shown in Figure 9, the majority of energy losses occur through the walls and roof. This effect is particularly pronounced in single-story flat buildings, where the roof accounts for a disproportionately large portion of total heat loss, thereby substantially increasing overall energy demand. In contrast, high-rise buildings, with multiple stacked floors and shared walls between units, typically exhibit reduced heat loss per unit due to decreased exposed surface area and increased thermal coupling between adjacent units.

These observations emphasize the importance of optimizing building envelope design, including wall and roof insulation, glazing selection, and orientation, to minimize energy consumption. Targeted improvements in these areas can significantly enhance thermal efficiency, reduce HVAC loads, and improve occupant comfort. Moreover, the findings suggest that design strategies should be adapted according to building typology, with particular attention to envelope performance in low-rise, detached structures and to façade optimization in high-rise developments, ensuring energy-efficient and sustainable residential solutions across diverse climates.

Given the recent disparities in energy consumption, the necessity of reducing electricity and gas usage has become increasingly evident. Figure 10 illustrates the breakdown of energy consumption across end-uses such as heating, cooling, lighting, and domestic hot water. Furthermore, Figures 11 presents the cumulative electricity and gas consumption for summer (cooling) and winter (heating) periods, respectively. As anticipated, this pattern is reflected in both heating and cooling load values: Scenario 1 exhibits the highest electricity and gas consumption, whereas Scenario 7 demonstrates the lowest energy demand. This trend highlights the influence of building design, floor configuration, and block arrangement on overall energy performance.

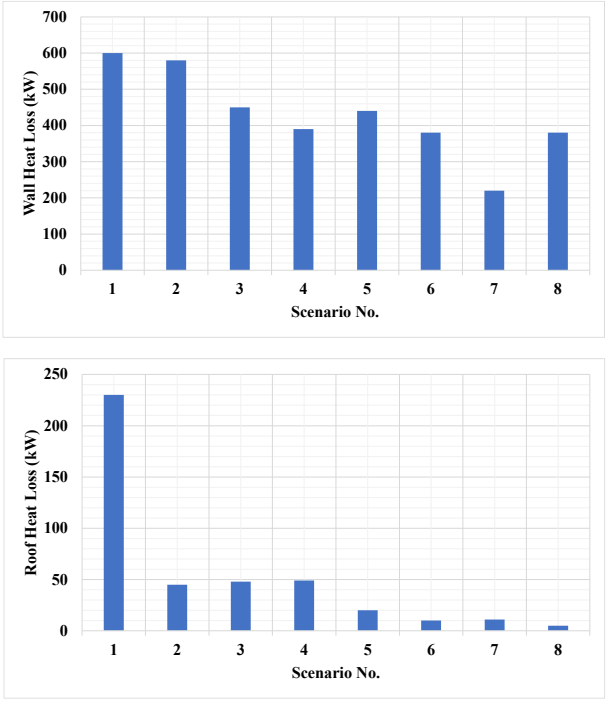

Figure 8. Comparative analysis of thermal losses through exterior walls and roof structures across the eight building scenarios.

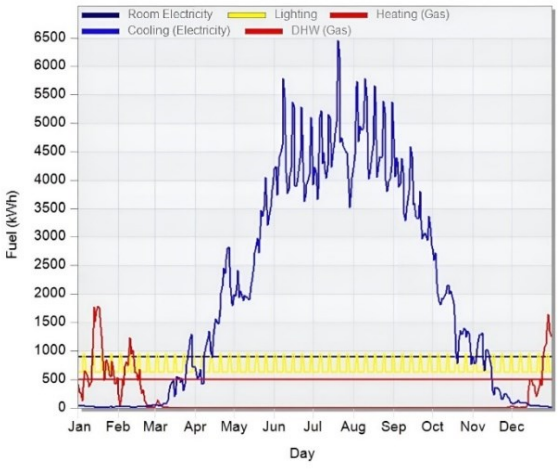

Figure 9. Composition of energy consumption by category, encompassing heating, cooling, lighting, and domestic hot water.

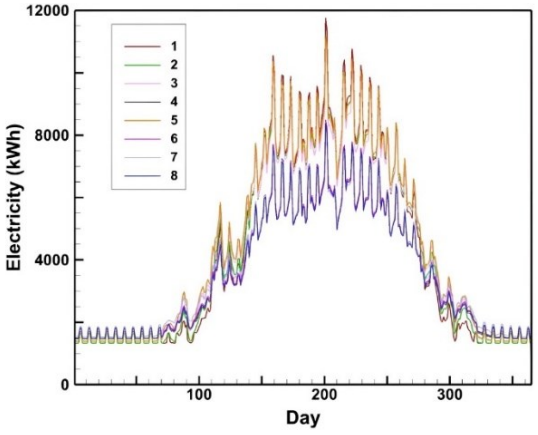

Figure 10. Cumulative electricity consumption in 365 days of the year (cooling) for eight scenarios.

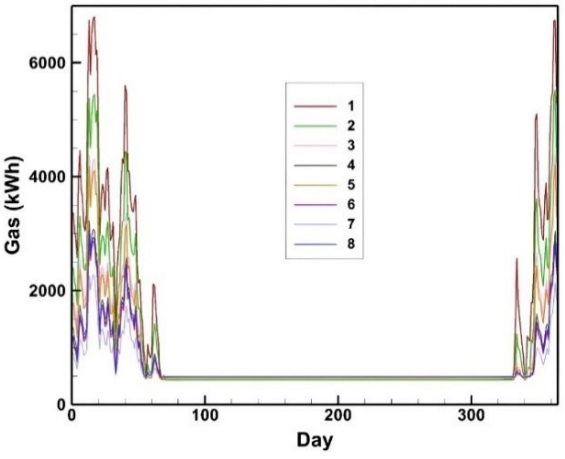

Figure 11. Cumulative gas consumption in 365 days of the year (heating) for eight scenarios.

Computational Fluid Dynamics (CFD) provides valuable insights into airflow behavior by revealing aspects that are not directly observable. Figures 12 and 13 illustrate the generated mesh, along with the pressure and velocity contours for the building in Scenario 8, taken as a representative case of all scenarios. As expected, in high-rise buildings, wind flow enhances heat transfer, a phenomenon that is consistent with and confirmed by the results presented in the preceding figures.

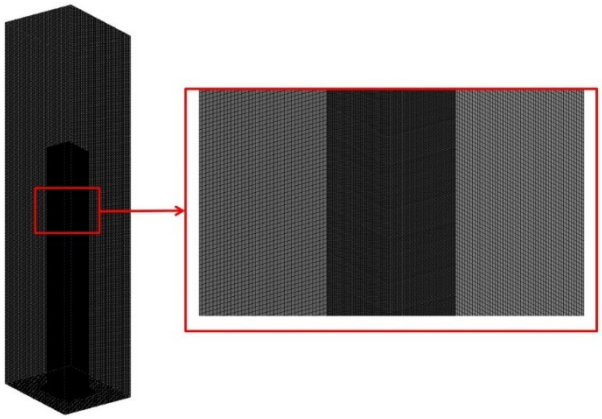

Figure 12. Example of the computational grid used for CFD simulations in this study.

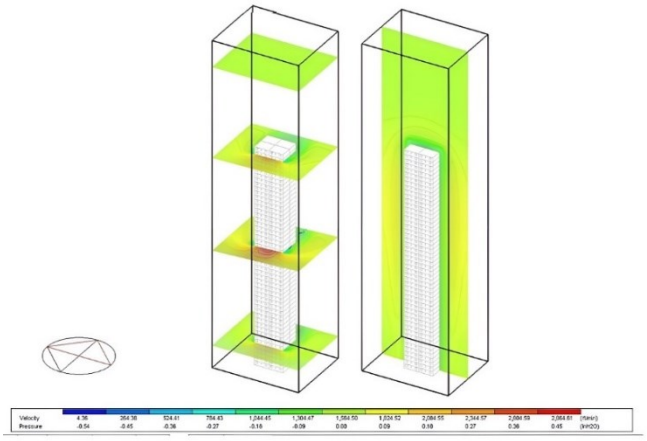

Figure 13. Pressure and velocity contours across various sections of the building for Scenario 8.

Overall, the results indicate that high-rise scenarios, which maximize the number of shared walls, can reduce heating and cooling energy consumption by nearly 60% across the examined cities.

6. Conclusion

This study analyzed and compared the cooling and heating energy consumption of high-rise and low-rise buildings, using the Fanger comfort index as the primary criterion for assessing thermal comfort. Energy demand for both heating and cooling was evaluated across eight distinct building scenarios, which differed in floor count and block configuration, under three representative climatic conditions corresponding to the Iranian cities of Yazd (hot), Arak (moderate), and Shahr-e Kord (cold). Simulations were conducted using DesignBuilder software to provide a detailed assessment of building performance. The scenarios included a range of building types, from single-story independent units to high-rise structures with up to 50 floors, as illustrated in Figure 3 and summarized in Table 1.

The results demonstrate that building geometry, floor configuration, and block arrangement significantly influence both energy consumption and thermal comfort. High-rise buildings with fewer shared walls and larger exposed surfaces tend to exhibit higher heating and cooling loads, whereas designs incorporating shared walls and optimized block layouts reduce energy demand while maintaining occupant comfort. These findings underscore the importance of integrating energy-efficient design strategies with climate-responsive planning to achieve sustainable and comfortable residential developments across diverse urban contexts.

The results demonstrated that the number of shared walls has a more significant influence on energy performance than the number of floors. Specifically, single-story buildings without shared walls exhibited up to 58.9% higher heating loads and 67.1% higher cooling loads compared to scenarios with greater wall adjacency. On average, the difference in energy consumption between the buildings with the maximum and minimum number of common walls was approximately 60%. Moreover, heat loss through the roof of a one-story building was found to be nearly 30 times greater than that of high-rise buildings with multiple units (Figure 9).

Additionally, exterior façade simulations were performed and analyzed to further assess their impact on energy performance. Future research will focus on examining the potential of phase change materials in reducing energy consumption in both high-rise and low-rise buildings.

Nomenclature

A	Surface area (m^2)	V	Volume of space (m^3)
ACH	Air changes per hour (1/h)	W	Mechanical work (W/m^2)
Clo	Clothing insulation unit (clo)	WB	Wet bulb temperature (°C)
DB	Dry bulb temperature (°C)	n	Number of floors
E	Total energy consumption (kWh)		
L	Energy loss (kWh)	Greek	
M	Metabolic rate (W/m^2)	η	System efficiency (-)
PMV	Predicted Mean Vote (thermal comfort index) (-)	ρ	Density (kg/m^3)
Q	Heat transfer (W)		
RH	Relative humidity (%)	Subscripts	
T	Temperature (°C or K)	a	Air
U	Overall heat transfer coefficient (U-value) ($W/(m^2 \cdot K)$)	w	Wall

References

[1] C. Cerezo Davila, C. F. Reinhart, and J. L. Bemis, "Modeling Boston: A Workflow for the Efficient Generation and Maintenance of Urban Building Energy Models from Existing Geospatial Datasets," *Energy*, vol. 117, pp. 237–250, 2016.

[2] C. F. Reinhart, and C. Cerezo Davila, "Urban Building Energy Modeling – A Review of a Nascent Field," *Building and Environment*, vol. 97, pp. 196–202, 2016.

[3] "EnergyPlus.," 2024. https://energyplus.net/.

[4] "DesignBuilder Software Ltd - Home," 2024. https://designbuilder.co.uk.

[5] T. Hong, Y. Chen, X. Luo, N. Luo, and S. H. Lee, "Ten Questions on Urban Building Energy Modeling," *Building and Environment*, vol. 168, 106508, 2020.

[6] B. Kim, Y. Yamaguchi, et al., "Urban Building Energy Modeling Considering the Heterogeneity of HVAC System Stock: A Case Study on Japanese Office Building Stock," *Energy and Buildings*, vol. 207, 109590, 2020.

[7] Y. Chen, T. Hong, X. Luo, and B. Hooper, "Development of City Buildings Dataset for Urban Building Energy Modeling," *Energy and Buildings*, vol. 183, pp. 252–265, 2019.

[8] S. Kimura, Y. Yamaguchi, B. Kim, and Y. Miyachi-, "Urban Scale Energy Demand Modelling of Commercial Building Stock Considering the Variety of HVAC System Configuration," *Building Simulation Conference Proceedings*, 2017.

[9] X. Yu, D. Yan, K. Sun, T. Hong, and D. Zhu, "Comparative Study of the Cooling Energy Performance of Variable Refrigerant Flow Systems and Variable Air Volume Systems in Office Buildings," *Applied Energy*, vol. 183, pp. 725–736, 2016.

[10] F. Gong, Z. Zeng, et al., "Mapping Sky, Tree, and Building View Factors of Street Canyons in a High-Density Urban Environment," *Building and Environment*, vol. 134, pp. 155–167, 2018.

[11] Z. Wang, T. Hong, and M. A. Piette, "Predicting Plug Loads with Occupant Count Data Through a Deep Learning Approach," *Energy*, vol. 181, pp. 29–42, 2019.

[12] J. Page, D. Robinson, N. Morel, and J. Scartezzini, "A Generalised Stochastic Model for the Simulation of Occupant Presence," *Energy and Buildings*, vol. 40, no. 2, pp. 83–98, 2008.

[13] G. Yalcin, and O. Selcuk, "3D City Modelling with Oblique Photogrammetry Method," *Procedia Technology*, vol. 19, pp. 424–431, 2015.

[14] C. Wang, S. Wei, et al., "A Systematic Method to Develop Three Dimensional Geometry Models of Buildings for Urban Building Energy Modeling," *Sustainable Cities and Society*, vol. 71, 102998, 2021.

[15] B. Dong, Y. Liu, et al., "Occupant Behavior Modeling Methods for Resilient Building Design, Operation and Policy at Urban Scale: A Review," *Applied Energy*, vol. 293, 116856, 2021.

[16] D. Yan, T. Hong, et al., "A Thorough Assessment of China's Standard for Energy Consumption of Buildings," *Energy and Buildings*, vol. 143, pp. 114–128, 2017.

[17] R. Buffat, A. Froemelt, N. Heeren, M. Raubal, and S. Hellweg, "Big Data GIS Analysis for Novel Approaches in Building Stock Modelling," *Applied Energy*, vol. 208, pp. 277–290, 2017.

[18] Y. Xu, C. Ren, et al., "Urban Morphology Detection and Computation for Urban Climate Research," *Landscape and Urban Planning*, vol. 167, pp. 212–224, 2017.

[19] P. Remmen, M. Lauster, et al., "TEASER: an Open Tool for Urban Energy Modelling of Building Stocks," *Journal of Building Performance Simulation*, vol. 11, no. 1, pp. 84–98, 2017.

[20] M. Ferrando, F. Causone, T. Hong, and Y. Chen, "Urban Building Energy Modeling (UBEM) Tools: A State-Of-The-Art Review of Bottom-Up Physics-Based Approaches," *Sustainable Cities and Society*, vol. 62, 102408, 2020.

[21] R. Nouvel, M. Zirak, V. Coors, and U. Eicker, "The Influence of Data Quality on Urban Heating Demand Modeling Using 3D City Models," *Computers, Environment and Urban Systems*, vol. 64, pp. 68–80, 2017.

[22] R. Nouvel, A. Mastrucci, et al., "Combining GIS-Based Statistical and Engineering Urban Heat Consumption Models: Towards a New Framework for Multi-Scale Policy Support," *Energy and Buildings*, vol. 107, pp. 204–212, 2015.

[23] B. Daemei, A. K. Limaki, and H. Safari, "Opening Performance Simulation in Natural Ventilation Using Design Builder (Case Study: A Residential Home in Rasht)," *Energy Procedia*, vol. 100, pp. 412–422, 2016.

[24] R. Vakilinezhad, and S. Khabir, "Energy Optimization for Façade Retrofit Design of Residential Buildings in Hot Climates Using Advanced Materials," *Energy and Buildings*, vol. 317, 114417, 2024.

[25] M. Su, P. Jie, et al., "A Review on the Mechanisms Behind Thermal Effect of Building Vertical Greenery Systems (VGS): Methodology, Performance and Impact Factors," *Energy and Buildings*, vol. 303, 113785, 2024.

[26] R. Verma, and D. Rakshit, "Comparison of Reflective Coating with Other Passive Strategies: A Climate Based Design and Optimization Study of Building Envelope," *Energy and Buildings*, vol. 287, 112973, 2023.

[27] N. Ashraf, and A. R. Abdin, "Biomimetic Design Synthesis and Digital Optimization of Building Shading Skin: A Novel Conceptual Framework for Enhanced Energy Efficiency," *Energy and Buildings*, vol. 323, 114824, 2024.

[28] B. Kim, Y. Yamaguchi, et al., "Urban Building Energy Modeling Considering the Heterogeneity of HVAC System Stock: A Case Study on Japanese Office Building Stock," *Energy and Buildings*, vol. 207, 109590, 2020.

[29] Y. Chen, T. Hong, X. Luo, and B. Hooper, "Development of City Buildings Dataset for Urban Building Energy Modeling," *Energy and Buildings*, vol. 183, pp. 252–265, 2019.

[30] J. Page, D. Robinson, N. Morel, and J. Scartezzini, "A Generalised Stochastic Model for the Simulation of Occupant Presence," *Energy and Buildings*, vol. 40, no. 2, pp. 83–98, 2008.

[31] G. Yalcin, and O. Selcuk, "3D City Modelling with Oblique Photogrammetry Method," *Procedia Technology*, vol. 19, pp. 424–431, 2015.

[32] C. Wang, S. Wei, et al., "A Systematic Method to Develop Three Dimensional Geometry Models of Buildings for Urban Building Energy Modeling," *Sustainable Cities and Society*, vol. 71, 102998, 2021.

[33] B. Dong, Y. Liu, et al., "Occupant Behavior Modeling Methods for Resilient Building Design, Operation and Policy at Urban Scale: A Review," *Applied Energy*, vol. 293, 116856, 2021.

[34] R. Nouvel, M. Zirak, V. Coors, and U. Eicker, "The Influence of Data Quality on Urban Heating Demand Modeling Using 3D City Models," *Computers, Environment and Urban Systems*, vol. 64, pp. 68–80, 2017.

Declaration of competing interest

The authors declare that they have no known competing financial interests or personal relationships that could have appeared to influence the work reported in this paper. The ethical issues, including plagiarism, informed consent, misconduct, data fabrication and/or falsification, double publication and/or submission, redundancy, have been completely observed by the authors.

Bibliography

Hamed Safikhani, born in 1986 in Arak, Iran, pursued his academic studies in Mechanical Engineering and obtained his B.Sc. degree from the University of Guilan, Iran, in 2008, his M.Sc. degree from the University of Tehran, Iran, in 2010, and his Ph.D. degree from Amirkabir University of Technology, Iran, in 2014. He joined the Department of Mechanical Engineering, Faculty of Engineering, Arak University, Iran, as an Assistant Professor in 2015. He was promoted to Associate Professor in 2019 and achieved the rank of Full Professor in 2023 at the same university. During his academic career, he has held several administrative and executive positions, including Vice-Chancellor for Research and Technology, Director of the Office for Industry and Society Relations, and Head of the Department of Mechanical Engineering at Arak University. Professor Safikhani has published more than 150 scientific papers in high-ranking international journals and in national and international conference proceedings, in addition to authoring several specialized books in the field of Mechanical Engineering. He also serves as an editorial board member and editor-in-chief of several international scientific journals. He was recognized as the Outstanding Researcher of Markazi Province in 2015 and 2020, and from 2020 to 2023, he has been consecutively listed among the world's top two percent of scientists in Mechanical Engineering, according to the Stanford University ranking. His research interests include optimization of energy systems, energy efficiency in buildings, and renewable energy technologies.
Email: h-safikhani@araku.ac.ir
ORCID: 0000-0002-9732-6861
Contribution Statement: Conceptualization, Software, Supervision, Roles/Writing - original draft.

Mohammad Farahani was born in 1990 in Arak, Iran. He received his B.Sc. degree in Mechanical Engineering from K. N. Toosi University of Technology, Tehran, Iran, in 2013, and his M.Sc. degree in Mechanical Engineering – Energy Conversion from Arak University of Technology, Arak, Iran, in 2020. He is currently pursuing his Ph.D. degree in Mechanical Engineering – Energy Conversion at Arak University of Technology, Arak, Iran. In parallel with his academic career, he serves as the Executive Director of Form Dama Company in Arak, where he is engaged in the design and production of heating, cooling, and HVAC systems. His research interests include the optimization of energy systems, energy efficiency in buildings, and renewable energy technologies.
Email: mmfarahani69@yahoo.com
ORCID: 0009-0008-5123-8007
Contribution Statement: Methodology, Software, Visualization.

Kimia Rezaei, born in 1998 in Arak, Iran, received her B.Sc. degree in Mechanical Engineering from Arak University, Iran, in 2022. She then obtained her M.Sc. degree in Energy Systems Engineering with a focus on Building Energy Simulation and Calibration from Eastern Mediterranean University, Turkey, in 2025. She is currently pursuing her Ph.D. in Mechanical Engineering – Energy Systems at Eastern Mediterranean University, where she also works as a Research and Teaching Assistant. Her main research interests include building energy simulation, HVAC optimization, energy model calibration, lithium-ion battery modeling, renewable energy integration, and sustainable energy systems.
Email: k.rezaei1998@gmail.com
ORCID: 0009-0008-6238-6419
Contribution Statement: Data curation, Formal analysis, Investigation, Software, Validation.

Dr. Asgar Minaei, associated professor at the University of Mohaghegh Ardabili, holds a BSc from the University of Tabriz, an MSc from the University of Tehran, and a PhD from Tarbiat Modares University. His research expertise lies in convective and conductive heat transfer, building energy systems, and renewable energy.
Email: a.minaei@uma.ac.ir
ORCID: 0000-0002-0829-2752
Contribution Statement: Resources, Supervision, Writing-review & editing.

Journal of Green Energy Research and Innovation

Modeling and Optimization of the Photovoltaic System Connected to the Grid

Reza Alayi, Yaser Ebazadeh, Babak Pordel Marageh, Mustafa Ghazi Sabri Al Sabti,

Ali Morsagh Dezfuli

Highlights

- **The study focuses on distributed generation using a photovoltaic (PV) system with battery storage.**
- **Power exchange with the grid is regulated based on the battery's state of charge (SOC).**
- **The system aims to maximize PV power extraction under varying temperature and irradiation conditions.**
- **A converter with proper switching control enables efficient energy management.**
- **With well-designed controllers, the proposed structure ensures optimal and reliable power management in distributed systems.**

Graphical Abstract

Use your device to scan and read the article online

Citation

R. Alayi, Y. Ebazadeh, B. P. Marageh, M. G. S. Al Sabti, and A. M. Dezfuli," Modeling and Optimization of the Photovoltaic System Connected to the Grid," *Journal of Green Energy Research and Innovation*, vol. 2, no. 3, pp. 14-26, 2025.

https://doi.org/10.61882/jgeri.2.3.14

Journal of Green Energy Research and Innovation 2.3 (2025) 14-26

Online ISSN: 3041-9018

Journal of Green Energy Research and Innovation

Journal Homepage: www.jgeri.araku.ac.ir

Modeling and Optimization of the Photovoltaic System Connected to the Grid

Reza Alayi [1,*] , Yaser Ebazadeh [2] , Babak Pordel Marageh [3] , Mustafa Ghazi Sabri Al Sabti [4] , Ali Morsagh Dezfuli [5]

[1] *Department of Mechanical Engineering, Ge.C., Islamic Azad University, Germi 5651763764, Iran.*

[2] *Department of Computer Engineering, Ge.C., Islamic Azad University, Germi 5651763764, Iran.*

[3] *Department of Civil Engineering, Ard.C., Islamic Azad University, Ardebil, Iran.*

[4] *Department of Energy Engineering and Industries, Science and research branch, Islamic Azad university, Tehran, Iran.*

[5] *Electrical Engineer, Khuzestan Steel Company (KSC), Ahvaz, Iran.*

A R T I C L E I N F O

Keywords:
Photovoltaic,
On-grid,
Electrical energy.

Article History:
Received: 18 March 2025;
Revised: 13 April 2025;
Accepted: 19 April 2025.

Article type:
Research Article

* ***Corresponding author***
E-mail address
reza.alayi@iau.ac.ir (R. Alayi)

A B S T R A C T

In recent years, distributed generation as a source of local loads and continuous economic operation has gathered attention. In this thread, this study focuses on distributed generation using a photovoltaic package with batteries, so that the power drawn from the distributed generation system for injection into the main grid or receiving it is adjusted based on the battery charge status. The goal is to absorb the maximum power received from the photovoltaic system at any temperature and hypothetical radiation. If the battery charge is not optimal, part of this power is applied to the battery for charging. By presenting a suitable structure, a photovoltaic system with a battery package is presented as a distributed generation source with the design of appropriate controllers. The results show that at any temperature and radiation, the maximum power received from the photovoltaic system can be estimated. By controlling a converter switching the required amount of energy can be obtained from the photovoltaic system. It can be concluded that such a structure, as a desirable distributed generation source, is realized. With the proper design of the necessary controllers, optimal management can be done for power management.

1. Introduction

Distributed generation as a source of local loads, as well as continuous and economic operation, has been considered by researchers in recent years. For this reason, different structures and several control algorithms have been presented in most different research [1-3]. In some research, the issue of islanding and the recognition of the necessity of islanding to continuously feed the local load has been considered [4-6] in which the islanding problem is investigated when the main grid is shut down and islanding the dis-tributed generation system is intelligently designed by terminal voltage and network frequency to detect transient errors from the total blackout of the system [7,8]. In the IEEE 929-2000 standard, the islanding conditions of the distributed generation system are described from the main grid, but the main issue in observing this standard is the detection of transient errors and disturbances caused by local load changes from the main grid blackout [9-11]. A control technique has been introduced to determine the necessity of islanding, in which only local and available parameters are measured and remote signals are excluded [12,13]. Also, without the use of telecommunication signals, the connection of the distributed system and the main grid is designed using a hybrid technique based on multi-inverter performance [14,15]. In addition, in [16,17] a method for safe detection of islanding based on reactive power flowing under normal conditions and its investigation during sudden changes is presented, and the same method has been car-ried out in [18] taking into account the power factor and its sudden changes, in which after deciding to islanding, the disconnection order is sent to the switch.

In [19, 20], considering the moment of a sharp drop in active and reactive power, the islanding problem was analyzed. Ref. 2022 [21] presented a collaborative optimization of PV greenhouses and clean energy systems in rural areas. The combined coordination model of agriculture and energy networks is established, and the combined model involves carbon, electrical energy, and thermal energy. Fu et al. [22] have done modeling with the purpose of stochastic optimal planning of distribution networks considering a dynamic correlation and dimension reduction. Fu et al. [23] presented a statistical machine-learning model for capacitor planning considering uncertainties in photovoltaic (PV) power. The results verify that the proposed model greatly improves planning performance while meeting accuracy requirements. The case study also considers a realistic power distribution system operating under stressed conditions.

This paper discusses the use of distributed generation with a PV system and batteries. The power from this system is adjusted based on the battery charge status when it is either being injected into the main grid or received. The goal is to maximize the power received from the PV system regardless of temperature and radiation levels. If the battery charge is not optimal, some of this power is used to charge the battery. The paper first describes the PV system model, then designs the necessary controllers. Finally, simulation results are presented to demonstrate the effectiveness of the proposed structure.

2. Materials and Methods

2.1. Structure description

The structure introduced in this paper consists of a PV system connected to a DC/DC converter whose output is connected to a battery package with the appropriate voltage, shown in Figure 1. The output of the converter is connected to a two-level inverter and after connecting to a transformer and a harmonic filter, the local load is fed through a distributed generation system and main grid. The distributed generation system is connected to the main grid through a distribution transformer, and the local load is combined through the distributed generation system and the main grid. In this structure, two separate controllers are designed as follows:

A. Power controller of a PV system, which absorbs reference and determines power from the PV system at any given temperature and radiation. This will be done by adjusting the pulse switching of the DC/DC converter, and in fact, the pulse switching controller of the mentioned converter adjusts the power received from the PV system to its reference value.

B. The power controller is exchanged between the distributed generation system and the main grid, which is done by adjusting the pulse switching of the inverter connected to the DC/DC converter and adjusting the transmission power of the PV/battery set to the reference value. It is obvious that when the power transferred from the distributed generation system is less than the power generated by the PV system, the rest of the absorbed power from the PV system is applied to the batteries and sets them in charging conditions. When the transmission power is higher, the batteries will supply the rest of the power and will be in a discharged state.

2.2. Modeling the PV system

A PV system consists of several series/parallel cells, as shown in Figure 2, as described in [12, 24-26] on how they are modeled. In modeling the system, a current source whose value depends on the sun's radiation is used, and the relationships governing the voltage and current of this system are per Equation (1) to (4).

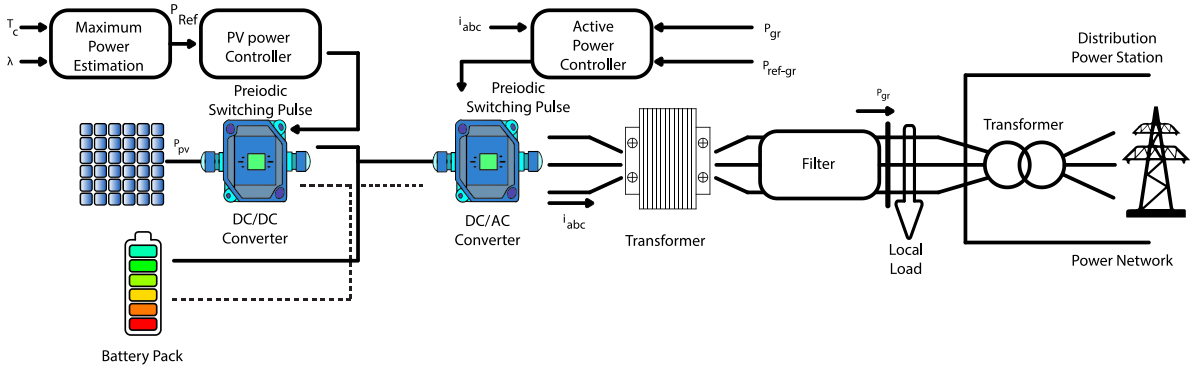

Figure 1. Power generation system with battery storage connected to the grid.

According to the above equations, voltage, current, and therefore the power of the system will depend on the temperature and radiation of the environment. In Figure 3, the sample curves of a PV system whose parameters are described in Table 1 are drawn from Equations (1) to (4).

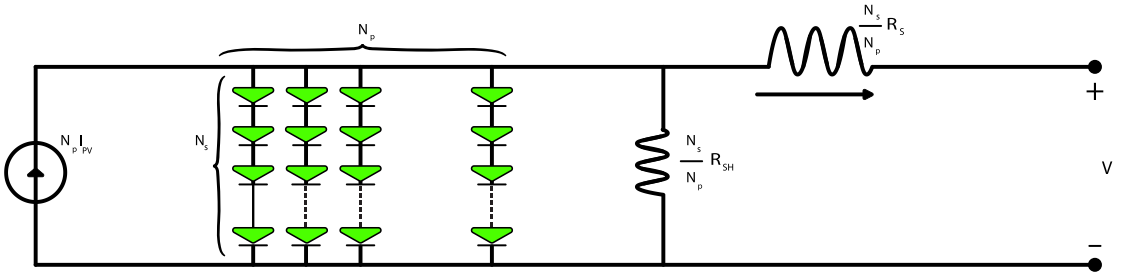

Figure 2. Model of the PV system consisting of series/parallel cells [12].

$$I_{PV} = \left[I_{sc} + K_I\left(T_{PV} - T_{ref}\right)\right], \lambda \tag{1}$$

$$I_{RS} = \frac{I_{sc}}{e^{\frac{q.V_{ec}}{N_S.k.A.T_{PV}}} - 1} \tag{2}$$

$$I_S = I_{RS}\left(\frac{T_{PV}}{T_{ref}}\right)^3 \cdot e^{\frac{q.G_i\left(\frac{1}{T_{ref}} \frac{T_{PV}}{}\right)}{k.A}} \tag{3}$$

$$I = N_P.I_{PV} - N_P.I_s\left[e^{\frac{q\left(\frac{V}{N_S} + \frac{R_S.I}{N_P}\right)}{k.T_{PV}.A}} - 1\right] - \frac{\frac{N_P V}{N_S} + R_s.I}{R_{sh}} \tag{4}$$

Table 1. Parameters of a PV system.

Parameter	Rate
N_s	1000
N_p	250
K_i	0.025
V_{oc}	1200 × 0.6 = 720
I_{sc}	300 × 3.6 = 1090
T_{ref}	25°C
R_{sH}	10000 Ω
R_s	10 μΩ
A	3.3

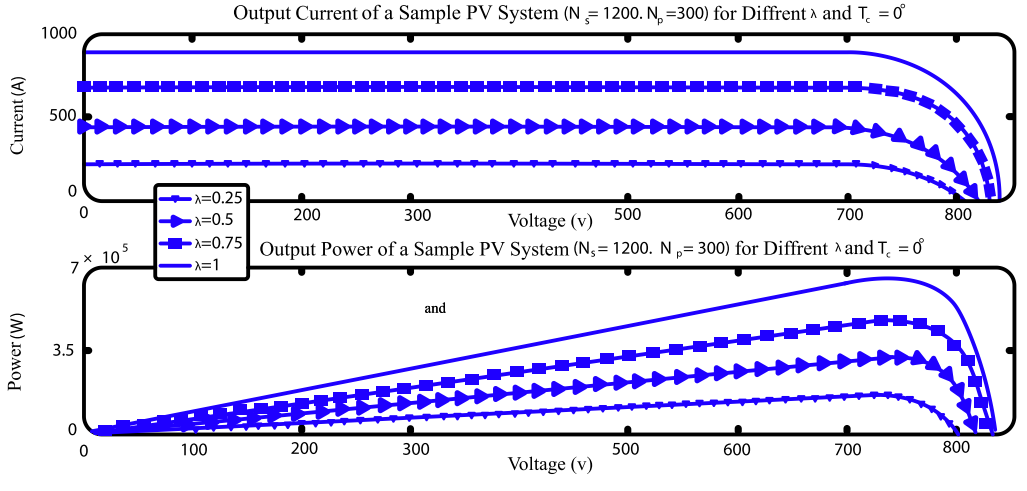

(a)

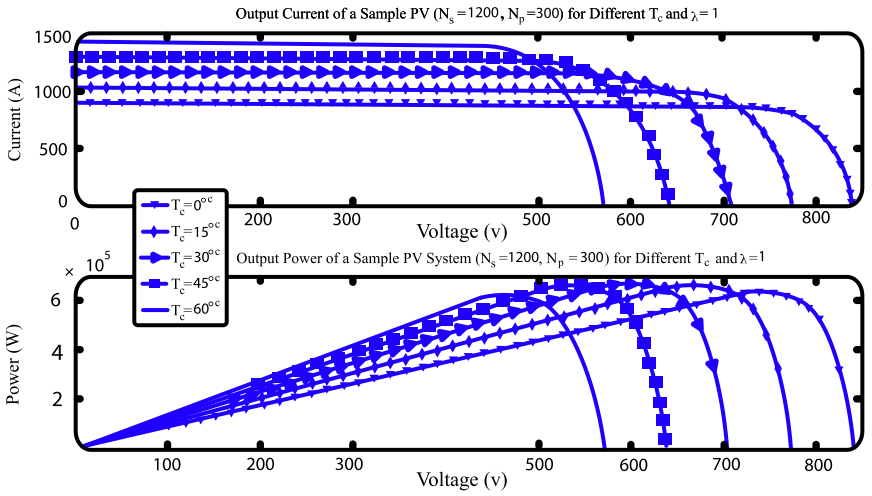

(b)

Figure 3. Voltage-current curve and power voltage of a sample PV package at (a) certain temperatures and different radiations, and (b) at different temperatures and certain radiations.

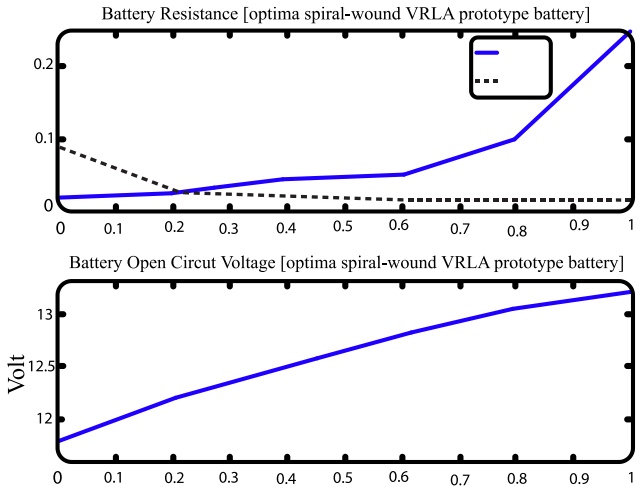

(a)

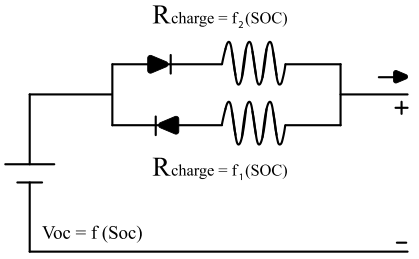

(b)

Figure 4. (a) Open-circuit voltage and internal resistance of a sample battery, (b) internal resistance model of the battery.

2.3. Battery modeling

A well-known battery model is the built-in resistance model [7,8,27,28], where the battery's internal resistance is modeled in charging and discharging modes and fits the charging status. Open-circuit voltage is also defined according to the charging state. This model is illustrated, and Figure 4 also shows the internal resistance and open-circuit voltage for a sample battery.

Battery charging mode, which is one of the most important control parameters of the system discussed in this paper, can be calculated from Equation (5) to (7) [7-9]:

$$\mathrm{SoC} = \frac{\mathrm{A,h} - \mathrm{Ah_{seed}}}{\mathrm{A.h}} \tag{5}$$

$$Ah_{\mathrm{used}} = \mathrm{Ah} \times \left(1 - SoC_{(0)}\right) + \int \frac{I_b}{3600} dt \tag{6}$$

$$I_b = \frac{V_{\mathrm{oc}} - \sqrt{4R_{\mathrm{int}} \cdot P_{\mathrm{el}}}}{2R_{\mathrm{int}}} \tag{7}$$

where Ah and $\mathrm{Ah_{seed}}$ are the instantaneous battery ampere-hour and ampere-hour consumed battery, respectively.

2.4. DC/DC and DC/AC inverters

According to the proposed structure of this paper, which is shown in Figure 1, a DC/DC converter is applied to control the absorbed power of the PV system, which is used through the switching pulse width of this model at a specified switching frequency. Figure 5(a) shows this incremental converter. In Figure 5(b), a two-level inverter used in the structure is shown, and its output power will be controlled by switching pulses.

2.5. Estimation of the maximum absorbable power from a PV system

According to the previous explanations, the maximum absorbable power from the PV system depends linearly on two parameters: temperature and ambient radiation. Therefore, it is necessary to estimate the maximum receivable power for each PV system with specific parameters. According to the parameters given in Table 1 used for the PV system in this paper, the maximum power received is obtained according to Figure 6(a). To estimate the maximum absorbable power, Figure 6(a), data have been applied to a form-matching neural fuzzy network, given in Figure 6(b). The membership functions of this network are considered by dividing radiation and temperature values into five different intervals according to Figure 12 and after network training, its fuzzy surface is formed according to Figure 11. To prevent damage to the PV system, after estimating the maximum power absorbed by the fuzzy neural network, 90% of this power is used as reference power and is applied to the absorbed power controller of the PV system.

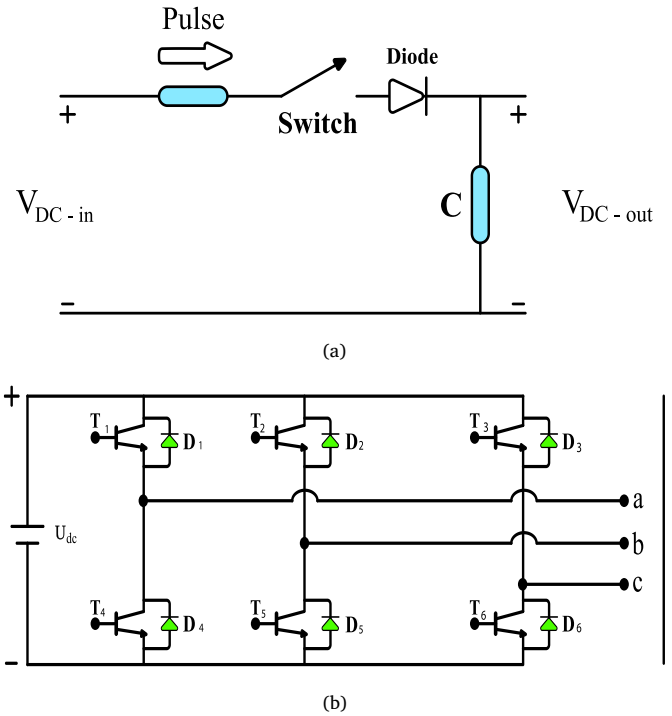

Figure 5. (a) Incremental DC/DC converter implemented, and (b) Two-level inverter used in the structure.

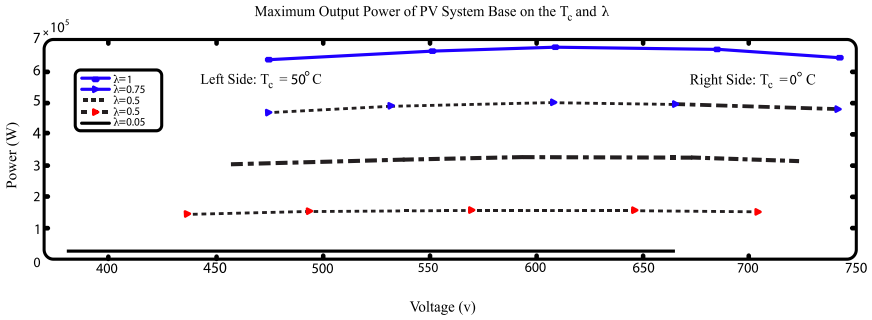

(a)

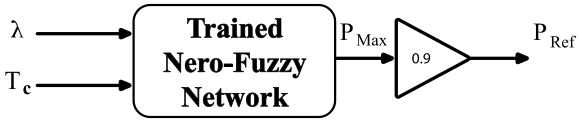

(b)

Figure 6. (a) Maximum power received from sample systems listed in Table 1 in terms of temperature and radiation, (b) Fuzzy-neural network.

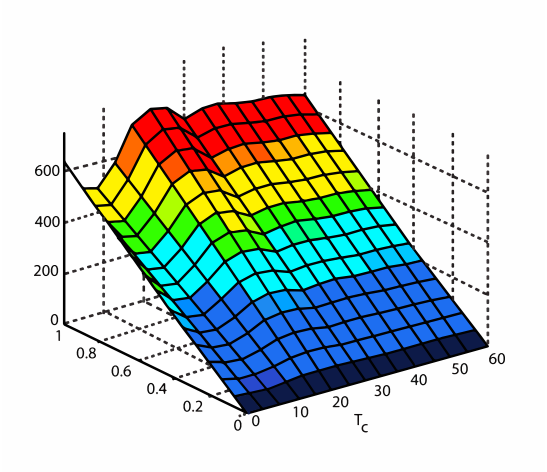

(a)

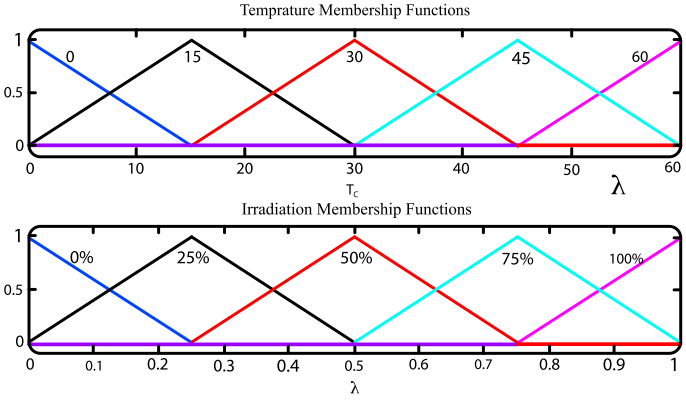

(b)

Figure 7. (a) Fuzzy surface of the sample fuzzy-neural network, (b) input membership functions of the trained network.

2.6. Design of essential controllers

It is necessary to design two separate controllers for the whole system as follows. The absorbed power controller of the PV system, which should be absorbed from the PV system at any temperature and radiation, can absorb the reference power determined by the fuzzy neural network. This controller performs power adjustment based on the DC/DC converter switching control described in the following sections.

The controller of power transfer to the main grid is required to adjust the transmission power to the network according to the reference value. This is done by controlling the inverter switching described in the following sections. The transmission power will also be determined from the battery charge mode. This is in such a way that if the battery charging mode is desirable, more power than the nominal of the PV system is transferred to the network, which in this case means provision will be part of the power injected by the batteries. Also, if the battery charging mode is low, the power to the network is less than the available power of the PV system, which indicates the transfer of part of the power generated by the PV system to the batteries and causes them to be charged.

2.7. Power controller absorbed from a PV system

This controller must adjust the power transmitted from the PV system according to the reference value generated by the trained fuzzy neural network. For this purpose, at a specified switching frequency, the pulse width of the switching is adjusted according to Figure 8.

2.8. Controller transferred to the network

For this purpose, the output current of the inverter is adjusted after converting to the dq0 frame by switching the controller with mend hysteresis. According to Figure 9, by stabilizing the two 0 and q components, the d component adjusts the current so that the transfer power to the network is equal to its reference value.

Herein, according to the control algorithm discussed previously, the amount of power reference transferred to the main grid should be determined according to the battery charge status, which is applied using a data table as shown in Table 2. K_p is defined as the available power factor of the PV system, and the transfer of power to the network is determined by Equation (8):

$$P_{\text{Ref-Tr}} = K_p, P_{\text{Ref-PV}} \quad (8)$$

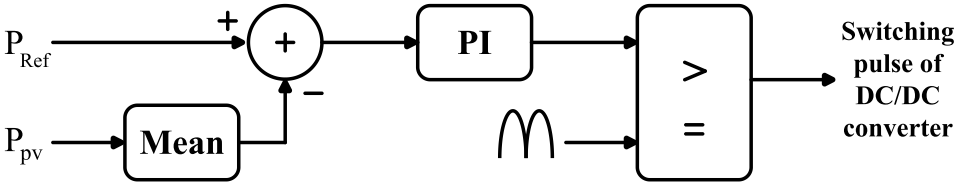

Figure 8. Generation procedure of pulse switching DC/DC converter to control the absorbed power of the PV system.

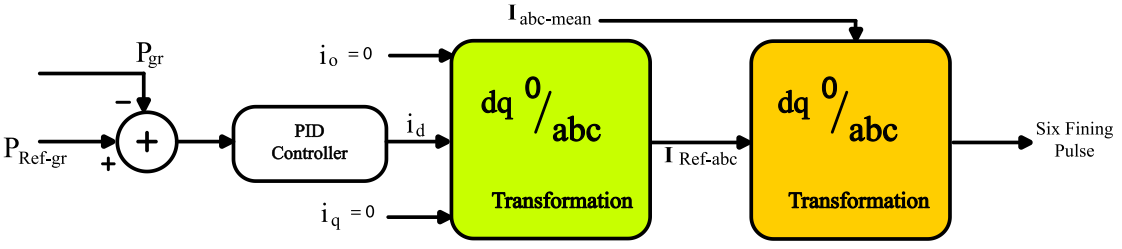

Figure 9. Injectable power controller to the network of the distributed generation system.

Table 2. Input data for battery charge status [29].

S_{oc}	100%	95%	90%	85%	80%	75%	70%
K_p	1.7	1.7	1.5	1.35	1.15	1	0.75

3. Results

3.1. Simulation

The structure shown in Figure 1 is simulated in the Simulink/Matlab environment according to Figure 10, and the parameters related to other parts of the system are under the values listed in Tables 3 to 6. To prove the proposed control performance, different conditions have been analyzed, which are discussed in the next section.

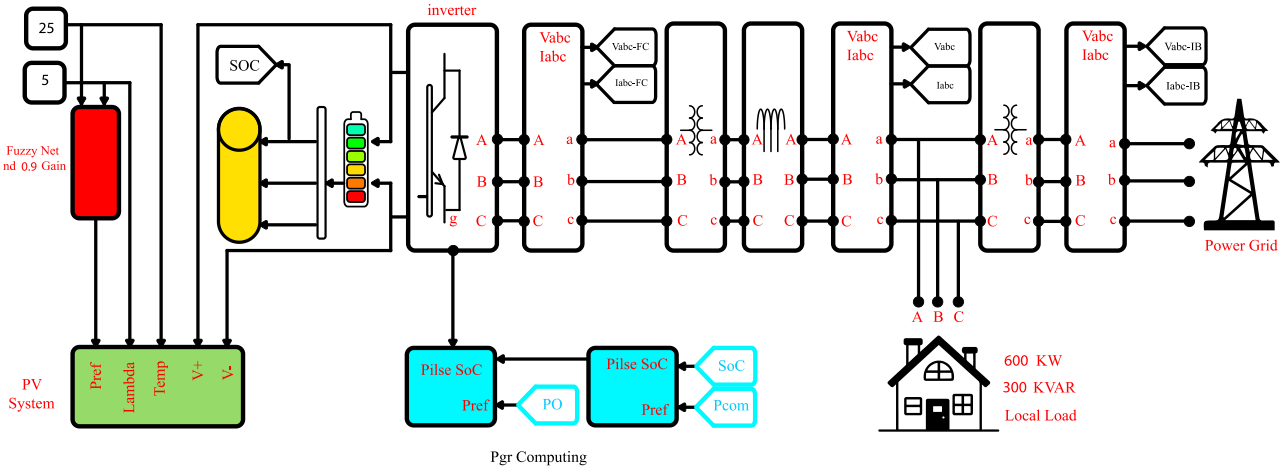

Figure 10. Injectable power controller to the network of the distributed generation system.

Table 3. Features of the implemented batteries.

Parameter	Quantity
N_p	65
$A.h_{Cap}$	110
V_b	10

Table 4. Transformer features connected to inverters.

Parameter	Quantity
N1/N2	0.5/0.5
Srate	1
Lm	470
Rc	470
L1 + L2	0.025
R1 + R2	0.0015

Table 5. Transformer features connected to the grid.

Parameter	Quantity
N_1/N_2	0.5/0.5
Srate	1
L_m	470
R_c	470
$L_1 + L_2$	0.025
$R_1 + R_2$	0.0015

Table 6. Features of the load and overall grid.

Parameter	Quantity
Ssc	520
V	30
F	50
P_L	750
Q_L	350
V_L	360 × 1.08

3.2. Maximum radiation status, maximum charging mode in battery, and variable temperature

In this section, the simulation is performed for a battery with a full charge and maximum radiation (λ = 1). The ambient temperature is considered a variable temperature according to Figure 11(a). In addition, the temperature variations are assumed to be more extreme and to occur at a faster rate than in reality, due to the shortened simulation time. If the system responds well under these conditions, it can be expected to perform equally well—or better—under real conditions, where temperature changes occur more gradually. In Figure 11(a), in addition to ambient temperature, the power drawn from the PV system (Ppv), injectable power to the global grid (Pπr), as well as the reference power commanded by the controller (P_{COM}) are displayed. In Figure 11(b), the voltage and current of the PV system are displayed, which are changed according to the variable temperature and adjusted by the controller at 90% of its peak value. Since the battery charging status has been favorable, the power transferred to the network exceeds the power drawn from the PV system, which means that part of the power is generated by the batteries, and conspicuously in these conditions, the battery is in discharging conditions. This is specified in the upper part of Figure 11(c). In addition, the load voltage is also stabilized by the inverter to the value of 1 p.u. as specified in the lower part of Figure 11(c).

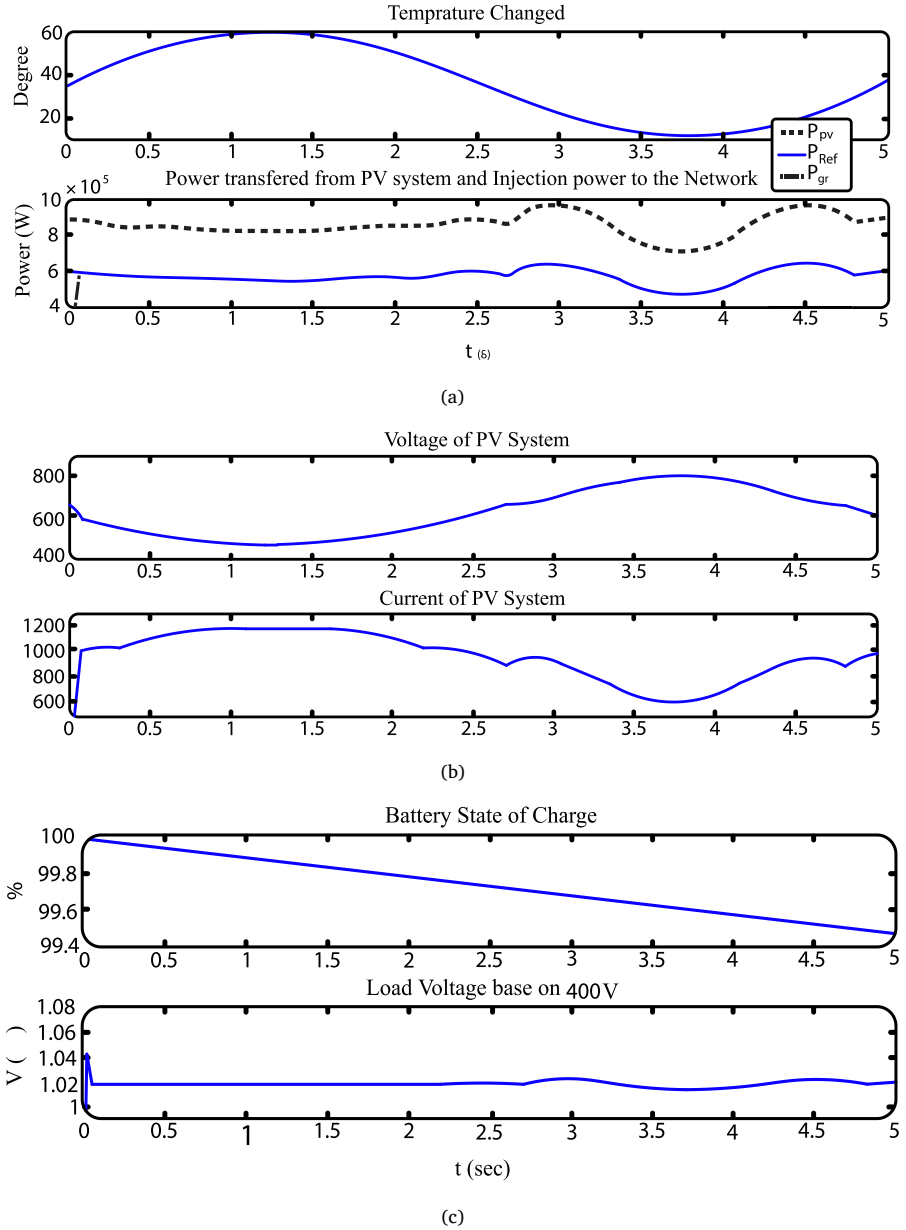

Figure 11. Maximum radiation status, maximum charging mode in battery, and variable temperature.

3.3. Temperature and specified charging mode and different radiation

In this section, a simulation is performed for a certain temperature of 25 °C, charging status of 80% battery, and variable radiation by Figure 12(a), which, due to the reduction of simulation time, radiation changes are considered more than real conditions. According to this figure, the power transferred to the network is exactly equal to the power absorbed from the PV system, and in other words, the battery has no involvement in the transmission of power to the network. The lack of power absorption from the battery is due to the rest state, which has a battery charge mode, and no power is absorbed from the battery. According to these results, it can be concluded that the performance of the controller is accurate, and the transmission power to the network and absorbed from the PV system is set to the desired and predetermined values. In Figure 12(b), to show the harmonic state of the system and the function of the embedded filter, the current waveform is shown along with a small part of it, and as it is known, the harmonic state of the flowing current is appropriate.

3.4. Specified temperatures and radiation, and different modes of battery charge

In this section, a simulation is performed for constant temperature and radiation, but with different charging conditions have been performed. The injectable active power is shown in the main grid in Figure 13(a). It is seen that when the charging situation is better, due to the battery's participation in the injection of active power, more power is transferred to the network. In addition, in Figure 13(b), the battery charging status is shown. Due to this, when the battery is charged more, the battery's discharge is done more quickly. Also, as is evident in the lower part of Figure 13(b), in 70% of the charge, the battery is in charge and the charging mode is incremental.

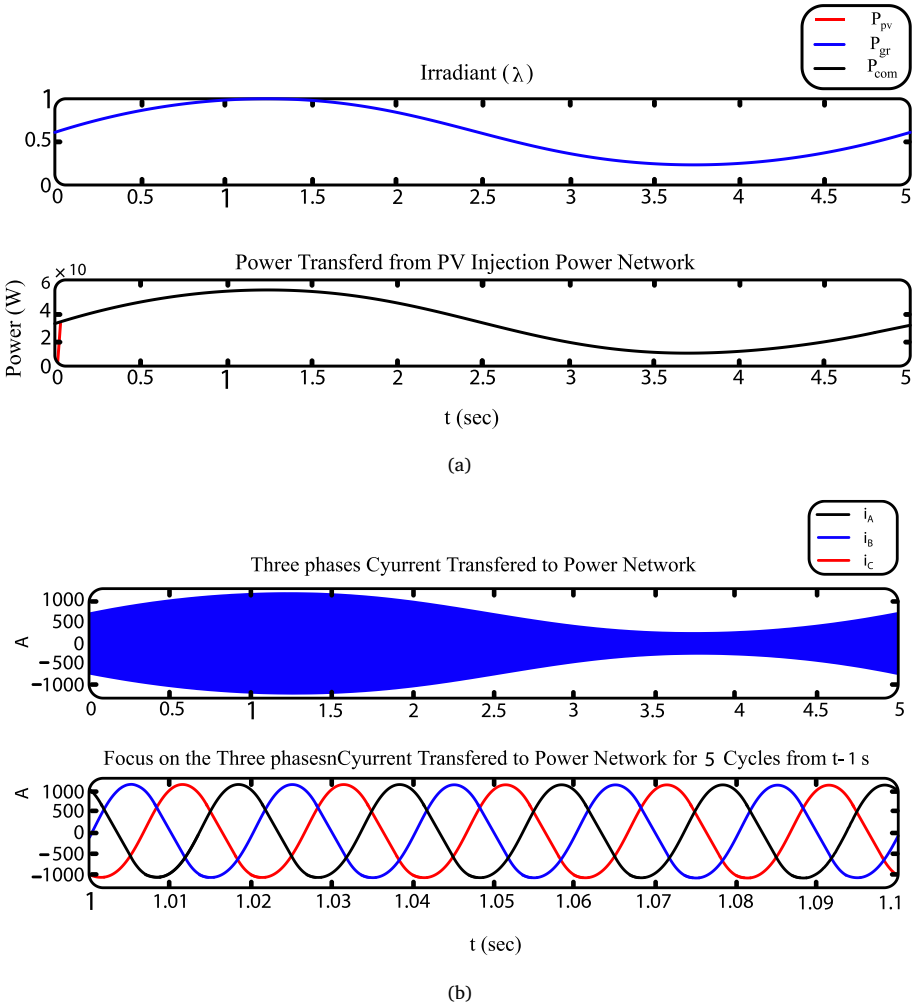

Figure 12. (a) Injectable power to the network and drawn from PV systems under variable radiation conditions, (b) Current waveform and part of it under variable radiation conditions.

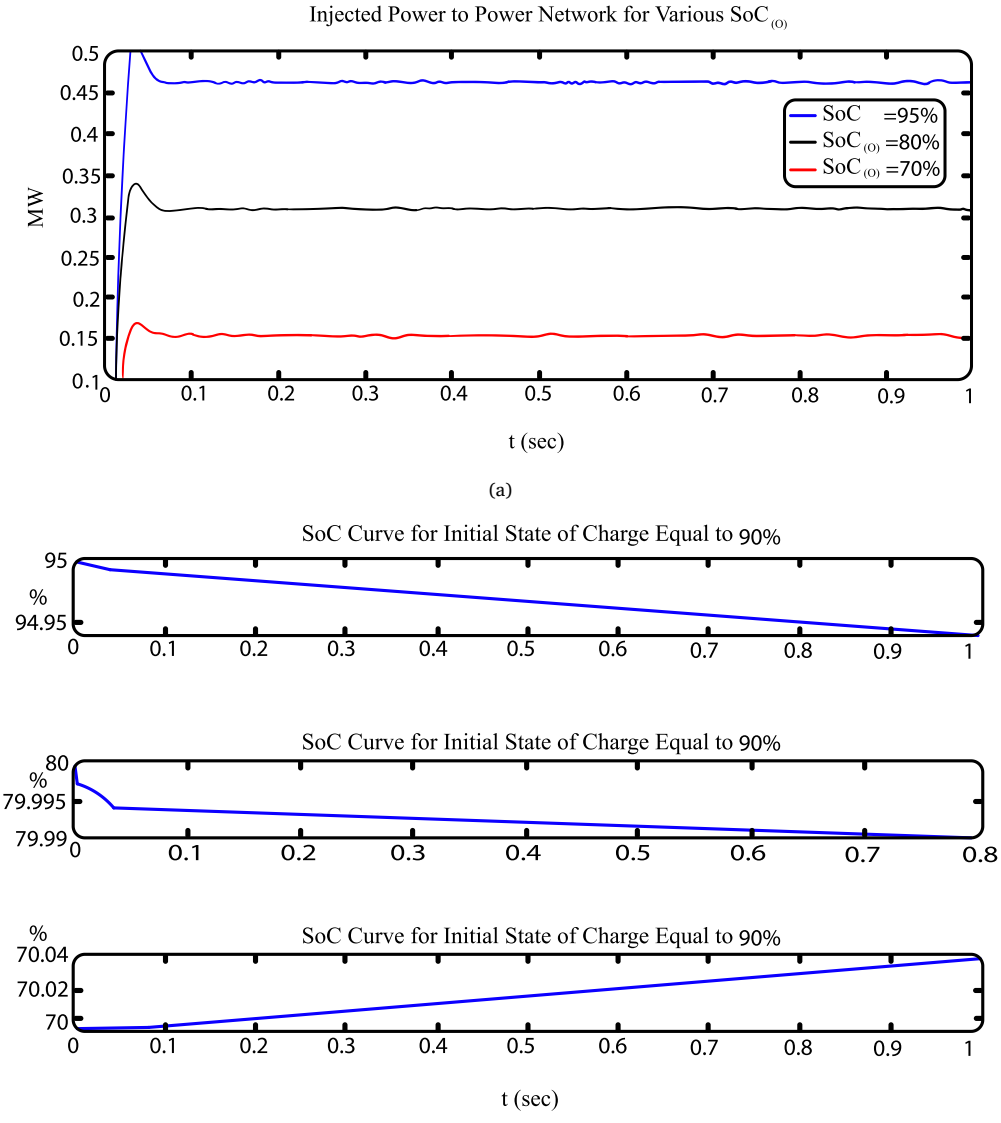

Figure 13. (a) Injectable power to the network in different battery charge situations, (b) Changes in battery charging mode under different battery mode conditions.

4. Conclusions

In this paper, by presenting a suitable structure, a PV system with a battery package as a distributed generation source, with the design of appropriate controllers. The results of this paper showed that at any temperature and radiation, the maximum power received from the PV system can be estimated, and by controlling switching, a converter, the required amount of power can be obtained from the PV system. On the other hand, by designing another control, and controlling the inverter switching, it managed the power transmitted from the battery set and the PV system, and divided between the two sources of battery and PV in a way that the battery charge mode always remained in the above-mentioned state. The results indicate that this structure can serve as an effective distributed generation source. With the appropriate design of the necessary controllers, optimal power management can be achieved. To continue the process of studying, it is recommended to provide different structures for controllers for better performance, as well as different switching structures of converters to reduce switching losses, or to use multilevel inverters.

References

[1] R. Alayi, F. Zishan, et al., "A Sustainable Energy Distribution Configuration for Microgrids Integrated to the National Grid Using Back-To-Back Converters in a Renewable Power System," *Electronics*, vol. 10, no. 15, 1826, 2021.

[2] L. Mehigan, J. Deane, B. Gallachóir, and V. Bertsch, "A Review of the Role of Distributed Generation (DG) in Future Electricity Systems," *Energy*, vol. 163, pp. 822–836, 2018.

[3] P. D. Huy, V. K. Ramachandaramurthy, J. Y. Yong, K. M. Tan, and J. B. Ekanayake, "Optimal Placement, Sizing and Power Factor of Distributed Generation: A Comprehensive Study Spanning from the Planning Stage to the Operation Stage," *Energy*, vol. 195, 117011, 2020.

[4] L. F. Fuentes-Cortés, and A. Flores-Tlacuahuac, "Integration of Distributed Generation Technologies on Sustainable Buildings," *Applied Energy*, vol. 224, pp. 582–601, 2018.

[5] A. M. Azmy, "Management of Distributed Generation for Smart Buildings," *Advances in Control Techniques for Smart Grid Applications*, pp. 173–199, 2022.

[6] A. Fleischhacker, H. Auer, G. Lettner, and A. Botterud, "Sharing Solar PV and Energy Storage in Apartment Buildings: Resource Allocation and Pricing," *IEEE Transactions on Smart Grid*, vol. 10, no. 4, pp. 3963–3973, 2019.

[7] F. Wei, B. Zeng, and F. Xu, "Evaluation on Load Restoration of Distribution System Based on Distributed Generation in Smart Buildings After Extreme Disasters," *Power Generation Technology*, vol. 40, no. 5, p. 440, 2019.

[8] A. D. Georgakarakos, M. Mayfield, and E. A. Hathway, "Battery Storage Systems in Smart Grid Optimised Buildings," *Energy Procedia*, vol. 151, pp. 23–30, 2018.

[9] S. M. Mirbagheri, D. Falabretti, and M. Merlo, "Voltage Control in Active Distribution Grids: A Review and a New Set-Up Procedure for Local Control Laws," *2018 International Symposium on Power Electronics, Electrical Drives, Automation and Motion (SPEEDAM)*, pp. 1203–1208, 2018.

[10] R. Alayi, F. Zishan, et al., "Optimal Load Frequency Control of Island Microgrids Via a PID Controller in the Presence of Wind Turbine and PV," *Sustainability*, vol. 13, no. 19, 10728, 2021.

[11] A. J. Babqi, Z. Yi, and A. H. Etemadi, "Centralized Finite Control Set Model Predictive Control for Multiple Distributed Generator Small-Scale Microgrids," *2017 North American Power Symposium (NAPS)*, pp. 1–5, 2017.

[12] A. Vukojevic, and S. Lukic, "Microgrid Protection and Control Schemes for Seamless Transition to Island and Grid Synchronization," *IEEE Transactions on Smart Grid*, vol. 11, no. 4, pp. 2845–2855, 2020.

[13] R. Bisht, A. Suresh, and S. Kamalasadan, "Multiple Single Phase Inverters Based Combined Active Power Management and Voltage Regulation of Power Distribution System Based on A Novel Optimal Control Architecture," *2019 North American Power Symposium (NAPS)*, pp. 1–6, 2019.

[14] X. Guo, and W. Chen, "Control of Multiple Power Inverters for More Electronics Power Systems: A Review," *CES Transactions on Electrical Machines and Systems*, vol. 2, no. 3, pp. 255–263, 2018.

[15] K. Naraghipour, K. Ahmed, and C. Booth, "A Comprehensive Review of Islanding Detection Methods for Distribution Systems," *2020 9th International Conference on Renewable Energy Research and Application (ICRERA)*, pp. 428–433, 2020.

[16] R. Sedaghati, and M. R. Shakarami, "A Novel Control Strategy and Power Management of Hybrid PV/FC/SC/Battery Renewable Power System-Based Grid-Connected Microgrid," *Sustainable Cities and Society*, vol. 44, pp. 830–843, 2019.

[17] M. Bajaj, and A. K. Singh, "Grid Integrated Renewable DG Systems: A Review of Power Quality Challenges and State-of-the-art Mitigation Techniques," *International Journal of Energy Research*, vol. 44, no. 1, pp. 26–69, 2019.

[18] S. Kumar, K. K. Mandal, and N. Chakraborty, "Optimal DG Placement by Multi-Objective Opposition Based Chaotic Differential Evolution for Techno-Economic Analysis," *Applied Soft Computing*, vol. 78, pp. 70–83, 2019.

[19] M. N. AlMallahi, M. El Haj Assad, S. AlShihabi, and R. Alayi, "Multi-Criteria Decision-Making Approach for the Selection of Cleaning Method of Solar PV Panels in United Arab Emirates Based on Sustainability Perspective," *International Journal of Low-Carbon Technologies*, vol. 17, pp. 380–393, 2022.

[20] A. Shaqour, H. Farzaneh, Y. Yoshida, and T. Hinokuma, "Power Control and Simulation of a Building Integrated Stand-Alone Hybrid PV-Wind-Battery System in Kasuga City, Japan," *Energy Reports*, vol. 6, pp. 1528–1544, 2020.

[21] X. Fu, and Y. Zhou, "Collaborative Optimization of PV Greenhouses and Clean Energy Systems in Rural Areas," *IEEE Transactions on Sustainable Energy*, vol. 14, no. 1, pp. 642–656, 2023.

[22] X. Fu, Q. Guo, and H. Sun, "Statistical Machine Learning Model for Stochastic Optimal Planning of Distribution Networks Considering a Dynamic Correlation and Dimension Reduction," *IEEE Transactions on Smart Grid*, vol. 11, no. 4, pp. 2904–2917, 2020.

[23] X. Fu, "Statistical Machine Learning Model for Capacitor Planning Considering Uncertainties in Photovoltaic Power," *Protection and Control of Modern Power Systems*, vol. 7, no. 1, 2022.

[24] R. Alayi, H. Harasii, and H. Pourderogar, "Modeling and Optimization of Photovoltaic Cells with GA Algorithm," *Journal of Robotics and Control (JRC)*, vol. 2, no. 1, 2020.

[25] R. Alayi, A. Sevbitov, M. E. H. Assad, R. Akhmadeev, and M. Kosov, "Investigation of Energy and Economic Parameters of Photovoltaic Cells in Terms of Different Tracking Technologies," *International Journal of Low-Carbon Technologies*, vol. 17, pp. 160–168, 2021.

[26] N. Ganjei, F. Zishan, et al., "Designing and Sensitivity Analysis of an Off-Grid Hybrid Wind-Solar Power Plant with Diesel Generator and Battery Backup for the Rural Area in Iran," *Journal of Engineering*, vol. 2022, pp. 1–14, 2022.

[27] R. Alayi, M. Jahangiri, et al., "Modelling and Reviewing the Reliability and Multi-Objective Optimization of Wind-Turbine System and Photovoltaic Panel with Intelligent Algorithms," *Clean Energy*, vol. 5, no. 4, pp. 713–730, 2021.

[28] M. Jahangiri, F. Karimi Shahmarvandi, and R. Alayi, "Renewable Energy-Based Systems on A Residential Scale in Southern Coastal Areas of Iran: Trigeneration of Heat, Power, And Hydrogen," *Journal of Renewable Energy and Environment*, vol. 8, no. 4, pp. 67–76, 2021.

[29] D. Azuatalam, K. Paridari, et al., "Energy Management of Small-Scale PV-Battery Systems: A Systematic Review Considering Practical Implementation, Computational Requirements, Quality of Input Data and Battery Degradation," *Renewable and Sustainable Energy Reviews*, vol. 112, pp. 555–570, 2019.

Declaration of competing interest

The authors declare that they have no known competing financial interests or personal relationships that could have appeared to influence the work reported in this paper. The ethical issues, including plagiarism, informed consent, misconduct, data fabrication and/or falsification, double publication and/or submission, redundancy, have been completely observed by the authors.

Bibliography

Reza Alayi holds a MSc. and a PhD in energy systems engineering from science and research branch Islamic Azad University (IAU) in Iran. He is leading the "Energy engineering" group the Saveh for Energy institute of higher education. He currently works Assistant Professor at the Department of Mechanical Engineering, Islamic Azad University Germi Branch. Dr. Alayi research is mainly focused energy systems analysis of renewable energy, especially solar energy and energy management in buildings and industry.
Email: reza.alayi@iau.ac.ir
ORCID: 0000-0003-2190-1185
Contribution Statement: Conceptualization, Project administration, Supervision.

Yaser Ebazadeh received the BS.c. in Computer Science from Tabriz University, Iran in 2004, MS.c. in Computer Engineering from Tabriz Branch, Islamic Azad University, Tabriz, Iran in 2017, and is currently pursuing the full-time Ph.D. degree in Computer Engineering of Qazvin Branch, Islamic Azad University, Qazvin, Iran. His major research interests include the resource management, task scheduling, and security of Cloud and Fog computing.
Email: Yaser.ebazadeh@iau.ac.ir
ORCID: 0000-0002-6106-6682
Contribution Statement: Data curation, Software, Validation, Visualization.

Babak Pordel Marageh holds a bachelor's degree in civil engineering from the University of Mohaghegh Ardabili, a master's degree in structural engineering from the University of Mohaghegh Ardabili, and a doctorate in structural engineering from the Islamic Azad University, Arak Branch. He is a faculty member of the Department of Civil Engineering at the Islamic Azad University, Ardabil Branch, and is an expert in the fields of retrofitting, progressive failure, and design of special concrete structures.
Email: pordel@samaard.ac.ir
ORCID: 0000-0002-7897-8944
Contribution Statement: Formal analysis, Investigation.

Mustafa Ghazi Sabri Al Sabti holds a bachelor's degree in Polymer & petrochemical engineering from the Islamic Azad university Tehran, a master's degree in Renewable energy Engineering from the Islamic Azad university Tehran, and is an expert in the fields of Renewable energy Engineering.
Email: mustafasabti95@gmail.com
ORCID: 0009-0003-3570-1421
Contribution Statement: Methodology, Resources.

Ali Morsagh Dezfuli was born in Dezful, Iran in 1992. He received the B.Sc.degree from the Jundi-Shapur University of Technology of Dezful, Dezful, Iran in 2015, the M.Sc. degree from the Shahid Rajaee Teacher Training University of Tehran, Tehran, Iran in 2017 and he is a PhD candidate at Shahid Chamran University of Ahvaz, Ahvaz, Iran all in Power Electrical Engineering. His research interests are: Voltage and Frequency Control of Microgrid, Power Electronics, FACTs Devices and Power System Protection.
Email: a.morsagh@ksc.ir
ORCID: 0009-0008-1661-5663
Contribution Statement: Roles/Writing-original draft, Writing-review & editing.

Journal of Green Energy Research and Innovation

Optimal Novel Fuzzy Control Design Method for Efficient Grid-Connected Photovoltaic System

Asaad Shemshadi, Hamidreza Haghighi

Highlights

- **A three-input fuzzy logic controller (E, CE, Vpv) is proposed for improved MPPT in grid-connected PV systems.**
- **PSO optimization enhances fuzzy membership functions, reducing oscillations and improving accuracy.**
- **The method outperforms the P&O algorithm under varying irradiance and temperature.**
- **Hysteresis current and PID control ensure stable grid synchronization and power injection.**
- **MATLAB simulations show reduced ripple and higher energy transfer efficiency.**

Graphical Abstract

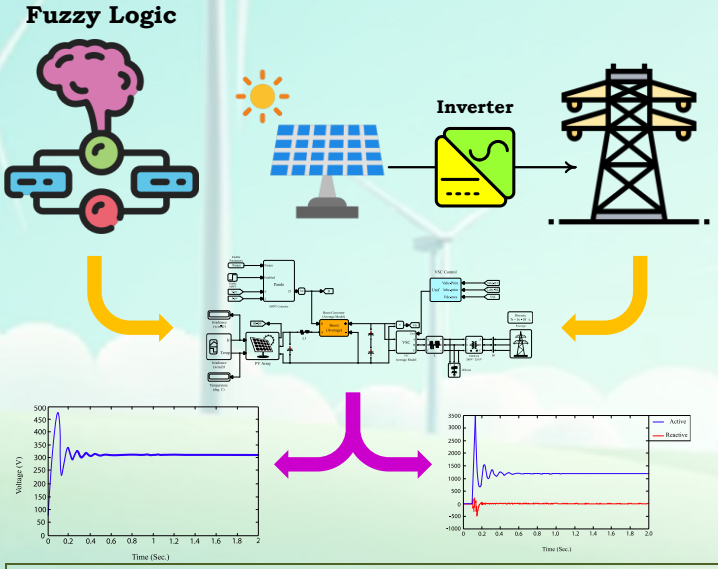

Use your device to scan and read the article online

Citation

A. Shemshadi and H. Haghighi," Optimal Novel Fuzzy Control Design Method for Efficient Grid-Connected Photovoltaic System," *Journal of Green Energy Research and Innovation*, vol. 2, no. 3, pp. 27-43, 2025.

https://doi.org/10.61882/jgeri.2.3.27

Journal of Green Energy Research and Innovation 2.3 (2025) 27-43

Online ISSN: 3041-9018

Journal of Green Energy Research and Innovation

Journal Homepage: www.jgeri.araku.ac.ir

Optimal Novel Fuzzy Control Design Method for Efficient Grid-Connected Photovoltaic System

Asaad Shemshadi * , Hamidreza Haghighi

Department of Electrical Engineering, Arak University of Technology, Arak, Iran.

A R T I C L E I N F O

Keywords:
fuzzy logic controller, power point tracking, inverter, particle swarm algorithm.

Article History:
Received: 02 March 2025;
Revised: 06 May 2025;
Accepted: 12 May 2025.

Article type:
Research Article

* ***Corresponding author***
E-mail address
shemshadi@arakut.ac.ir (A. Shemshadi)

A B S T R A C T

In this article, the modified fuzzy controller tracks the maximum power point (MPP) in a photovoltaic (PV) system connected to the grid under variable and standard solar radiation and variable temperature conditions. The perturb and observe (P&O) method has also been employed for MPP tracking (MPPT), and it has been compared with the modified fuzzy method. Ultimately, the superiority of the modified fuzzy method has been proven. In addition, the particle swarm algorithm (PSO) is employed to make the fuzzy groups optimal, thereby enhancing the performance of the fuzzy controller. In conclusion, implementing the designed phase control for the PV system connected to the single-phase grid is paramount. Furthermore, utilizing the hysteresis current control method facilitates inverter switching, thereby ensuring the injection of maximum power into the grid.

1. Introduction

The grid-connected PV system comprises a PV module, a boost converter, and a maximum power point tracking (MPPT) system, which together enable integration with the main power grid. In this method, the electrical energy generated by the PV system is integrated into the main grid through grid-connected inverters, which modify the waveform and adjust key parameters such as voltage level, phase angle, and frequency to ensure compatibility [1-4].

1.1. Research Necessity and Novelty

The growing global energy demand and environmental concerns have led to the increased integration of PV systems into modern power grids. However, variations in solar radiation and temperature cause continuous fluctuations in PV output, reducing system reliability and energy utilization. An intelligent and adaptive MPPT method is essential to maintain optimal operation and guarantee efficient grid interaction. The necessity of this study arises from the need for an improved control strategy capable of minimizing power ripple, improving transient response, and ensuring seamless grid synchronization. The key novelty of this work lies in proposing a modified fuzzy logic controller optimized using the PSO algorithm. Unlike conventional two-input fuzzy controllers, the proposed method introduces a third input (PV voltage) to enhance decision precision. PSO is used to optimally adjust the membership function parameters—centers and spreads—thereby reducing power fluctuations and improving MPPT accuracy. Moreover, the proposed controller is integrated into a grid-connected PV configuration, where hysteresis current control and a PID-based synchronization system ensure efficient power injection into the grid [5-9].

1.2. Contributions

The main contributions of this study are summarized as follows:

1. Development of an enhanced fuzzy MPPT controller with three inputs (E, CE, and V_{pv}) for improved tracking performance.
2. Optimization of fuzzy membership functions using PSO, leading to reduced oscillations and enhanced steady-state accuracy.
3. Implementation of the proposed control method in a grid-connected PV system with effective hysteresis-based current synchronization.
4. Comparative analysis demonstrating superior efficiency and stability compared to the conventional P&O algorithm under dynamic conditions.

1.3. Paper Organization

The remainder of this paper is organized as follows. Section 2 provides a general overview of solar energy and power systems, discussing the role of PV technologies in sustainable energy generation and the challenges of their integration into modern grids. Section 3 describes the modeling of MPPT in PV systems, including equivalent electrical circuit representation, operational characteristics, and the governing current–voltage relationships under variable irradiance and temperature conditions. Section 4 presents the proposed optimal fuzzy controller design for MPPT, explaining its structural framework, control mechanism, and advantages over conventional methods. Section 5 outlines the Particle Swarm Optimization (PSO) algorithm used to fine-tune the fuzzy controller's parameters, detailing its mathematical formulation, optimization strategy, and convergence process. Section 6 elaborates on the fuzzy logic controller design and optimization procedure, covering the fuzzification, rule inference, and defuzzification stages, as well as the incorporation of PSO-based parameter adjustment. Section 7 reports the MATLAB-based simulation results, providing a comparative performance analysis between the proposed optimized fuzzy control method and the conventional Perturb and Observe (P&O) algorithm for both standalone and grid-connected PV systems. Finally, Section 8 concludes the paper by summarizing the key findings, verifying the effectiveness of the proposed control strategy, and suggesting possible directions for future research.

2. Solar Energy and Power Systems

Currently, large-scale PV systems, configured as renewable power substations, are integrated into the power grid through power electronic converters, as illustrated in Figure 1.

Figure 2 illustrates that the equivalent circuit of a PV cell incorporates both series and parallel resistances. The series resistance represents the cumulative resistive effects of the semiconductor material and electrical interconnections, and its value increases with the number of cells connected in series. The parallel, or shunt, resistance models power losses due to small leakage currents through alternate conduction paths. While series resistance can significantly influence performance, the impact of parallel resistance is generally minimal. Additionally, the behavior of non-ohmic currents in the depletion region can be represented by introducing a second diode into the equivalent circuit model.

Considering all parameters, the current equation of the PV cell will be as described in Equation (1):

$$I = I_{ph} - I_o * (e^{q*(V+I*Rs)/(n*k*T)} - 1) - (V + I * R_S/R_{Sh}) \quad (1)$$

To calculate the value of R_S, we will have Equation (2):

$$R_S = -\frac{dI}{dv} - \frac{n*k*\frac{T}{q}}{Io*e^{\left(q*\frac{V+I*Rs}{n*k*T}\right)}} \quad (2)$$

The value $(\frac{dI}{dv})$ will be determined using the voltage-current characteristic of the PV module.

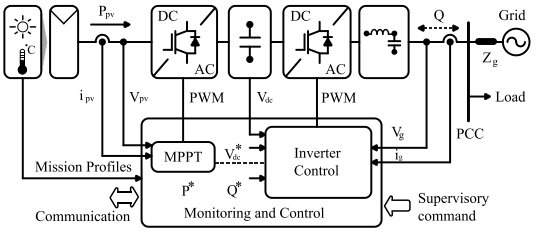

Figure 1. Overview of the PV system connected to the power grid.

3. MPPT in PV systems

Over the past decade, significant attention has been directed toward enhancing the efficiency of PV systems, with MPPT emerging as a key area of focus. MPPT techniques are designed to optimize the extraction of electrical power from PV modules by continuously adjusting the operating point to correspond with the maximum power output. Typically implemented through electronic power converters, these systems actively respond to variations in environmental factors such as solar irradiance and temperature, as well as changes in electrical load, to maintain optimal energy conversion performance.

MPPT is a key factor in improving the energy conversion efficiency of PV systems, thereby enhancing their economic viability. The current–voltage (I–V) curve of PV modules exhibit strong nonlinearity and are affected by several dynamic parameters, such as cell temperature, incident solar radiation, charge carrier lifetime, and the electrical load profile. For any given set of environmental conditions—specifically, irradiance and temperature—there exists a unique operating point on the I–V curve where the module achieves its peak power output. A plethora of methods have been introduced for MPP detection, and they can be classified into four main methodological categories based on their underlying principles [10-12].

The first category includes techniques based on basic algorithmic approaches, with P&O and Incremental Conductance (INC) being the most widely used. The P&O technique functions by slightly adjusting the terminal voltage and observing the corresponding change in output power. If power output rises, the adjustment continues in the same direction; if it falls, the direction of perturbation is reversed. One of the main strengths of this method is its independence from the specific parameters of the PV module [13,14].

However, its primary drawback is the tendency to oscillate around the MPP, especially under rapidly fluctuating environmental conditions, which may result in diminished tracking accuracy.

The second category comprises methods grounded in solar cell modeling. These techniques entail the development of a mathematical or electrical model of the solar cell and the subsequent derivation of its characteristic relationships. The model is then used to predict the behavior of the PV module, thereby serving as the basis for system design and implementation. While such approaches can offer high precision under controlled conditions, their primary limitation lies in their lack of adaptability. Specifically, these methods are customized to the characteristics of a particular solar cell, making it difficult to substitute or upgrade components without requiring a complete redesign of the system [15-18].

The third category comprises techniques that utilize the empirical relationship between the operating point and specific parameters of the PV cell. Notable examples include the short-circuit current method and the open-circuit voltage method. These approaches estimate the MPP based on proportionality assumptions, such as a fixed ratio between the MPP current and the short-circuit current, or between the MPP voltage and the open-circuit voltage. However, their accuracy is limited due to the inherent nonlinearity of the current–voltage characteristics, which undermines the validity of the linear approximations on which these methods rely. The fourth category is intelligent control designs, in which fuzzy logic control or artificial neural networks are used. The fuzzy logic control method can work with imprecise and non-linear inputs and does not require a precise mathematical model. Fuzzy control has three stages: fuzzification, determining rules based on lookup tables, and defuzzification [19,20].

In the fuzzification process, numerical input variables are turned into linguistic variables using predefined membership functions. For fuzzy controllers applied in MPPT, the typical inputs are the error (E) and the change in error (ΔE or CE). The calculation of E and CE can be defined by the system designer, offering flexibility in controller design as in Equations (3) to (4).

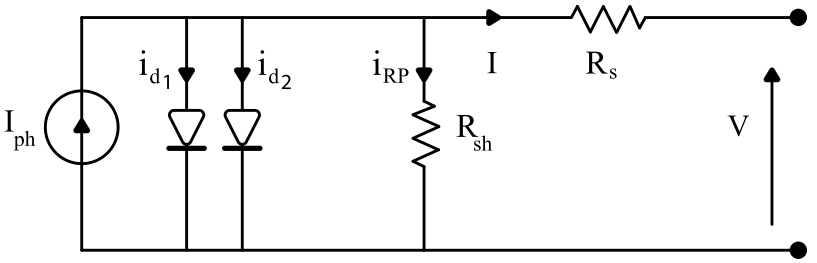

Figure 2. The exact equivalent circuit of the PV cell.

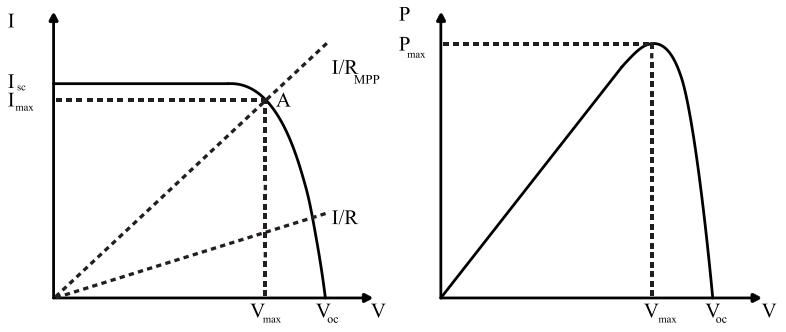

Figure 3. The point of maximum power in the nonlinear PV characteristic.

One common approach involves using the condition where the derivative of power with respect to voltage (dP/dV) approaches zero, which indicates the operating point corresponding to the maximum power.

$$E(n) = \frac{p(n)-p(n-1)}{V(n)-V(n-1)} \quad (3)$$

$$CE(n) = E(n) - E(n-1) \quad (4)$$

CE and E are calculated and converted into linguistic variables. The output of the controller is usually the change in duty cycle of the converter (ΔD) and is searched in the rules table. In the defuzzification step, the output of the fuzzy controller is converted from linguistic variables to numerical variables that are still used in the membership function.

These controllers demonstrate effective performance under varying weather conditions. Experimental results indicate that they achieve rapid convergence to the MPP while exhibiting minimal oscillations around it. The accuracy and stability of the tracking process are significantly influenced by the selection of the membership function, which plays a critical role in shaping the controller's responsiveness and precision.

Each method of finding MPPT has its advantages and disadvantages. In this article, since the goal of optimization is achieved, the maximum efficiency of the PV system, the fuzzy method is used with corrections to reach the maximum efficiency, and the simulation results It is compared with the common P&O method.

4. Optimal Fuzzy Controller Design for MPPT

The MPP of a PV module varies in response to changing environmental conditions, such as irradiance and temperature. Consequently, achieving maximum power transfer would ideally require continuous adjustment of the load, which is not feasible in practical applications. To address this limitation, an intermediate stage is introduced to ensure optimal power extraction from the PV module under constant load conditions and varying environmental inputs. This stage typically involves a DC–DC converter, which may be configured as a step-up, step-down, or bidirectional (buck–boost) converter, depending on the system design requirements. When interfacing with an AC load or the utility grid, a DC–AC inverter must be added following the DC–DC converter [21-24]. This inverter may employ pulse-width modulation (PWM) to boost efficiency and lead to low harmonic distortion, or a simpler square-wave design that offers easier control at the expense of increased harmonic content.

4.1. Boost converter

The converter's placement between the PV module and the consumer is pivotal for effective power extraction. When utilized in conjunction with appropriate control mechanisms, this configuration enables the PV module to operate at its optimal power output level. The boost converter is a device that functions to amplify the direct current (DC) voltage. It is a component of various peak power tracking methods. Given that the maximum voltage produced by the array is negligible, this converter can be utilized to augment the voltage. The ideal model of a boost converter is as follows:

The circuit's operation can be described in two distinct modes. In the first mode, initiated at time $t = t_0 = 0$, the switch is closed, causing the input voltage to be applied across the inductor. As a result, an increasing current flow through the inductor LL and the closed switch. The second mode begins at $t = D \cdot T$, where DD is the duty cycle and TT represents the switching period. At this point, the switch opens, redirecting the inductor current through the diode, capacitor, and load. During this interval, the inductor releases its stored energy to the load, causing the current to gradually decrease. In the subsequent cycle, when the switch closes again, the inductor begins a new energy storage phase. This cyclical operation enables controlled energy transfer to the load (Figure 5).

As illustrated in Figure 6, the status when the switch is closed is as follows in Equations (5) to (7):

$$I_{c1}(t) = C_1 \frac{dv_1(t)}{dt} = i(t) - i_l(t) \quad (5)$$

$$I_{c2}(t) = C_2 \frac{dv_o(t)}{dt} = -i_o(t) \quad (6)$$

$$V_1(t) = L \frac{di_l(t)}{dt} = v_i(t) \quad (7)$$

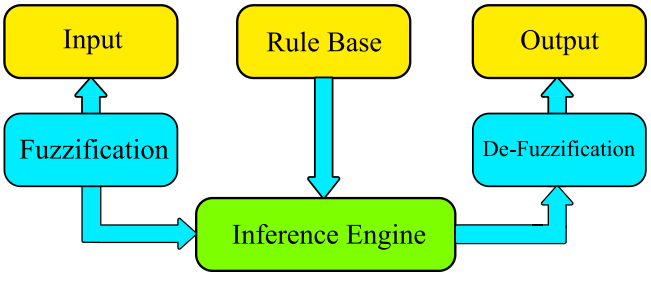

Figure 4. Fuzzy system overview.

As illustrated in Figure 7, the status when the switch is closed is as follows in Equations (8) to (10):

$$I_{c1}(t) = C_1 \frac{dv_1(t)}{dt} = i(t) - i_l(t) \tag{8}$$

$$I_{c2}(t) = C_2 \frac{dv_o(t)}{dt} = i_l(t) - i_o(t) \tag{9}$$

$$V_l(t) = L \frac{di_l(t)}{dt} = v_i(t) - v_o(t) \tag{10}$$

Therefore, it can be concluded that the inductor voltage waveform is illustrated in Figure 8. Voltage and current waveforms for the case where the load current is continuous are as mentioned in Figures 9 to 11.

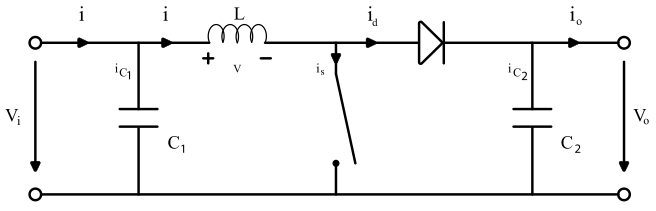

Figure 5. Equivalent circuit of ideal boost converter.

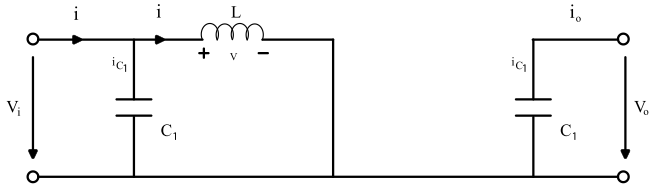

Figure 6. Boost converter in switch closed mode.

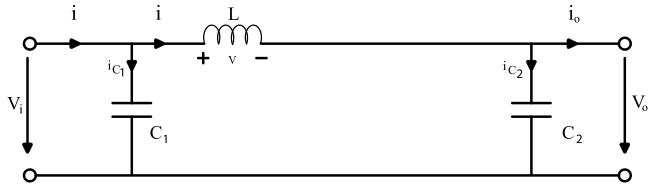

Figure 7. Boost converter in open mode.

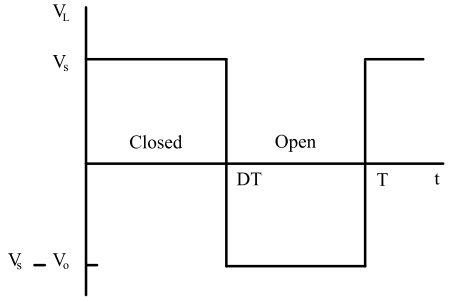

Figure 8. Inductor voltage.

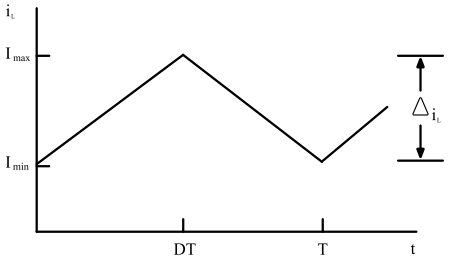

Figure 9. Inductor current.

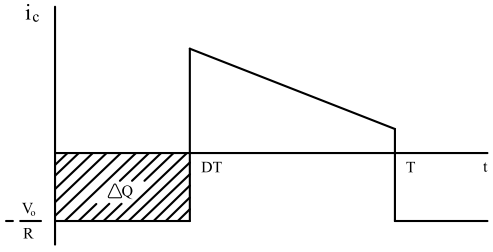

Figure 10. diode current.

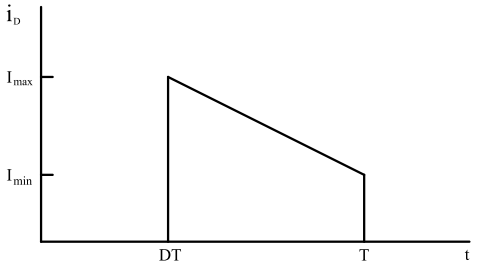

Figure 11. Capacitor current.

The following relations can be obtained for the DC-DC step-up converter (Equation (11) and Equation (12)):

$$V_O = \frac{VS}{1-D} \tag{11}$$

Boost factor:

$$\frac{Vo}{Vin} = \frac{Iin}{Io} = \frac{1}{1-D} \tag{12}$$

4.2. Boost converter design

To have a continuous current flow, the minimum inductance value would be calculated as follows in Equation (13):

$$L_{min} = \frac{(1-D)^2 DR}{2F} \tag{13}$$

In Equation (13), D is the working parameter, R is the consumer resistance in ohms, and F is the switching frequency in Hz. The output capacitor in the boost converter supplies the output current to the consumer when the diode is off. The minimum capacity of the capacitor in this converter is obtained by considering the voltage fluctuation from the Equation (14):

$$C_{min} = \frac{D \times Vo}{2RF} \tag{14}$$

In Equation (14), V_O is the output voltage of the converter.

4.3. Inverter

Solar panels inherently produce direct current, which must be converted to alternating current (AC) for grid connection or AC load applications. This conversion is accomplished using an inverter. A typical single-phase bridge inverter consists of four power electronic switches arranged to alternate the direction of current flow, thereby generating an AC output from a DC input. The type of switching devices, commonly insulated gate bipolar transistors (IGBTs) or metal-oxide-semiconductor field-effect transistors (MOSFETs), is selected based on design requirements. IGBTs are generally preferred for high-frequency switching, while MOSFETs are suitable for applications involving lower frequencies and higher power levels. Various switching control strategies are employed to regulate inverter operation, including conventional pulse width modulation (PWM), sinusoidal PWM (SPWM), and square-wave control with adjustable pulse widths. Each method presents trade-offs in terms of harmonic content, efficiency, and implementation complexity, and the choice depends on the specific performance goals of the inverter system.

The circuit model of a single-phase inverter is illustrated in Figure 12. As shown, the inverter comprises four power switches arranged in a bridge configuration, which facilitate the conversion of DC input to AC output by appropriately controlling the conduction of each switch. To protect the switches during load commutation, especially in the presence of inductive (self-reactive) loads, a freewheeling diode is connected in parallel with each switch. These diodes provide an alternative current path during switch-off intervals, preventing voltage spikes and minimizing the risk of damage to the switching devices.

The inverter has two modes of operation. In the first case, the work cycle interval D, when the switches S1 and S2 are closed, and in the second case, the complementary time 1-D, when the switches S3 and S4 are closed (Figure 13).

5. Particle Swarm Optimization

To enhance the performance of the fuzzy logic controller, the particle swam optimization (PSO) algorithm is employed to optimize the membership functions. PSO is a population-based metaheuristic inspired by the principles of collective intelligence and social behavior, particularly as observed in flocking birds or schooling fish. In this approach, each potential solution—referred to as a 'particle'—navigates the search space with an associated fitness value, which is determined based on its position relative to the objective function. Each particle retains knowledge of its personal best position (Pbest), the best position found by its neighbors (Nbest), and the best position discovered globally by the swarm (Gbest). When the neighborhood includes the entire swarm, Nbest and Gbest are identical. Particles adjust their velocities and positions by considering both their individual experiences and those of their peers. This iterative process allows the swarm to converge toward an optimal or near-optimal solution. By leveraging this algorithm, the fuzzy system can dynamically refine its rule base or membership functions, thereby improving overall tracking accuracy and controller performance. The particle mass optimization algorithm is as follows:

- N particles are created randomly.
- For all particles, speed and position are generated randomly.
- As long as the completion conditions are not met:
  - One unit is added to t.
  - Calculates the value of the objective function for each particle.
  - For i from one to n:

- Calculates $X^{i,best}[t]$
- Next value i is entered.
- Calculates $X^{g,best}[t]$.
- For i from one to n:
  - for j from one to d:

$$V_j^i[t+1] = WV_j^i[t] + c_1r_1(X_j^{i,best}[t] - X_j^i[t]) + c_2r_2(X_j^{g,best}[t] - X_j^i[t])$$
$$X_j^i[t+1] = Xji[t] + V_j^i[t+1]$$

  - Next value j is entered.
- The next value i is entered.

6. Fuzzy Logic controller design and optimization

Given the inherently variable nature of solar irradiance, the MPP of a PV module shifts dynamically along different current–voltage (I–V) curves. Therefore, the MPPT controller must respond rapidly and accurately to these changes to minimize power fluctuations and reduce energy losses. Among the various MPPT strategies, intelligent control techniques—particularly fuzzy logic-based methods—have gained prominence in recent years, often outperforming conventional approaches such as P&O and INC. Due to their heuristic nature, robustness, and effectiveness in both linear and nonlinear systems, fuzzy controllers are well-suited for real-time MPP tracking under variable environmental conditions. In a typical fuzzy MPPT system, the input variables are the PV module's voltage and current, which are processed to evaluate the control output. Based on a predefined reference model, the fuzzy controller adjusts the duty cycle of the DC–DC converter to modulate the array's output impedance. This ensures that the operating point remains aligned with the MPP despite fluctuations in irradiance and temperature.

6.1. Fuzzification

The initial step in designing a fuzzy logic controller involves defining fuzzy sets for both input and output variables. This process requires a foundational understanding of the range and behavior of each variable involved in the system. Fuzzification serves as the interface between real-world input signals and the fuzzy inference engine, translating crisp numerical values into linguistic variables represented by fuzzy sets. These sets are characterized by membership functions, which describe the degree to which an input belongs to a particular fuzzy category. Membership functions are inherently system-dependent, with their shapes varying according to the nature and range of the variables they represent. In large-scale systems, configuring appropriate membership functions becomes a challenging and complex task, as it requires balancing precision, interpretability, and computational efficiency.

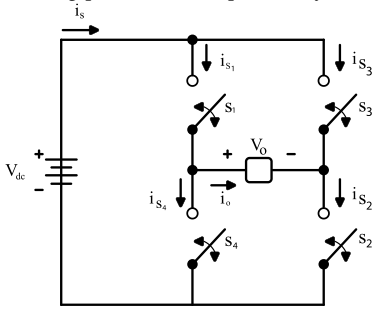

Figure 12: Equivalent circuit of a single-phase inverter.

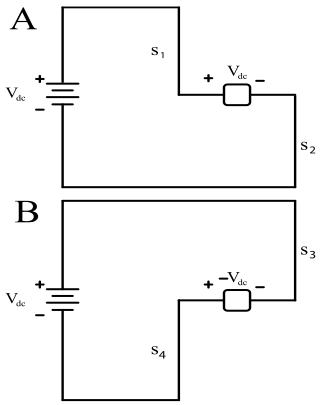

Figure 13. A: Connection state of switches S1, S2 B: Connection state of switches S3, S4.

6.2. Rules and deductions

During the inference stage of a fuzzy logic controller, a set of fuzzy rules is formulated to determine the control signal based on the input variables—typically the error and its derivative. Each fuzzy rule comprises two components: an antecedent (the 'if' part) and a consequent (the 'then' part). These rules represent expert knowledge or heuristic strategies and serve as the decision-making logic within the fuzzy inference system. By evaluating the degree to which input conditions satisfy each rule, the fuzzy controller generates an output that represents the required change in the control signal. This incremental output is then added to the previous control value at each sampling interval, effectively adjusting the system's behavior dynamically and adaptively.

6.3. Defuzzification

The output of the fuzzy controller is a fuzzy set, but a real quantity is required at the output. Therefore, the output of the fuzzy controller must be defuzzified.

The novel approach to fuzzy control involves the utilization of three inputs in lieu of two inputs, in conjunction with intelligent methods. In the phase controller, the inputs (E) are typically the power changes to the voltage changes and their changes (CE) in time t, which are expressed by the Equations (15) to (17). The output voltage of the module has also been utilized as the third input to enhance the output power of the PV module. It has been determined that the output of the phase controller is also a ΔD duty cycle.

$$E(t) = \frac{Ppv(t)-Ppv(t-1)}{Vpv(t)-Vpv(t-1)} \quad (15)$$

$$CE(t) = E(t) - E(t\text{-}1) \quad (16)$$

$$V_{pv}(t) \quad (17)$$

The structure of the fuzzy controller used to track the MPP is shown in Figure 14.

In this system, the Mamdani multiplication inference engine is used with a single fuzzifier as well as defuzzification of average centers and Gaussian membership functions, whose input and output relationship is as follows in Equation (18).

$$Y(X) = \frac{\sum_{L=1}^{M} \gamma^{L} \times [\prod_{i=1}^{n} \exp(-(\frac{Xi - Xi^{L}}{\sigma i}))]}{\sum_{L=1}^{M} [\prod_{i=1}^{n} \exp(\frac{Xi - Xi^{L}}{\sigma i}))]} \quad (18)$$

Y(X): Fuzzy system output
M: The number of fuzzy system rules
n: The number of input groups of the fuzzy system
γ^{L}: Centers of fuzzy system output groups
X_i^{L}: The centers of the input groups of the fuzzy system
σ_i: The degree of dispersion of the input groups of the fuzzy system.

In Equation (18), γ^{L}, X_i^{L}, and σ_i are factors that play a very important role in the accuracy of the fuzzy system. The more precisely these three parameters are adjusted in the fuzzy system, the better the fuzzy system performs. For this reason, we use particle swarm optimization (PSO) algorithms to adjust these three parameters.

The work process is such that the optimization algorithm determines the centers and sigmas of the fuzzy groups so that the cost function reaches its minimum value. The optimization process is done OFFLINE, and when the optimization algorithm determines the best centers and sigmas for the lowest cost function, it applies them to the fuzzy system, and after that, the fuzzy system consists of the centers and sigmas that the optimization algorithm has determined.

As illustrated in Figures 15 to 18, the fuzzy controller employs membership functions for its three input variables. The first input, typically representing the error (E), defined as the rate of change of power with respect to voltage, and the second input, its temporal derivative (CE), are each categorized into three linguistic labels: Negative (N), Zero (Z), and Positive (P). The third input, which corresponds to the module's output voltage, is also partitioned into the same three fuzzy sets (N, Z, P) to reflect its influence on the control process. The output variable of the fuzzy controller, which dictates the change in duty cycle (ΔD), is described by a broader range of linguistic terms, extending from Negative Very Large (NVL) to Positive Very Large (PVL), to capture fine variations in control action.The fuzzy rule base, as summarized in Table 1, is constructed based on the three input variables, each defined by three membership functions: N, Z, and P. Given that the fuzzy controller operates with three inputs and each input has three fuzzy sets, the total number of possible rule combinations is 33 = 2733 = 27.

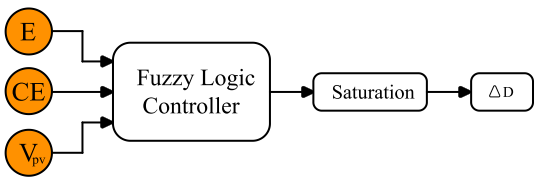

Figure 14. The adopted Fuzzy system.

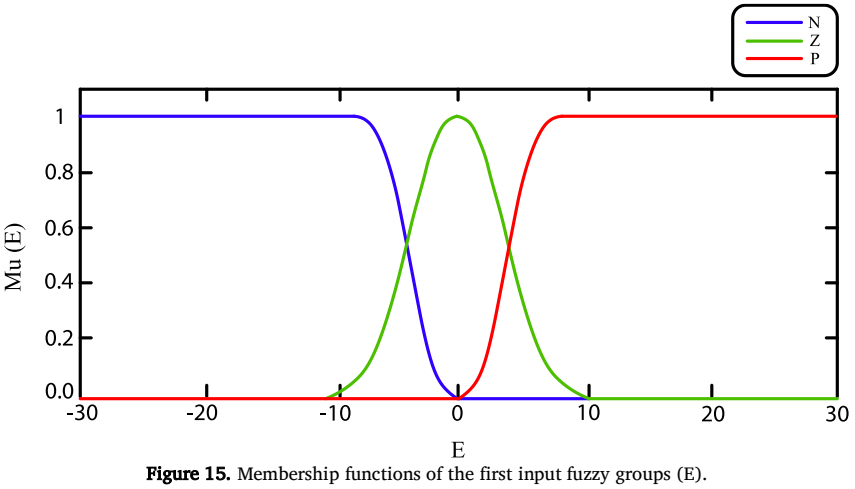

Figure 15. Membership functions of the first input fuzzy groups (E).

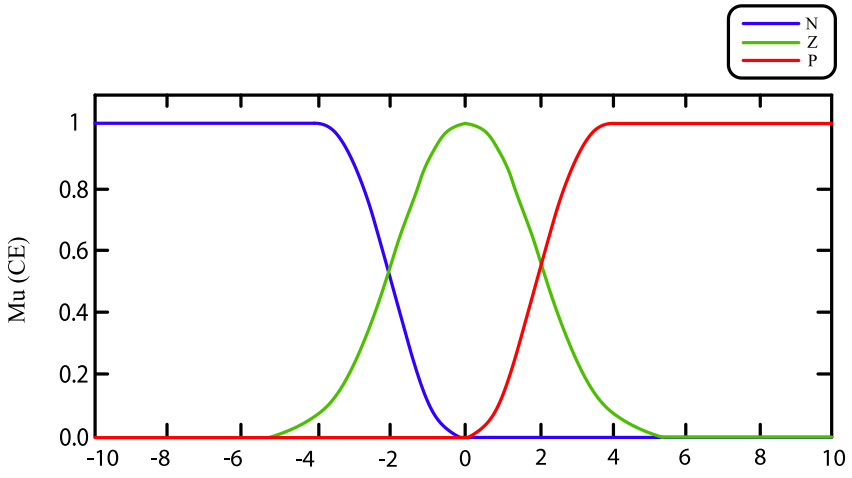

Figure 16. Membership functions of the second input fuzzy groups (CE).

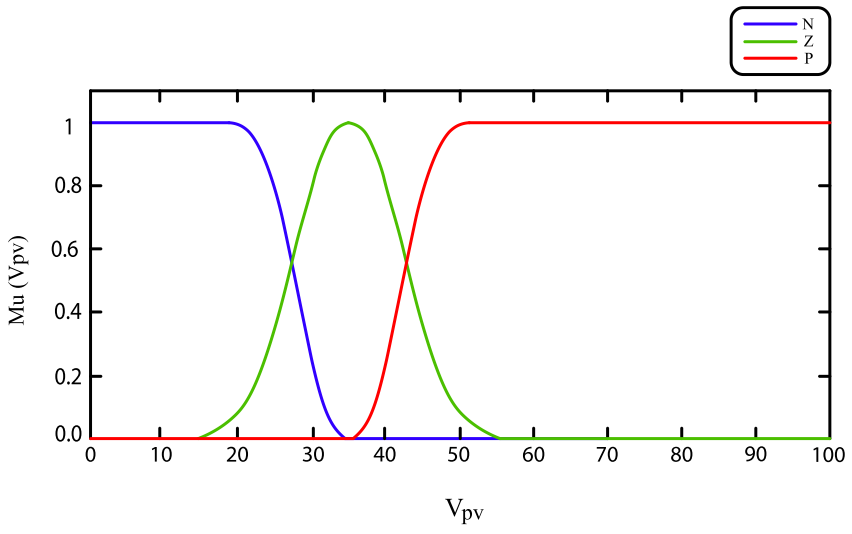

Figure 17. Membership functions of the third input fuzzy groups (Vpv).

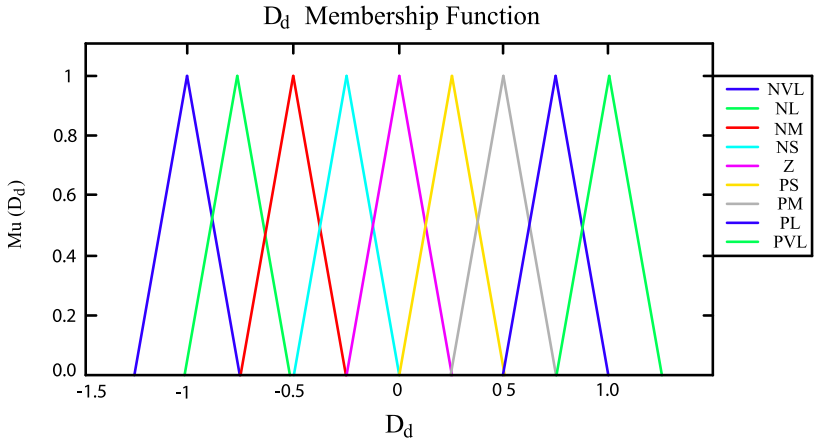

Figure 18. Membership functions of output fuzzy groups (ΔD).

Table 1. Fuzzy logic rules.

1.	Input 1	2.	Input 2	3.	Input 3	4.	Output
5.	N	6.	N	7.	N	8.	Z
9.	N	10.	N	11.	Z	12.	NS
13.	N	14.	N	15.	P	16.	NVL
17.	N	18.	Z	19.	N	20.	Z
21.	N	22.	Z	23.	Z	24.	NM
25.	N	26.	Z	27.	P	28.	NVL
29.	N	30.	P	31.	N	32.	PS
33.	N	34.	P	35.	Z	36.	Z
37.	N	38.	P	39.	P	40.	NS
41.	Z	42.	N	43.	N	44.	PS
45.	Z	46.	N	47.	Z	48.	NS
49.	Z	50.	N	51.	P	52.	NL
53.	Z	54.	Z	55.	N	56.	PM
57.	Z	58.	Z	59.	Z	60.	Z
61.	Z	62.	Z	63.	P	64.	NM
65.	Z	66.	P	67.	N	68.	PL
69.	Z	70.	P	71.	Z	72.	PS
73.	Z	74.	P	75.	P	76.	NS
77.	P	78.	N	79.	N	80.	PM
81.	P	82.	N	83.	Z	84.	Z
85.	P	86.	N	87.	P	88.	NM
89.	P	90.	Z	91.	N	92.	PM
93.	P	94.	Z	95.	Z	96.	PS
97.	P	98.	Z	99.	P	100.	Z
101.	P	102.	P	103.	N	104.	PVL
105.	P	106.	P	107.	Z	108.	PM
109.	P	110.	P	111.	P	112.	Z

These 27 fuzzy rules form the core of the decision-making mechanism, enabling the controller to generate appropriate adjustments to the duty cycle (ΔD) in response to changes in system behavior and environmental conditions.
Fuzzy controller parameters have been optimized to reduce power fluctuations around the MPP using the particle swarm algorithm. For optimization, it is necessary to choose the criterion or cost function as in Equation (19).

$$J = \frac{1}{N}\sum_{k=1}^{N}(Pref - P)^2 = 0 \quad (19)$$

npop**:** Number of particles
MAXit: Number of iterations
c_1, c_2: PSO parameters
W**:** Coefficient of inertia

The graph of the cost function will be shown in Figure 19. After optimization by PSO algorithm, membership functions of fuzzy controller are optimized as follows in Figure 20:

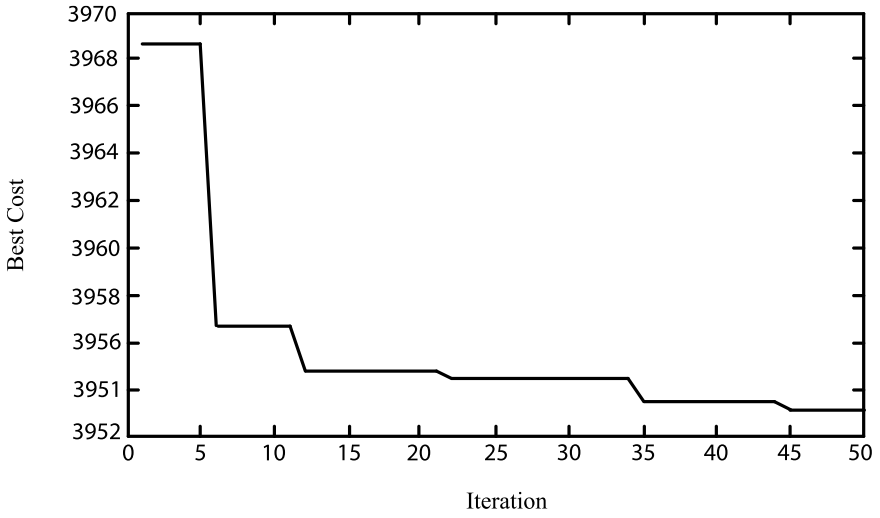

Figure 19. Cost function.

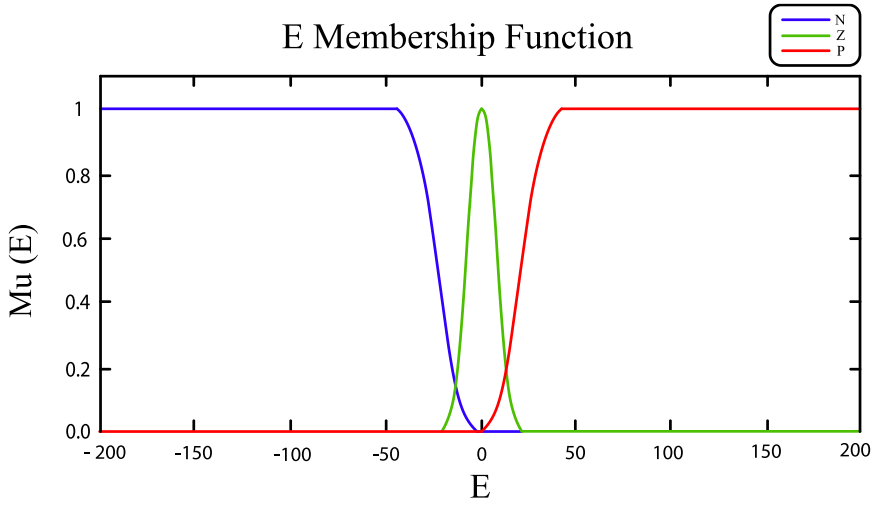

Figure 20. Membership functions of the first input fuzzy groups (E) after optimization.

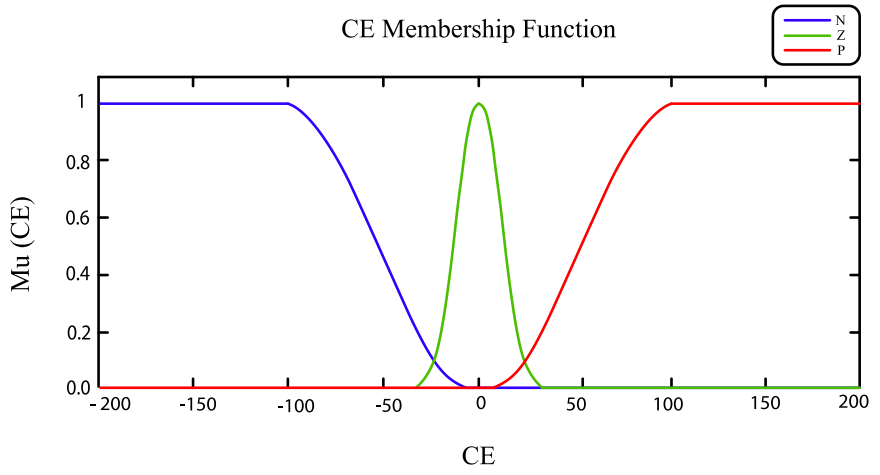

Figure 21. Membership functions of the second input fuzzy groups (CE) after optimization.

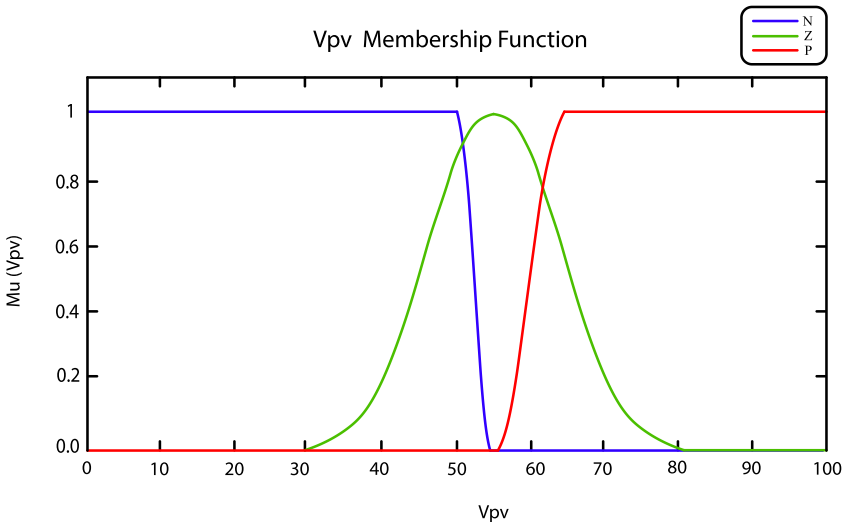

Figure 22. Membership functions of the third input fuzzy groups (Vpv) after optimization.

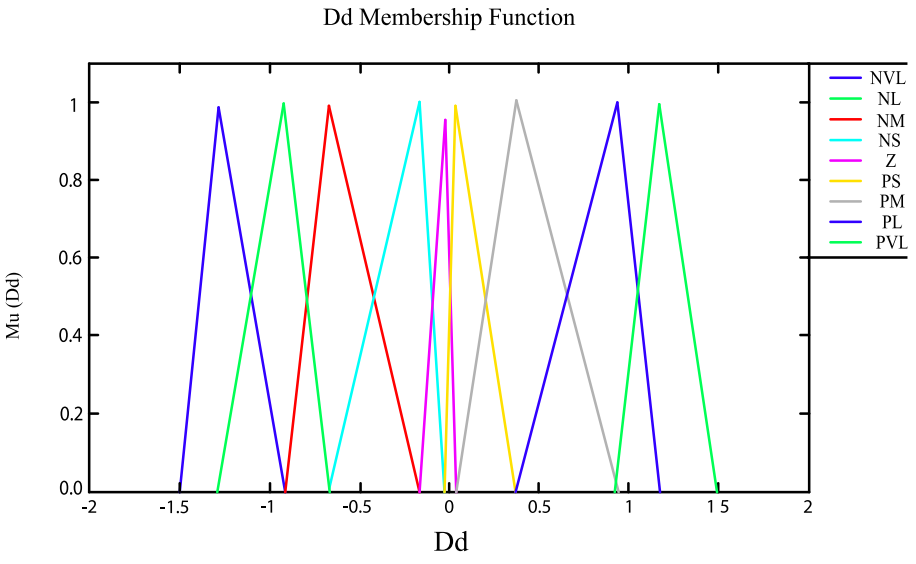

Figure 23. Membership functions of output fuzzy groups (ΔD) after optimization.

7. Simulation Results Utilizing MATLAB

"For simulation purposes in this study, the BP SX 150S PV module is selected. The simulation is implemented using MATLAB, where the PV module is modeled through a MATLAB Function Block. This block accepts two input parameters: solar irradiance (in kW/m^2) and cell operating temperature (in Celsius degrees), which is internally converted to Kelvin for accurate computation. These inputs are essential for dynamically replicating the behavior of the PV module under varying environmental conditions.

To evaluate the performance and efficiency of the proposed fuzzy logic control system, the simulation is first conducted on a standalone (grid-independent) PV system.

The MPPT algorithm is responsible for continuously tracking the optimal operating point to extract the maximum available power from the PV module. The actual regulation of PV operation at this point is achieved through a DC–DC converter, which adjusts its duty cycle based on the MPPT controller's output to ensure the module operates at or near the MPP.

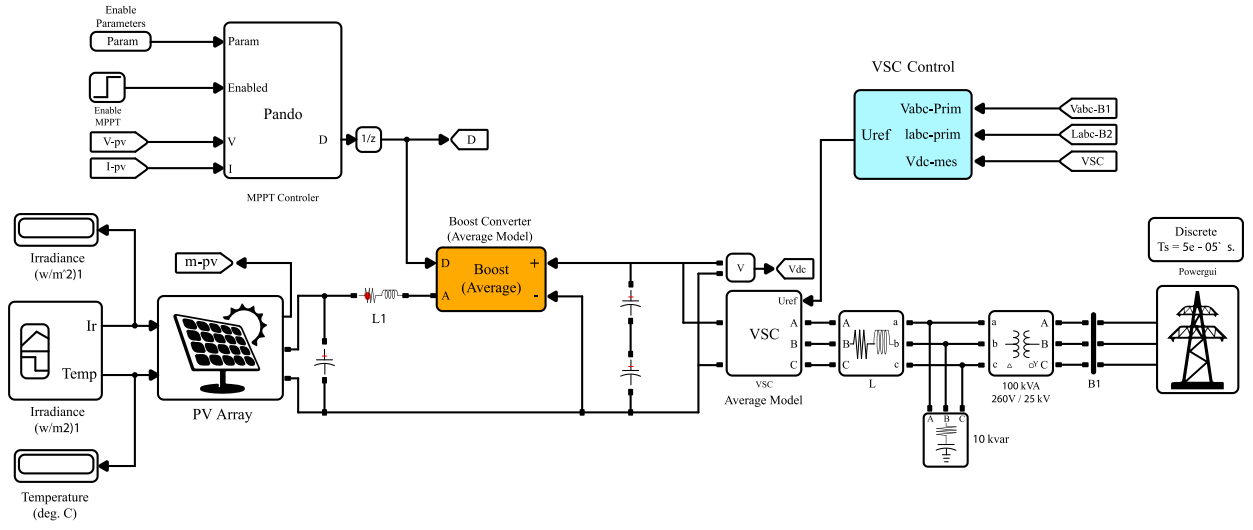

Figure 24. Grid-independent PV system.

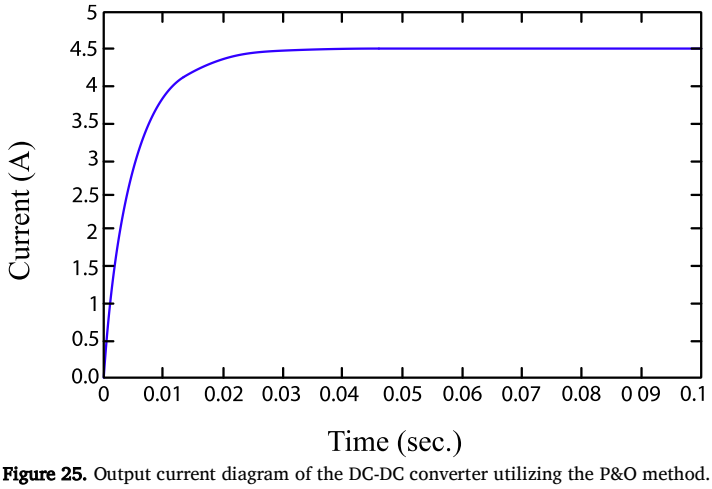

Figure 25. Output current diagram of the DC-DC converter utilizing the P&O method.

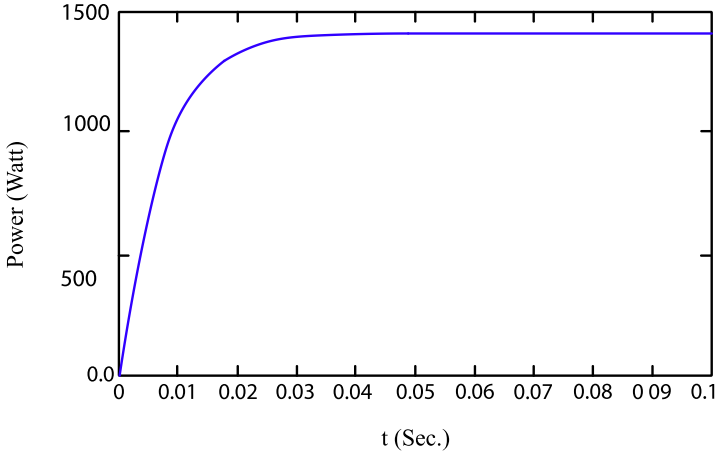

Figure 26. Output power diagram of the DC-DC converter utilizing the P&O method.

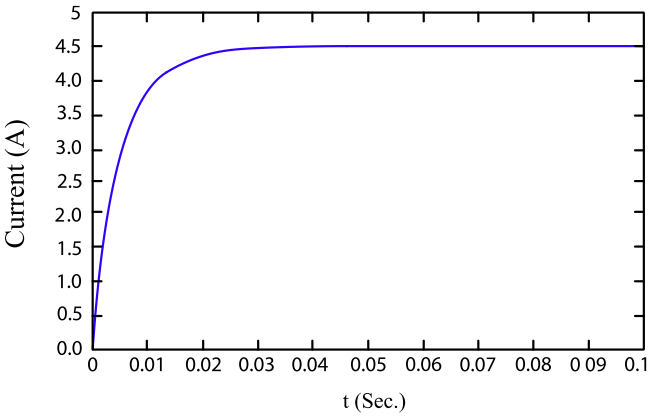

Figure 27. Output current diagram of the DC-DC converter utilizing fuzzy optimal control method.

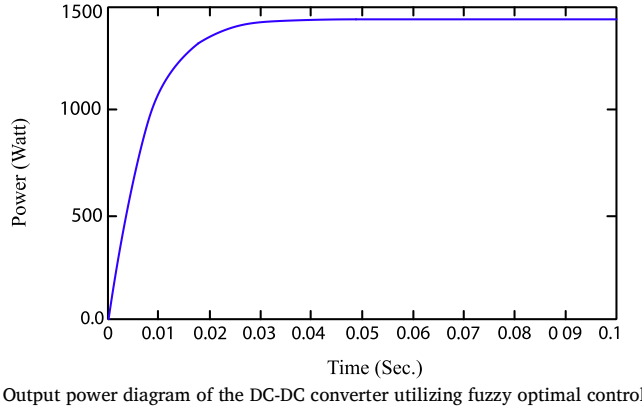

Figure 28. Output power diagram of the DC-DC converter utilizing fuzzy optimal control method.

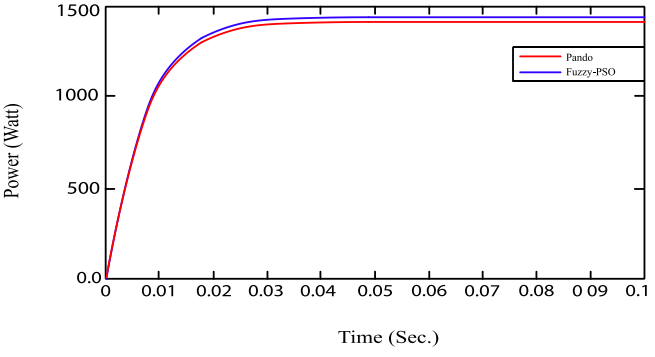

Figure 29. Comparison of tracked power by the optimal fuzzy method and the P&O method.

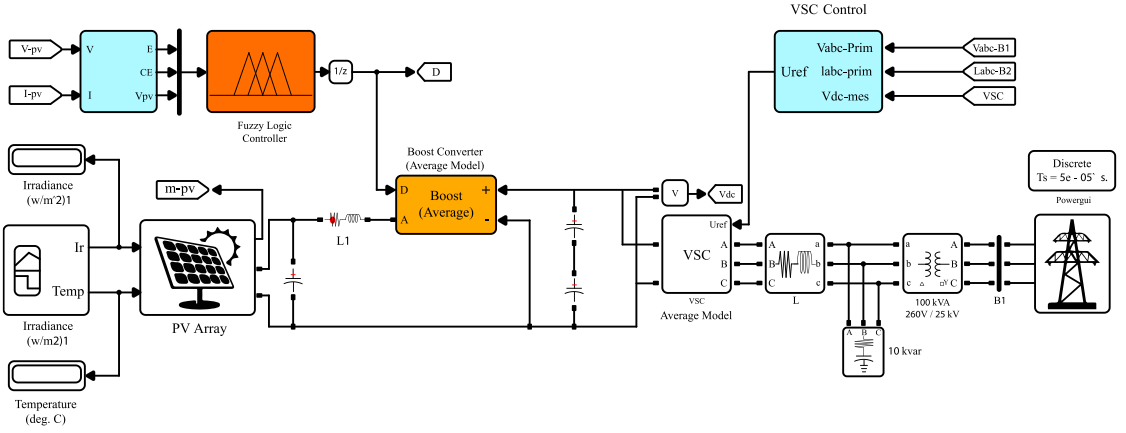

Figure 30. Grid-connected PV system with optimal fuzzy controller.

According to the results of the simulations, it is clear that the current and voltage ripple of the optimal phase control method is less than the P&O method, and also the power ripple will be less, and its better performance is proven. In the tracked power part, the optimal fuzzy control method has a higher value than the P&O method, which proves the proper performance of the proposed method.

In the following paragraphs, we simulate the designed PV system connected to the grid. First, the output power of the PV array is adjusted by the DC-DC converter, and then it is converted to alternating power by the direct power inverter. The single-phase voltage source inverter is used to connect to the low-voltage distribution network. The goal is to inject the maximum production power of the PV system into the grid. As a result, the injection current must be in phase with the network current. The network used includes a phase-locked loop (PLL) for synchronizing the power injected into the network, as well as an L-filter to reduce unwanted harmonics. A PLL is used to track the grid voltage even under severe harmonic conditions.

7.1. Network synchronization

One of the most important aspects of distributed production systems is synchronization with the network. The PV module and inverter must be able to adapt to the grid frequency and phase. The hysteresis current control method is used in this article.

7.2. Hysteresis current control method

In circumstances where the inverter is connected to the distribution network, the current control method is employed for synchronization.

At first, the network voltage is sent to the PLL to determine the frequency and phase of the network, and then, using the determined frequency and phase, we create the reference current. Then, the reference current is compared with the network current and determined by the hysteresis method and band determination. The inverter gates are switched. A PID controller is also used to control the range of the reference current. Multiply the coefficient obtained from the PID controller by the reference current so that the input voltage of the inverter does not exceed a desired value and is controlled.

7.3. PID controller

The Proportional–Integral–Derivative (PID) controller is a widely used feedback control mechanism that aims to minimize the error between a desired reference input and the system output. The effectiveness of a PID controller relies on the appropriate tuning of its three parameters: the proportional gain (Kp), the integral gain (Ki), and the derivative gain (Kd). These coefficients determine the controller's responsiveness, steady-state accuracy, and ability to predict system behavior, respectively.

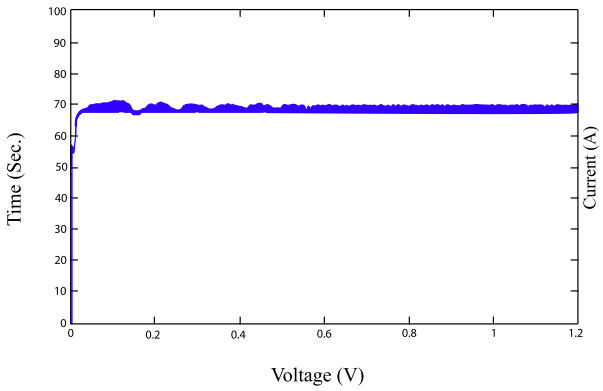

Figure 31. The output voltage of the PV module.

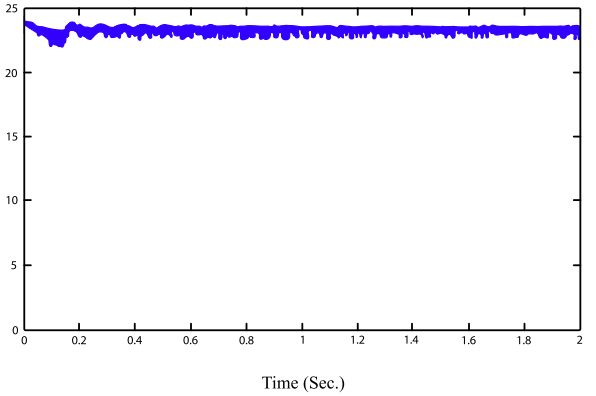

Figure 32. The output current of the PV module.

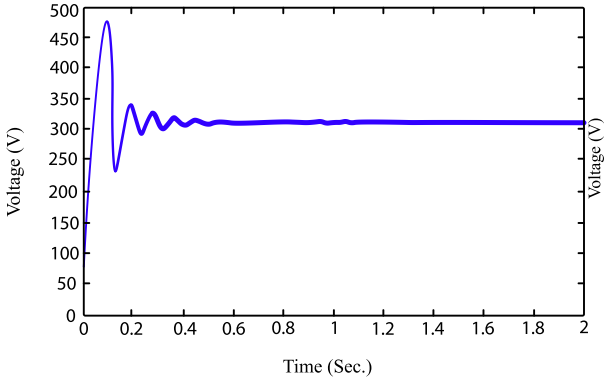

Figure 33. Boost converter output voltage.

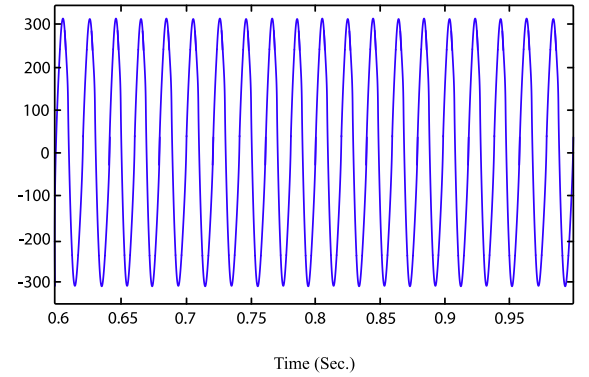

Figure 34. Network voltage.

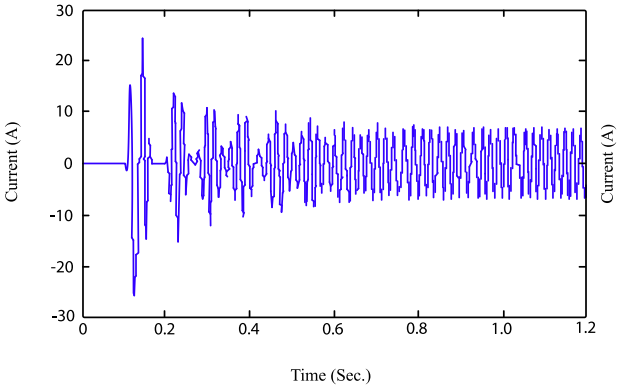

Figure 35. Reference current.

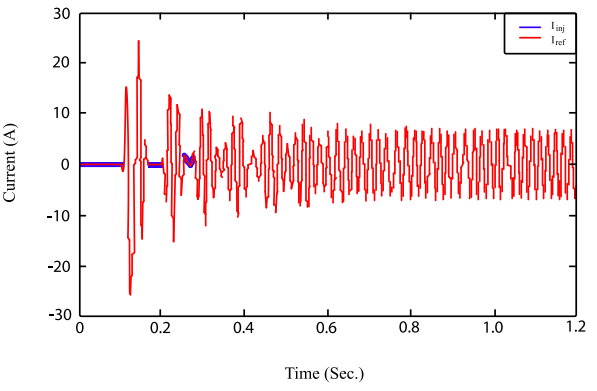

Figure 36. Reference current along with injected current to the grid.

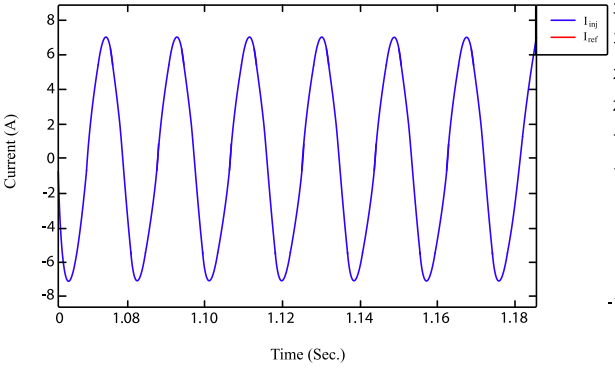

Figure 37. Reference current tracking by injecting current into the grid.

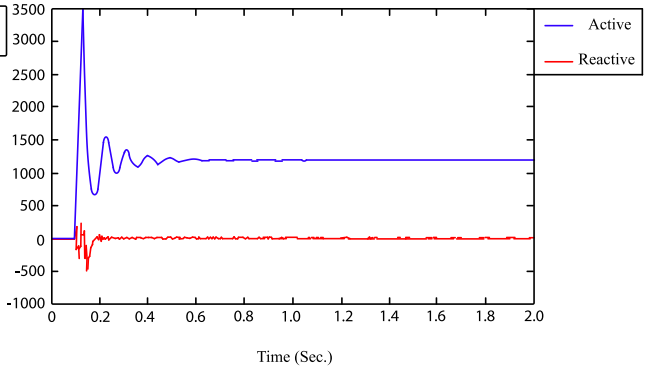

Figure 38. Active and reactive power injected into the network.

8. Conclusions

This study presented an intelligent, modified optimal fuzzy control strategy for MPPT in standalone PV systems. The objective was to minimize power fluctuations and enhance overall system efficiency. The proposed method was benchmarked against the conventional P&O technique, demonstrating superior performance in terms of tracking accuracy and stability. To further refine the controller's effectiveness, the PSO algorithm was employed to optimize the fuzzy controller's parameters, ensuring appropriate switching behavior. The optimized fuzzy controller significantly reduced ripple at the MPP and maintained stable operation under varying irradiance and temperature conditions. Additionally, the fuzzy-optimal control strategy was extended to a grid-connected PV system, successfully enabling maximum power transfer to the utility grid.

Abbreviations

K: Boltzmann's constant
I_{ph}: current generated from received photons
$I_{O.}$ Diode reverse saturation current
V: Voltage across the diode
Q: electrical charge
T: Junction temperature in Kelvin
N: Ideal diode coefficient (between 1 and 2)

References

[1] U.S. Energy Information Administration, *International Energy Outlook 2014*. Washington DC, 2014.
[2] L. D. Partian, *Solar Cells and Their Applications*. New York, NY, USA: John Wiley & Sons, 1995.
[3] M. R. Patel, and O. Beik, "Wind Power Systems," *Wind and Solar Power Systems*, pp. 37–62, 2021.
[4] International Energy Agency, *World Energy Outlook 2004*. Paris, France: IEA/OECD, 2004.
[5] M. Yaghoubi, "Studies of Environmental Compatible Buildings Using Domed Roof Architectures for Passive Cooling in Hot Arid Regions of Iran," *in Proceedings of Sustainable Energy Development in Asia Conference*, Beijing, China, Nov. 2008.
[6] M. S. Sivagamasundari, P. M. Mary, and V. K. Velvizhi, "Maximum Power Point Tracking for Photovoltaic System By Perturb And Observe Method Using Buck Boost Converter," *International Journal of Advanced Research in Electrical, Electronics and Instrumentation Engineering*, vol. 2, no. 6, pp. 2433–2439, 2013.
[7] K. Kobayashi, I. Takano, and Y. Sawada, "A Study of a Two Stage Maximum Power Point Tracking Control of a Photovoltaic System Under Partially Shaded Insolation Conditions," *Solar Energy Materials and Solar Cells*, vol. 90, no. 18-19, pp. 2975–2988, 2006.
[8] K. Irisawa, T. Saito, I. Takano, and Y. Sawada, "Maximum Power Point Tracking Control of Photovoltaic Generation System Under Non-Uniform Insolation by Means of Monitoring Cells," *Conference Record of the Twenty-Eighth IEEE Photovoltaic Specialists Conference - 2000 (Cat. No.00CH37036)*, pp. 1707–1710, n.d.
[9] T. Esram, J. Kimball, P. Krein, P. Chapman, and P. Midya, "Dynamic Maximum Power Point Tracking of Photovoltaic Arrays Using Ripple Correlation Control," *IEEE Transactions on Power Electronics*, vol. 21, no. 5, pp. 1282–1291, 2006.
[10] T. Noguchi, S. Togashi, and R. Nakamoto, "Short-Current Pulse Based Adaptive Maximum-Power-Point Tracking for Photovoltaic Power Generation System," *ISIE'2000. Proceedings of the 2000 IEEE International Symposium on Industrial Electronics (Cat. No.00TH8543)*, vol. 1, pp. 157–162.

[11] M. Masoum, H. Dehbonei, and E. Fuchs, "Theoretical and Experimental Analyses of Photovoltaic Systems with Voltage and Current-Based Maximum Power-Point Tracking," *IEEE Transactions on Energy Conversion*, vol. 17, no. 4, pp. 514–522, 2002.
[12] J. A. Jaleel, A. Nazar, and A. R. Omega, "Simulation on Maximum Power Point Tracking of the Photovoltaic Module Using LabVIEW," *International Journal of Advanced Research in Electrical, Electronics and Instrumentation Engineering*, vol. 1, no. 3, pp. 190–199, 2012.
[13] E. Jimenez-Brea, A. Salazar-Llinas, E. Ortiz-Rivera, and J. Gonzalez-Llorente, "A Maximum Power Point Tracker Implementation for Photovoltaic Cells Using Dynamic Optimal Voltage Tracking," *2010 Twenty-Fifth Annual IEEE Applied Power Electronics Conference and Exposition (APEC)*, pp. 2161–2165, 2010.
[14] C. Ben Salah, and M. Ouali, "Comparison of Fuzzy Logic and Neural Network in Maximum Power Point Tracker for PV Systems," *Electric Power Systems Research*, vol. 81, no. 1, pp. 43–50, 2011.
[15] B. N. Alajmi, K. H. Ahmed, S. J. Finney, and B. W. Williams, "Fuzzy-Logic-Control Approach of a Modified Hill-Climbing Method for Maximum Power Point in Microgrid Standalone Photovoltaic System," *IEEE Transactions on Power Electronics*, vol. 26, no. 4, pp. 1022–1030, 2011.
[16] R. Raja, L. U. Kumar, and S. R. Kumar, "Fuzzy logic controller for photovoltaic array simulator," 2013.
[17] S. Pirouzi, and A. Naderi, "Applying Sliding Mode Control Along with Particle Swarm Algorithm in Order to Optimally Control the System Wind Turbines with Variable Speed," *Journal of Green Energy Research and Innovation*, vol. 1, no. 2, pp. 64–80, 2024.
[18] BP SX051 – 051-watt multi crystalline photovoltaic module datasheet, 2001.
[19] B. Alatas, E. Akin, and A. B. Ozer, "Chaos Embedded Particle Swarm Optimization Algorithms," *Chaos, Solitons & Fractals*, vol. 40, no. 4, pp. 1715–1734, 2009.
[20] R. Poli, J. Kennedy, and T. Blackwell, "Particle Swarm Optimization," *Swarm Intelligence*, vol. 1, no. 1, pp. 33–57, 2007.
[21] M. A. Mahmud, H. R. Pota, and M. J. Hossain, "Nonlinear Current Control Scheme for a Single-Phase Grid-Connected Photovoltaic System," *IEEE Transactions on Sustainable Energy*, vol. 5, no. 1, pp. 218–227, 2014.
[22] Anonymous, "Power Electronics Converters Processing AC Voltage and Power Blocks Geometry," *ADVANCED POWER ELECTRONICS CONVERTERS*, pp. 56–87, 2014.
[23] S. E. Aminoroayaye yamani, M. Bahramian, and A. A. Ghadimi, "Improving Low Voltage Ride-Through Capability of Doubly-Fed Induction Generator Wind Farms Using Superconducting Fault Current Limiter," *Journal of Green Energy Research and Innovation*, vol. 1, no. 2, pp. 15–30, 2024.
[24] M. Mohseni, A. Niknam Kumleh, M. Alibakhshi, and M. Sheikhi Abou Masoudi, "Improving the Maximum Power Point Tracking in a Photovoltaic System Based on the Resistance-Predictive Method," *Journal of Green Energy Research and Innovation*, vol. 1, no. 2, pp. 81–102, 2024.

Declaration of competing interest

The authors declare that they have no known competing financial interests or personal relationships that could have appeared to influence the work reported in this paper. The ethical issues, including plagiarism, informed consent, misconduct, data fabrication and/or falsification, double publication and/or submission, redundancy, have been completely observed by the authors.

Bibliography

Asaad Shemshadi was born on Nov 1, 1979. He received the B.Sc. degree from the Shiraz University, in 2003, the M.Sc. degree from the Kashan University, Iran in 2007, and PhD degree from Khaje Nasir Toosi University of Technology in 2014, all in Electrical engineering. His research interests are: Vacuum Interrupters design and analysis, high voltage simulations, thermal plasma modeling, high voltage equipments design, transients in vacuum arc quenching, renewable energies and pulsed power.
Email: shemshadi@arakut.ac.ir
ORCID: 0000-0002-7271-9933
Contribution Statement: Conceptualization, Data curation, Formal analysis, , Validation, Roles/Writing - original draft, Writing-review & editing.

Hamidreza Haghighi was born on October 2, 1999 in Esfahan, Iran. He received his B.Sc and MSc. degrees from Arak University of Technology, in the field of electrical engineering. His Interests are: power systems transients, Electricity market, power system dynamics and renewable energies.
Email: k-khandani@araku.ac.ir
ORCID: 0009-0004-1737-5666
Contribution Statement: Formal analysis, Investigation, Software, Roles/Writing-original draft, Writing-review & editing.

Journal of Green Energy Research and Innovation

Stochastic Scheduling of Integrated System of Solar Resources and Hydrogen Storage in the Smart Distribution Network Considering a Multi-Objective Energy Management Model

Ehsan Akbari

Highlights

- **Energy management should be implemented in the distribution network using an integrated PV-hydrogen storage system to improve the network's technical and financial performance.**
- **Modeling the distribution network's operational, economic, and environmental indicators concurrently as a multi-objective optimization problem. This methodology proficiently encapsulates the multi-criteria goals of the DSO, furnishing an all-encompassing structure for making decisions.**
- **The incorporation of a hydrogen storage system with PVs to offset variations in PV power, improving the integrated energy system's capacity to regulate network indices by doing so.**

Graphical Abstract

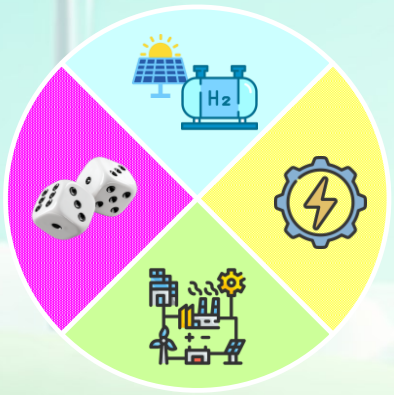

Multi-Objective Energy Management Model

Use your device to scan and read the article online

Citation

E. Akbari," Stochastic Scheduling of Integrated System of Solar Resources and Hydrogen Storage in the Smart Distribution Network Considering a Multi-Objective Energy Management Model," *Journal of Green Energy Research and Innovation*, vol. 2, no. 3, pp. 44-53, 2025.

https://doi.org/10.61882/jgeri.2.3.44

Journal of Green Energy Research and Innovation 2.3 (2025) 44-53

Online ISSN: 3041-9018

Journal of Green Energy Research and Innovation

Journal Homepage: www.jgeri.araku.ac.ir

Stochastic Scheduling of Integrated System of Solar Resources and Hydrogen Storage in the Smart Distribution Network Considering a Multi-Objective Energy Management Model

Ehsan Akbari *

Department of Electrical Engineering, Mazandaran University of Science and Technology, Babol, Iran.

A R T I C L E I N F O

Keywords:
Integrated Energy System,
Photovoltaic (PV),
Hydrogen storage,
Multi-objective Optimization,
Stochastic Optimization.

Article History:
Received: 12 March 2025;
Revised: 27 March 2025;
Accepted: 27 March 2025.

Article type:
Research Article

* ***Corresponding author***
E-mail address
e.akbari@ustmb.ac.ir (E. Akbari)

A B S T R A C T

This study proposes an integrated framework that combines photovoltaic (PV) generation with hydrogen-based storage to enhance energy management in smart distribution systems. The framework is designed to address the multi-objective concerns of distribution system operators (DSOs), focusing on minimizing operating costs, reducing energy losses, and mitigating greenhouse gas emissions. To ensure technical rigor and practical applicability, the model incorporates alternating current (AC) power flow equations along with operational constraints and system-specific performance characteristics. Recognizing the inherent uncertainties associated with load demand, renewable PV output, and fluctuating market prices, the research employs a scenario-based stochastic optimization method. This approach integrates the Kantorovich method, which efficiently manages complex multi-dimensional problems, with the Roulette Wheel Mechanism (RWM), a probabilistic selection tool that enhances solution robustness under uncertainty. Numerical simulations validate the effectiveness of the proposed method, demonstrating significant improvements compared with conventional load flow analyses. The results show reductions of approximately 14.5% in operational costs, 28.9% in energy losses, and 21% in emissions, indicating the capacity of the approach to promote sustainable and cost-efficient system operation. Beyond its quantitative achievements, the study provides meaningful insights for DSOs, offering a structured roadmap to navigate the technical, economic, and environmental challenges posed by evolving energy systems. Ultimately, the research underscores the transformative potential of PV-hydrogen integration for building resilient, efficient, and environmentally responsible distribution networks, contributing both theoretical advancements and practical guidance to the broader discourse on sustainable energy management.

1. Introduction

1.1. Motivation

The global shift towards renewable energy sources (RES) has gained significant momentum in recent years, driven primarily by escalating environmental concerns associated with the extensive reliance on fossil fuels. This transition is not merely a trend but a necessary response to the pressing challenges posed by climate change and the depletion of non-renewable resources. Among the diverse array of RES technologies, photovoltaic (PV) systems stand out as particularly appealing options. Their advantages include relatively low land requirements, ease of installation, and scalability, which make them more accessible compared to other renewable alternatives such as wind or geothermal energy [1]. However, the increasing integration of PV systems into distribution networks presents a set of operational challenges that must be addressed to ensure the stability and reliability of the electrical grid. One significant issue is the potential for overvoltage conditions, which can arise when the generation from PV systems exceeds the local demand, particularly during peak sunlight hours. Additionally, the inherent intermittency and variability of solar energy introduce uncertainties that can lead to discrepancies between day-ahead forecasts and real-time operational conditions [2].

These mismatches often result in imbalances between electricity supply and demand, which can compromise the reliability of the power system and lead to potential disruptions. To mitigate these challenges, the integration of energy storage systems with PV technology has emerged as a highly effective solution. Storage systems can absorb excess energy generated during peak production periods and release it during times of low generation or high demand, thereby compensating for the fluctuations associated with solar energy production. This capability not only enhances the reliability of the power supply but also contributes to the overall stability of the distribution network [2]. Consequently, the implementation of effective energy management strategies within distribution networks has become increasingly essential. The coordinated operation of PV-storage systems in conjunction with the distribution system operator (DSO) represents a practical pathway toward optimizing network operations. Such coordination can lead to enhanced technical reliability, reduced environmental impacts, and improved economic performance. By strategically managing the interplay between generation, storage, and consumption, DSOs can facilitate a more resilient and efficient energy distribution system that aligns with the broader goals of sustainability and energy transition. In summary, as the world continues to embrace renewable energy technologies, the challenges associated with their integration into existing infrastructure must be proactively addressed. The development and implementation of innovative energy management strategies that leverage the synergies between PV systems and storage solutions will be critical in ensuring a reliable, sustainable, and economically viable energy future.

1.2. Literature review

A substantial body of research has been dedicated to the exploration of energy management within contemporary distribution networks, with scholars examining a wide array of technical, economic, and environmental dimensions under various operational conditions. For instance, the study presented in [3] delves into the analysis of expected energy not-supplied (EENS) and the voltage stability index (VSI) within the context of dynamic reconfiguration strategies in distribution networks. This research broadens its focus to encompass both balanced and unbalanced systems, while also addressing the critical integration of RES and energy storage systems (ESSs). Such contributions are pivotal in enhancing the resilience and stability of distribution operations, particularly as the energy landscape evolves. In another significant contribution, the concept of economic flexible–securable operation (EFSO) is introduced for smart distribution networks (SDNs) in [4]. This innovative formulation integrates distributed generation and storage resources to improve the delivery of environmentally sustainable electricity. The authors frame the problem as a constrained optimization task, aiming to minimize overall operational costs while simultaneously fulfilling requirements related to optimal power flow, environmental impact mitigation, system security, and operational flexibility. This multifaceted approach underscores the importance of balancing economic viability with environmental stewardship in the management of modern energy systems. Further advancing the discourse, the research in [5] focuses on optimizing the management of electric vehicle (EV) charging systems connected to distribution networks. The proposed model, which is primarily powered by solar and wind resources, categorizes EVs into four distinct groups based on their contributions to the grid. By employing the normal distribution function, the model captures the random spatial distribution of EVs while also accounting for the stochastic variability of wind speed and solar irradiation. This approach acknowledges the inherent intermittency and lack of coordination between renewable generation sources and EV demand, offering strategies to mitigate these challenges effectively. The work presented in [6] proposes a novel energy management framework aimed at determining the optimal operation of a grid-connected microgrid. This framework explicitly considers uncertainties associated with renewable-based distributed generation units, such as wind turbines (WTs) and PV systems, thereby ensuring a more reliable and practical operational scheme. Similarly, the research in [7] investigates energy management strategies for a microgrid integrated with battery charging and swapping stations. This study highlights the dual role of such infrastructure in facilitating renewable energy integration while simultaneously addressing the growing demand for EVs. In a shift towards real-time applications, [8] emphasizes the active participation of distribution networks in energy markets. The authors explore the coordinated use of price-responsive demand, inverter-based PV generation units, and battery energy storage systems (BESSs) within an active distribution network (ADN). This approach not only strengthens the role of distributed networks in dynamic energy trading but also enhances system flexibility and resilience, thereby contributing to a more robust energy ecosystem. Complementing this, [9] introduces a control framework based on multi-agent deep reinforcement learning (MADRL). By employing an actor–critic algorithm enhanced with a shared attention mechanism, this model adeptly manages energy flows in interconnected greenhouses, thereby extending the scope of energy management research to agricultural applications. Innovative optimization techniques have also been proposed to tackle the challenges associated with energy management in distributed systems. For example, [10] presents the Golden Jackal Optimization (GJO) algorithm, a nature-inspired metaheuristic designed to optimize distributed generation systems that comprise hybrid energy sources (HESs) and battery storage systems (BSSs). Similarly, [11] proposes a multi-objective tuna swarm optimization technique for active distribution networks. This method introduces enhancements in initialization, population diversity, and objective transformation, thereby enabling more effective solutions to the multi-objective optimization problems that characterize energy management. Collectively, these contributions underscore the diversity of methodologies employed to enhance energy management in distribution networks, ranging from classical optimization models and stochastic formulations to advanced artificial intelligence and bio-inspired metaheuristics. They highlight the increasing complexity of distribution systems in the context of renewable energy integration, storage technologies, and flexible loads. Furthermore, these studies emphasize the central role of optimization and intelligent control in ensuring the sustainability, reliability, and cost-effectiveness of modern energy systems. As the energy landscape continues to evolve, ongoing research in these areas will be crucial for developing innovative solutions that address the challenges and opportunities presented by the transition to a more sustainable energy future.

1.3. Research gaps and contributions

Despite the considerable advancements made in the field of energy management within distribution networks, existing research continues to exhibit several shortcomings that hinder its comprehensiveness and practical applicability. A significant gap in the literature is the predominant emphasis on economic and operational indicators, often at the expense of a thorough examination of the interplay with technical factors. In real-world scenarios, distribution networks are characterized by a complex interaction among technical, operational, economic, and environmental indicators. Improvements in one dimension do not necessarily yield positive outcomes in others; for instance, a reduction in operational costs may inadvertently lead to overvoltage conditions, which can subsequently increase power losses and compromise the overall reliability of the system. This underscores the critical need to incorporate multiple, and frequently conflicting, indices into the energy management problem, thereby ensuring a more holistic and realistic optimization framework. Another recurring limitation in the existing literature is the insufficient consideration of the co-location of renewable energy resources and storage systems. In many studies, distributed energy resources (DERs), such as PV units and storage devices, are modeled as being geographically dispersed across various buses within the network. However, when these components are co-located and integrated into a unified system, their synergistic interactions can significantly enhance both the economic and technical performance of the network. For example, the output power of a PV system can be effectively stabilized when combined with hydrogen storage, resulting in a more reliable and flexible operational framework. This potential for synergy remains largely underexplored in current research. Moreover, the majority of previous works have predominantly employed batteries as the primary storage technology within integrated energy systems. While batteries offer notable advantages, such as high power density and efficiency, they are also constrained by limitations, including relatively short operational lifespans, high installation costs, and challenges associated with scaling capacity. In contrast, hydrogen storage presents a promising alternative due to its extended operational life, lower installation costs, and favorable efficiency characteristics. Despite these advantages, the integration of hydrogen storage with PV systems has received limited attention in the literature, leaving a significant research avenue largely unexplored. To address these identified gaps, the present study investigates the energy management of a smart distribution network that incorporates an integrated PV-hydrogen storage system. The proposed framework explicitly models the technical, economic, and environmental objectives of the DSO within a multi-objective optimization formulation. This design is constrained by the operational model of the integrated PV-hydrogen storage system, network operational limits, and the AC power flow equations, ensuring that the model adheres to practical operational realities. To effectively capture uncertainties related to load demand, energy prices, and renewable power generation, a scenario-based stochastic optimization (SBSO) approach is employed. This method allows for a more robust analysis of potential future states of the system, accommodating the inherent variability associated with renewable energy sources. Furthermore, fuzzy decision-making techniques are applied to identify compromise solutions that systematically balance conflicting objectives, thereby facilitating a more nuanced approach to energy management.

In summary, this study aims to contribute to the existing body of knowledge by providing a comprehensive framework that addresses the multifaceted challenges of energy management in distribution networks. By integrating an innovative PV-hydrogen storage system and employing advanced optimization techniques, the research seeks to enhance the operational efficiency, reliability, and sustainability of modern energy systems, ultimately paving the way for more resilient and adaptable distribution networks in the face of evolving energy demands.

The novel contributions of this research are summarized as follows:

- Implementation of integrated PV–hydrogen storage systems for energy management in distribution networks, thereby improving both the technical reliability and the financial performance of the network.
- Concurrent modeling of operational, economic, and environmental indicators within a unified multi-objective optimization problem, providing the DSO with a comprehensive decision-making framework.
- Integration of hydrogen storage with PV systems to mitigate PV output variability and enhance the network's ability to regulate key operational indices.

The remainder of this paper is organized as follows: Section 2 presents the detailed modeling of the proposed strategy as a multi-objective optimization problem. Section 3 introduces the stochastic optimization framework for modeling uncertainties. Section 4 analyzes the numerical results obtained from several case studies, and Section 5 concludes the paper with a discussion of the findings and their implications.

2. Formulation

This section delineates the proposed framework for energy management within a distribution network that incorporates an integrated PV and hydrogen storage system. The strategy is meticulously designed to simultaneously address the operational, economic, and environmental objectives of the DSO, thereby offering a balanced and comprehensive approach to energy management. The formulation of this framework is subject to several technical constraints, which are critical for ensuring the integrity and reliability of the system. Among these constraints, the AC power flow equations play a pivotal role in governing the dynamics of the distribution network. These equations are essential for accurately modeling the flow of electrical power through the network, taking into account the voltage levels, phase angles, and power losses that occur during transmission. Additionally, the operational characteristics of the integrated PV-hydrogen storage system are incorporated into the model, ensuring that the unique performance attributes of these technologies are adequately represented. By imposing these constraints, the optimization framework is designed to remain both technically feasible and practically applicable in real-world scenarios. This ensures that the solutions generated by the model are not only theoretically sound but also implementable within the existing infrastructure of the distribution

network. The mathematical formulation of the proposed model is presented as follows in Equation (1-19):

$$\min F = v_1 Cost + v_2 EL + v_3 EM \tag{1}$$

Subject to:

$$Cost = \sum_{t,w} \pi_w p_{t,w} P^{DS}_{b=r,t,w} \tag{2}$$

$$EL = \sum_{b,t,w} \pi_w (P^{DS}_{b,t,w} + P^{I}_{b,t,w} - P^{C}_{b,t,w}) \tag{3}$$

$$EM = \sum_{t,w} \pi_w (CO2 + SO2 + NOX) P^{DS}_{b=r,t,w} \tag{4}$$

$$P^{DS}_{b,t,w} + P^{I}_{b,t,w} + \sum_{i} A_{b,j} P^{L}_{b,j,t,w} = P^{C}_{b,t,w} \quad \forall b,t,w \tag{5}$$

$$Q^{DS}_{b,t,w} + \sum_{i} A_{b,j} Q^{L}_{b,j,t,w} = Q^{C}_{b,t,w} \quad \forall b,t,w \tag{6}$$

$$P^{L}_{b,j,t,w} = G^{L}_{b,j}(V_{b,t,w})^2 - V_{b,t,w}V_{j,t,w}\{G^{L}_{b,j}\cos(\varphi_{b,t,w} - \varphi_{j,t,w}) + B^{L}_{b,j}\sin(\varphi_{b,t,w} - \varphi_{j,t,w})\} \quad \forall b,j,t,w \tag{7}$$

$$Q^{L}_{b,j,t,w} = -B^{L}_{b,j}(V_{b,t,w})^2 + V_{b,t,w}V_{j,t,w}\{B^{L}_{b,j}\cos(\varphi_{b,t,w} - \varphi_{j,t,w}) - G^{L}_{b,j}\sin(\varphi_{b,t,w} - \varphi_{j,t,w})\} \quad \forall b,j,t,w \tag{8}$$

$$\varphi_{b,t,w} = 0 \quad \forall b = r,t,w \tag{9}$$

$$V_{b,t,w} = 1 \quad \forall b = r,t,w \tag{10}$$

$$V^{min}_{b} \le V_{b,t,w} V^{max}_{b} \quad \forall b,t,w \tag{11}$$

$$\sqrt{(P^{L}_{b,j,t,w})^2 + (Q^{L}_{b,j,t,w})^2} \le S^{L,max}_{b,j} \quad \forall b,j,t,w \tag{12}$$

$$\sqrt{(P^{DS}_{b,t,w})^2 + (Q^{DS}_{b,t,w})^2} \le S^{DS,max}_{b} \quad \forall b = r,t,w \tag{13}$$

$$P^{I}_{b,t,w} = P^{PV}_{b,t,w} + (P^{DCH}_{b,t,w} - P^{CH}_{b,t,w}) \tag{14}$$

$$P^{PV}_{b,t,w} = \mu_{t,w} P^{PV,max}_{b} \quad \forall b,t,w \tag{15}$$

$$0 \le P^{DCH}_{b,t,w} \le DR_b x_{b,t} \quad \forall b,t,w \tag{16}$$

$$0 \le P^{CH}_{b,t,w} \le CR_b(1 - x_{b,t}) \quad \forall b,t,w \tag{17}$$

$$E_{b,t,w} = E_b(0) + \sum_{h=1}^{t} (\eta^{CH} P^{CH}_{b,h,w} - \frac{1}{\eta^{DCH}} P^{DCH}_{b,h,w}) \quad \forall b,t,w \tag{18}$$

$$E^{min}_{b} \le E_{b,t,w} \le E^{max}_{b} \tag{19}$$

The objective of the proposed framework is to minimize a weighted sum of three key performance measures in the distribution network: total operational cost, energy losses, and environmental emissions. This goal is expressed in Equation (1). The projected cost of the distribution network (Cost) is defined in Equation (2) [1]. Anticipated energy losses (EL), defined as the difference between energy consumed and energy produced, are formulated in Equation (3). Equation (4) models network emissions (EM), which result from the upstream energy supply. Specifically, emissions from SO_2, NO_x, and CO_2 are considered in this work [12].

The weighted combination of these three performance measures constitutes the overall objective function (F). The associated weight coefficients are denoted by v_1, v_2, and v_3. By varying these coefficients, different trade-offs between Cost, EL, and EM can be achieved, thereby generating multiple Pareto-optimal solutions. The resulting Pareto front of the proposed scheme is obtained by plotting these functions in three-dimensional space [13].

To determine the optimal compromise solution, a fuzzy decision-making approach is applied. First, the minimum and maximum values of each function are determined by setting $v_1 = 1$, $v_2 = 1$, and $v_3 = 1$ in turn. A linear membership function (f_l) is then defined. For a given set of weight coefficients, $f_l = 0$ if the function value exceeds Fmax, and $f_l = 1$ if the function value is less than F_{min}. Otherwise, f_l is calculated as $(f - F^{max})/(F^{min} - F^{max})$, where f is the actual function value. This procedure is repeated for the Cost, EL, and EM functions. The minimum f_l among them is selected, and the corresponding weight coefficients are adjusted. For each Pareto front solution, the value of σ and the associated f_l are calculated. Ultimately, the compromise solution is defined as the Pareto front point with the maximum σ value [13].

The optimization problem under consideration is further constrained by a series of technical and operational limitations that are critical for ensuring the feasibility and reliability of the system. Specifically, Equations (5) to (10) delineate the AC power flow equations pertinent to the distribution network. These equations encompass essential parameters such as the angles and magnitudes of bus voltages, as well as the active and reactive power flows traversing the distribution lines [1,3]. The integrity of the power distribution system is contingent upon adhering to these equations, which are fundamental to the analysis of power systems.

In addition to the power flow equations, Equations (11) to (13) encapsulate various operational restrictions that must be observed. These include the bounds on bus voltage magnitudes, as articulated in Equation (11), which ensures that voltage levels remain within acceptable limits to prevent equipment damage and maintain system stability. Furthermore, Equation (12) imposes limits on the apparent power flow across distribution lines, thereby safeguarding against overloading and ensuring efficient operation. Lastly, Equation (13) addresses the capacity constraints of the substation, which is pivotal for maintaining the overall reliability of the distribution network. It is noteworthy that the network is assumed to comprise a singular distribution substation that is interconnected with the upstream grid at the reference bus. Consequently, for the purposes of analysis, the bus index *b* is set equal

to the reference bus r in Equations (2), (4), and (13), thereby simplifying the representation of the network.

The operational constraints governing the integrated PV and hydrogen storage system are articulated through Equations (14) to (19). Equation (14) serves to regulate the net electricity exchanged between the distribution network and the PV-hydrogen storage system, thereby facilitating a balanced energy exchange that is essential for system stability. In Equation (15), the generation of electricity from the PV system is quantified as the product of the installed PV capacity and the PV power rate [2]. This relationship is crucial for accurately modeling the contribution of solar energy to the overall energy mix.

The operational dynamics of the hydrogen storage system are further constrained by Equations (16) to (19) [14]. Specifically, Equations (16) to (17) delineate the power limits for both charging and discharging processes, respectively, while simultaneously ensuring that these two processes cannot occur concurrently. To facilitate this operational logic, a binary decision variable x is introduced, where $x=0$ signifies that the system is in charging mode, and $x=1$ indicates that it is in discharging mode. This binary variable is instrumental in modeling the operational state of the hydrogen storage system.

Equation (18) provides a mathematical representation of the state of charge of the hydrogen storage system, which is updated based on the initial energy stored, the net energy charged, and the energy discharged. This dynamic modeling is essential for accurately tracking the energy balance within the storage system. Finally, Equation (19) stipulates the maximum storage capacity, thereby ensuring that the system operates within its physical limits and maintains operational integrity. Collectively, these constraints form a comprehensive framework that governs the optimization problem, ensuring that both technical and operational requirements are met in the design and operation of the integrated PV-hydrogen storage system.

3. Modeling Uncertainties

In the proposed framework, several parameters in Equations (1) to (19), including load demand (P^C and Q^C), energy price (p), and PV power production rate (μ), are subject to uncertainty. To ensure a reliable solution capable of addressing the prediction errors associated with these uncertain variables, this study employs a SBSO approach. The adopted SBSO method integrates the Kantorovich technique with the RWM [15].

In this procedure, a large number of scenarios are first generated using the RWM. For each scenario, the probability of the selected values for the load and energy price is determined using a normal probability distribution, while the PV production rate is modeled with a beta probability distribution. Consequently, the probability of each generated scenario, denoted as π^0, is obtained as the product of the individual probabilities of the uncertainties.

To reduce the computational burden, the Kantorovich approach is applied as a scenario-reduction technique. This method identifies and retains a representative subset of scenarios that are most similar to one another, thereby maintaining the essential probabilistic characteristics of the original set while improving computational efficiency. The optimization problem defined in Equations (1) to (19) is then solved using this reduced scenario set.

Finally, the probability of each selected scenario is recalculated as the ratio of its corresponding π^0 value to the sum of π^0 values across all retained scenarios. This ensures that the reduced scenario set preserves the probabilistic integrity of the original uncertainty model [15].

4. Numerical Results

4.1. Data

The proposed methodology is validated using the IEEE 33-bus distribution network [16], illustrated in Figure 1. The system operates with a base voltage of 12.66 kV and a base apparent power of 1 MVA. The distribution substation, located at Bus 1 (the reference bus), connects the distribution network to the upstream transmission system. The permissible voltage range at all buses is restricted between 0.90 and 1.05 p.u. Peak active and reactive load values for each bus, as well as distribution line and substation parameters, are adopted from [16].

The actual hourly load demand is obtained by multiplying the peak load values by the daily load factor curve, as shown in Figure 2 [1]. The energy price structure of the system is time-dependent and follows a three-tier tariff scheme [1]:

- 01:00–07:00: $16/MWh
- 17:00–22:00: $30/MWh
- All other hours: $24/MWh

Additionally, emissions associated with electricity purchased from the upstream network are considered. The emission coefficients of the major pollutants are as follows [12]:

- CO_2: 764.3 ton/MWh
- SO_2: 2.4 ton/MWh
- NO_x: 0.7 ton/MWh

This test system provides a realistic basis for evaluating the operational, environmental, and economic impacts of the proposed PV–hydrogen storage integration and energy management framework.

This network has six integrated PV-hydrogen storage systems, as shown in Figure 1, where the locations of various energy systems are given. Every system consists of 0.6 MW worth of PVs. Figure 2 [1] shows the predicted power generation rate curve of the PV. Note that, 2 MWh hydrogen storage with beginning and minimum energy levels set at 0.2 MWh is also included with each system. The hydrogen storage is anticipated to have a 0.6 MW charge and discharge rate, with a 93% charge and discharge efficiency [14].

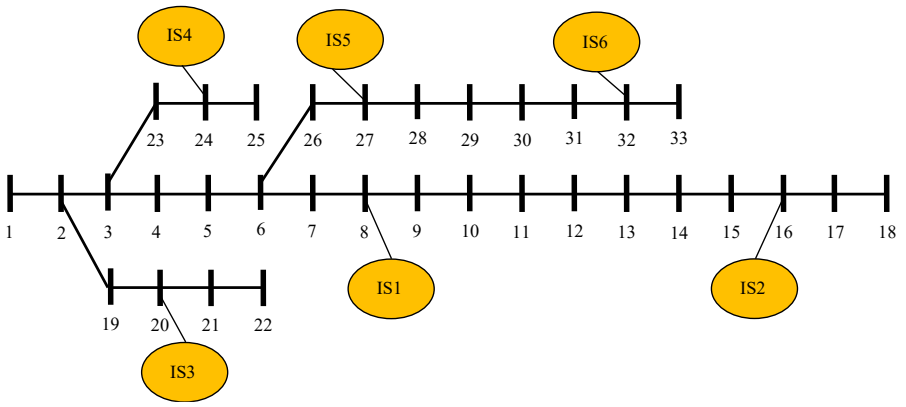

Figure 1. IEEE 33-bus distribution network [16] along with integrated PV-hydrogen storage units.

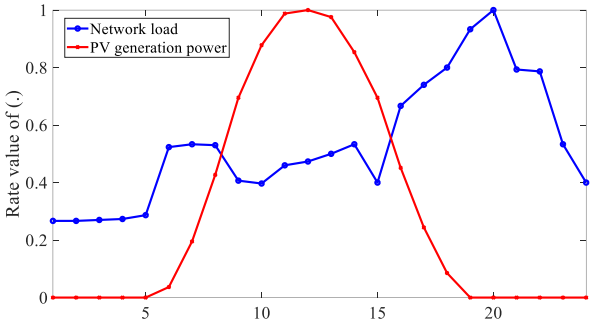

Figure 2. Expected daily curve of load factor and PV power generation rate [1].

4.2. Results and discussion

This part uses the GAMS optimization software environment to encode the problem given by Equations (1) to (19), which correspond to the data provided in section 4.1. A Mixed Integer Non-Linear Programming (MINLP) issue is how this one is classified. To solve it, the BONMIN algorithm [17] is used.

A) *Evaluation of Multi-Objective Energy Management in the Distribution Network*: The Pareto front of the proposed strategy at a 100% load level is summarized in Table 1. As observed, the trends of the objective functions—Cost, Energy Loss (EL), and Emissions (EM)—do not follow the same pattern. Specifically, cost minimization is often associated with an increase in EL. This is primarily because achieving lower costs requires the combined PV–hydrogen storage system to inject a considerable amount of active power into the network. Consequently, reverse power flow toward the distribution substation may occur, leading to higher current magnitudes and, therefore, greater energy losses.

According to Table 1, the minimum achievable values of Cost, EL, and EM are $894.2, 1.12 MWh, and 21.3 tons, respectively. Conversely, their maximum values are $3612.1, 2.61 MWh, and 38.4 tons, respectively. Hence, the ranges of variation are $2717.9 for Cost, 1.49 MWh for EL, and 17.1 tons for EM. Employing fuzzy decision-making methodologies, the optimal compromise solution across a spectrum of load levels is systematically detailed in Table 2. At the 100% load level, the identified compromise point yields specific values of $1289.3 for Cost, 1.55 MWh for EL, and 24.9 tons for EM. These metrics are critical as they reflect the trade-offs inherent in the optimization process, where multiple objectives must be balanced to arrive at a satisfactory solution. A thorough comparative analysis between Tables 1 and 2 reveals significant insights regarding the performance of the compromise solution relative to the optimal points. Specifically, the deviation of the compromise solution from the minimum point is quantified as 14.5% for Cost, 21% for EL, and 28.9% for EM. These percentages indicate that while the compromise solution is not the absolute optimal solution, it is strategically positioned in close proximity to the optimal values. This proximity suggests that the selected compromise effectively balances the competing objectives of minimizing costs, reducing energy losses, and lowering emissions, thereby reflecting a well-considered trade-off among these critical factors. Moreover, the results encapsulated in Table 2 provide compelling evidence that all three functions—Cost, EL, and EM—exhibit a discernible increasing trend as load levels rise. This trend can be attributed to the intensified utilization of the distribution network, which inherently amplifies both technical and environmental impacts under conditions of heightened demand. As the load increases, the distribution network experiences greater stress, leading to increased energy losses due to resistance in the lines and higher emissions resulting from the additional energy generation required to meet the demand. The implications of these findings are significant for stakeholders involved in energy management and policy-making. They underscore the necessity of considering the interplay between load levels and the associated impacts on cost, energy loss, and

emissions. In particular, the results highlight the importance of developing strategies that not only aim for cost efficiency but also prioritize sustainability and environmental stewardship. In conclusion, the application of fuzzy decision-making in this context not only facilitates the identification of a compromise solution that is close to optimal but also emphasizes the critical need for a holistic approach to energy management. By acknowledging the trade-offs among cost, energy loss, and emissions, decision-makers can better navigate the complexities of energy distribution and contribute to a more sustainable energy future.

B) *Performance of integrated PV- hydrogen storage systems:* The operational behavior of the integrated PV–hydrogen storage system across different load levels is illustrated in Figure 3, which presents the predicted daily active power curves of the PV units and hydrogen storage. As shown in Figure 3(a), the daily PV power generation profile closely follows the general trend depicted in Figure 2, reflecting the typical solar irradiance pattern. In this context, the PV units are able to operate at their full rated capacity during peak sunshine hours, which corresponds to the constraints defined in Equation (15). The complementary operation of hydrogen storage is highlighted in Figure 3(b). During the early hours of the day, specifically from 01:00 to 16:00, the hydrogen storage units predominantly remain in charging mode, with the highest charging demand occurring between 01:00 and 07:00. This period coincides with the lowest electricity prices, making it economically advantageous for the storage system to absorb power and minimize overall costs. Conversely, during the evening peak hours from 17:00 to 22:00, when energy prices reach their maximum, the hydrogen storage units transition into discharge mode. In this phase, they inject a significant amount of power into the network, thereby reducing both operating costs and emissions. Furthermore, from 08:00 to 16:00, the hydrogen storage is also occasionally switched to discharge mode in response to high PV generation levels. This strategy helps mitigate the risk of overvoltage that may arise from the injection of surplus PV power into the grid. The aggregated active power profile of the combined PV–hydrogen storage system for different load conditions is presented in Figure 4. According to Equation (14), this profile is calculated as the summation of PV generation and hydrogen storage discharge power, minus the hydrogen storage charging power. The results reveal that during the low-price period (01:00 to 07:00), the system predominantly behaves as a consumer, as the hydrogen storage absorbs power while PV generation remains minimal. For the remaining hours of the day, the system operates as a net producer, supplying power through both PV generation and storage discharge. In mathematical terms, the aggregated active power profile can be expressed as $P_{total} = P_{PV} + P_{discharge} - P_{charge}$, where, P_{total} is the total active power, P_{PV} is the power generated by the PV units, $P_{discharge}$ is the power discharged from the hydrogen storage, P_{charge} is the power absorbed by the hydrogen storage.

This equation encapsulates the dynamic interaction between the PV generation and hydrogen storage, highlighting the system's ability to adapt to varying load conditions and electricity prices. An important observation is that the PV daily generation curve remains unchanged across different load levels, as it is solely dependent on solar irradiance and independent of network demand. By contrast, the operation of the hydrogen storage system is highly responsive to load variations. As the load level increases, both charging and discharging capacities of the hydrogen storage expand, thereby amplifying the system's contribution in both consumption and generation modes. Consequently, the integrated PV–hydrogen storage system demonstrates enhanced flexibility and adaptability, offering improved support to the distribution network under varying load conditions.

Table 1. Pareto front of the suggested plan for a load level of 100%.

v_1	v_2	v_3	Cost ($)	EL (MWh)	EM (ton)
1	0	0	894.2	2.61	33.4
0	1	0	3612.1	1.12	38.4
0	0	1	2932.4	2.48	21.3
0.75	0.25	0	1145.6	2.18	35.3
0.75	0	0.25	1008.5	2.49	28.8
0.25	0.75	0	2198.1	1.97	36.7
0	0.75	0.25	3252.5	1.86	34.2
0.25	0	0.75	3025.2	2.41	25.3
0	0.25	0.75	2989.1	2.81	26.4
0.5	0.5	0	1431.2	2.05	35.8
0.5	0	0.5	1344.1	2.51	26.8
0	0.5	0.5	3068.9	2.03	26.5
0.33	0.33	0.33	1678.2	2.31	27.1

Table 2. Optimal compromise solution between the Cost, Energy Loss (EL), and Emissions (EM) functions under different load levels.

Load level (%)	Cost ($)	EL (MWh)	EM (ton)
100	1289.3	1.55	24.9
110	1307.1	1.71	27.0
120	1418.6	1.85	29.1

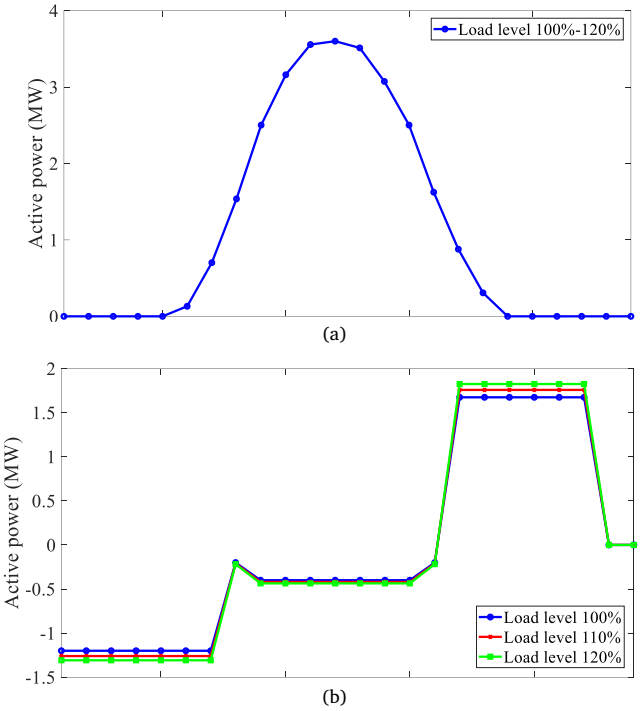

Figure 3. Predicted daily curves of the integrated PV–hydrogen storage system at different load levels: (a) PV power generation profile, showing consistency with the irradiance-based trend; (b) hydrogen storage charging and discharging patterns, highlighting load-dependent operation and price-responsive scheduling.

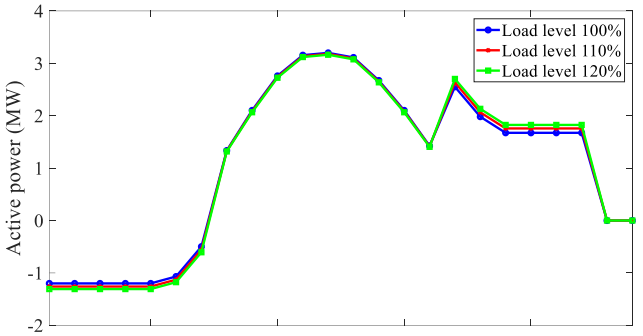

Figure 4. Predicted daily active power profile of the combined PV–hydrogen storage system under various load levels, computed as the net power (PV generation plus hydrogen discharge minus hydrogen charge), indicating the transition from consumer behavior during low-price hours (01:00–07:00) to net producer behavior during the remaining hours.

C) *Evaluation of the technical, economic, and environmental status of the distribution network*: The economic (Cost), environmental (EM), operational (EL), maximum voltage drop (MVD), and maximum overvoltage (MOV) indicators for the 100% load level are summarized in Table 3 across three case studies: Case I (base network without PV or storage), Case II (PV-only integration), and Case III (integrated PV–hydrogen storage system). As shown in the table, Case I yields the highest values of Cost, EM, EL, and MVD, since all energy is supplied by the upstream network. Introducing PVs into the distribution network (Case II) reduces all indicators compared to Case I, except for MOV, which increases due to voltage rise effects. In Case III, the integrated PV–hydrogen storage system achieves the most significant reductions in Cost, EL, EM, and MOV relative to Case I, demonstrating its effectiveness in improving system performance. Additionally, peak load carrying capacity (PLCC)—an operational index representing the maximum load the network can support under the daily load factor curve of Figure 2—remains unchanged between Cases I and II, as PVs are inactive during the peak load hour (20:00). However, in Case III, PLCC is notably higher due to hydrogen storage's substantial power injection during peak hours (17:00–22:00).

Table 3. Comparison of economic (Cost), environmental (EM), operational (EL), maximum voltage drop (MVD), maximum overvoltage (MOV), and peak load carrying capacity (PLCC) indicators across three scenarios (Case I: base network, Case II: PV-only integration, Case III: integrated PV–hydrogen storage system) at 100% load level.

Index	Parameter	Case I	Case II	Case III
Economic	Cost ($)	3971.2	1404.3	1289.3
Environment	EM (ton)	48.9	25.8	24.9
Operation	EL (MWh)	3.12	1.67	1.55
	MVD (p.u.)	0.087	0.051	0.048
	MOV (p.u.)	0	0.024	0.011
	PLCC (MW)	3.715	3.715	4.59

5. Conclusion

This study investigated the energy management of a distribution network with a focus on the operational, economic, and environmental objectives of the DSO in the context of integrated PV–hydrogen storage systems. The proposed framework, constrained by optimal power flow equations and the operational model of the network, aimed to minimize a weighted sum of operating costs, energy losses, and emissions. To address uncertainties in load demand, PV generation, and electricity prices, a stochastic optimization approach was employed, and fuzzy decision-making was applied to identify the best compromise solution. The numerical results demonstrated that this compromise point maintains the values of operating cost, energy losses, and emissions within 14.5%, 28.9%, and 21% of their respective minimum values, ensuring a near-optimal balance across objectives. Comparative analysis revealed that integrating PV systems alone can reduce maximum voltage drop, emissions, costs, and energy losses; however, this improvement is offset by a substantial increase in overvoltage. By contrast, the incorporation of hydrogen storage alongside PV generation not only alleviates the overvoltage issue but also provides the most significant enhancements across operational, environmental, and economic indicators. Demand-side management (DSM) is one of the promising energy management strategies that can enhance both the technical and economic performance of distribution networks. Incorporating DSM into the proposed framework is therefore suggested as a direction for future research. In addition, EVs are emerging as significant new consumers whose charging behavior directly influences network operation. Effective management of EV demand can provide valuable operational flexibility and improve network performance. Consequently, integrating EVs into the proposed scheme is also identified as an important avenue for future work.

Nomenclature

Indices

b, t, w, r	Bus, Operating Hour, Scenario, Reference Bus
j	Auxiliary Index Corresponding to the Bus

Variables

$Cost, EL, EM$	Expected Network Operation Cost ($), Expected Network Energy Losses (MWh), Network Pollution Level (ton)
E	Energy Stored in hydrogen tank (MWh)
F	Objective Function
$P^{DS}, P^{L}, P^{I}, P^{PV}, P^{CH}, P^{DCH}$	Active Power Passing Through Distribution Substation and Distribution Line, Active Power of Integrated PV-Hydrogen Storage System, PV Active Power, Active Power of Hydrogen Storage in Charge and Discharge Modes (MW)
Q^{DS}, Q^{L}	Reactive Power Passing Through the Distribution Substation and Distribution Line (MVAr)
V, φ	Voltage Amplitude (p.u.) and Voltage Angle (rad)
x	Binary Variable Corresponding to Hydrogen Storage Charge/Discharge Operation

Parameters

A, G^{L}, B^{L}	Cross Matrix of Bus, Distribution Line Conductance (p.u.), Distribution Line Susceptance (p.u.)
$CO2, SO2, NOX$	Pollution Coefficients (ton/MWh)
CR, DR	Charge and Discharge Rate of Hydrogen Storage (MW)
$E(0), E^{min}, E^{max}$	Primary Energy, Minimum and Maximum Energy Stored in Hydrogen Storage (MWh)
p	Energy Price ($/MWh)
P^{C}, Q^{C}	Active Power (MW) and Reactive Power (MVAr) of the Load
$P^{PV,max}$	PV Capacity (MW)
$S^{L,max}, S^{DS,max}$	Maximum Apparent Power of Distribution Line and Distribution Substation (MVA)
v_1, v_2, v_3	Weight Coefficients in the Objective Function
V^{min}, V^{max}	Minimum and Maximum Voltage Magnitude (p.u.)
π, μ	Scenario Probability, PV Power Generation Rate
η^{CH}, η^{DCH}	Charge and Discharge Efficiency

References

[1] J. Nikoukar, S. Mohammadi, et al., "Optimal Operation and Management of Energy Resources in Microgrids in the Presence of Renewable Resources and Energy Storage by Modified Grey Wolf Optimization Algorithm," *Journal of Green Energy Research and Innovation*, vol. 2, no. 1, pp. 1–13, 2025.

[2] F. Khalafian, N. Iliaee, et al., "Capabilities of Compressed Air Energy Storage in the Economic Design of Renewable Off-Grid System to Supply Electricity and Heat Costumers and Smart Charging-Based Electric Vehicles," *Journal of Energy Storage*, vol. 78, 109888, 2024.

[3] A. Azizivahed, A. Arefi, et al., "Energy Management Strategy in Dynamic Distribution Network Reconfiguration Considering Renewable Energy Resources and Storage," *IEEE Transactions on Sustainable Energy*, vol. 11, no. 2, pp. 662–673, 2020.

[4] Z. Yan, Z. Gao, R. B. Navesi, M. Jadidoleslam, and A. Pirouzi, "Smart Distribution Network Operation Based on Energy Management System Considering Economic-Technical Goals of Network Operator," *Energy Reports*, vol. 9, pp. 4466–4477, 2023.

[5] Z. Yang, F. Yang, et al., "RETRACTED: Energy Management Programming to Reduce Distribution Network Operating Costs in the Presence of Electric Vehicles and Renewable Energy Sources," *Energy*, vol. 263, 125695, 2023.

[6] A. Ali Dashtaki, S. Mehdi Hakimi, A. Hasankhani, G. Derakhshani, and B. Abdi, "Optimal Management Algorithm of Microgrid Connected to the Distribution Network Considering Renewable Energy System Uncertainties," *International Journal of Electrical Power & Energy Systems*, vol. 145, 108633, 2023.

[7] M. Ahmadi Jirdehi, and V. Sohrabi Tabar, "Risk-Aware Energy Management of a Microgrid Integrated with Battery Charging and Swapping Stations in the Presence of Renewable Resources High Penetration, Crypto-Currency Miners and Responsive Loads," *Energy*, vol. 263, 125719, 2023.

[8] M. Azarnia, M. Rahimiyan, and P. Siano, "Offering of Active Distribution Network in Real-Time Energy Market by Integrated Energy Management System and Volt-Var Optimization," *Applied Energy*, vol. 358, 122635, 2024.

[9] A. Ajagekar, B. Decardi-Nelson, and F. You, "Energy Management for Demand Response in Networked Greenhouses with Multi-Agent Deep Reinforcement Learning," *Applied Energy*, vol. 355, 122349, 2024.

[10] R. P. Kumar, and G. Karthikeyan, "A Multi-Objective Optimization Solution for Distributed Generation Energy Management in Microgrids with Hybrid Energy Sources and Battery Storage System," *Journal of Energy Storage*, vol. 75, 109702, 2024.

[11] L. Li, B. Ji, M. K. Lim, and M. Tseng, "Active Distribution Network Operational Optimization Problem: A Multi-Objective Tuna Swarm Optimization Model," *Applied Soft Computing*, vol. 150, 111087, 2024.

[12] M. A. Ashraf, Z. Liu, et al., "Designing an Optimized Configuration for a Hybrid PV/Diesel/Battery Energy System Based on Metaheuristics: A Case Study on Gobi Desert," *Journal of Cleaner Production*, vol. 270, 122467, 2020.

[13] S. M. Mohseni-Bonab, A. Rabiee, and B. Mohammadi-Ivatloo, "Voltage Stability Constrained Multi-Objective Optimal Reactive Power Dispatch Under Load and Wind Power Uncertainties: A Stochastic Approach," *Renewable Energy*, vol. 85, pp. 598–609, 2016.

[14] M. Norouzi, J. Aghaei, S. Pirouzi, T. Niknam, and M. Fotuhi-Firuzabad, "Flexibility Pricing of Integrated Unit of Electric Spring and EVs Parking in Microgrids," *Energy*, vol. 239, 122080, 2022.

[15] J. Aghaei, M. Barani, M. Shafie-khah, A. A. Sanchez de la Nieta, and J. P. S. Catalao, "Risk-Constrained Offering Strategy for Aggregated Hybrid Power Plant Including Wind Power Producer and Demand Response Provider," *IEEE Transactions on Sustainable Energy*, vol. 7, no. 2, pp. 513–525, 2016.

[16] P. R. Babu, C. P. Rakesh, M. N. Kumar, G. Srikanth, and D. P. Reddy, "A Novel Approach for Solving Distribution Networks," *2009 Annual IEEE India Conference*, pp. 1–5, 2009.

[17] Generalized Algebraic Modeling Systems (GAMS). http://www.gams.com.

Declaration of competing interest

The author declares that there are no known competing financial interests or personal relationships that could have appeared to influence the work reported in this paper. All ethical standards, including avoidance of plagiarism, informed consent, research misconduct, data fabrication or falsification, duplicate publication or submission, and redundancy, have been fully observed by the author.

Bibliography

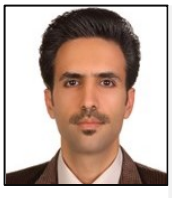

Ehsan Akbari was born in 1987 in Borujerd, Iran. He received his Diploma and Pre-university degrees from Shahid Beheshti High School in Borujerd in 2004 and 2005, respectively all in Mathematics and Physics fields. received the B.Sc. degree in Electrical Power Engineering from Mazandaran University, Babolsar, Iran, in 2009 and M.S. degree in Electrical Power Engineering from Mazandaran University of Science and Technology, Babol, Iran, in 2014. He received Ph.D. in Electrical Power Engineering from Isfahan University of Technology, Isfahan, Iran in 2022. He is now an Assistant Professor at Department of Electrical Engineering, Mazandaran University of Science and Technology, Babol, Iran. He is the author of 20 books and more than 295 papers in reputed journals and conferences and won six patents in his research fields. He has obtained five provincial scientific and technological progress awards. His main areas of research are power quality, flexible AC transmission systems (FACTS), application of power electronics in power systems, power electronics multilevel converters, smart grids, control of grid-connected converters, micro-grids, harmonics, reactive power control using hybrid filters and renewable energy systems. He has served as an organizer and a program committee member for many conferences.

Email: e.akbari@ustmb.ac.ir

ORCID: 0000-0002-5318-5673

Contribution Statement: Conceptualization, Data curation, Formal analysis, Funding acquisition, Investigation, Methodology, Project administration, Resources, Software, Supervision, Validation, Visualization, Roles/Writing - original draft, Writing-review & editing.

Journal of Green Energy Research and Innovation

Enhancing Power Quality in Distribution Networks Through the Optimal Allocation and Sizing of Capacitor Banks and Distributed Generation Sources, Utilizing A New Evolutionary Algorithm

Leila Mohammadian

Highlights

- **A new algorithm is proposed for simultaneous power quality improvement and optimal allocation/sizing of DGs and capacitor banks in radial distribution networks.**
- **The optimization goal is to minimize power losses and improve voltage profiles through proper DG and capacitor placement.**
- **Constraints include voltage limits, DG and capacitor sizes, and candidate bus locations.**
- **The method uses Biogeography-Based Optimization (BBO), which models solutions as islands exchanging features via immigration and emigration.**
- **Tested on the IEEE 33-bus radial distribution network, results were compared and validated against other references.**

Graphical Abstract

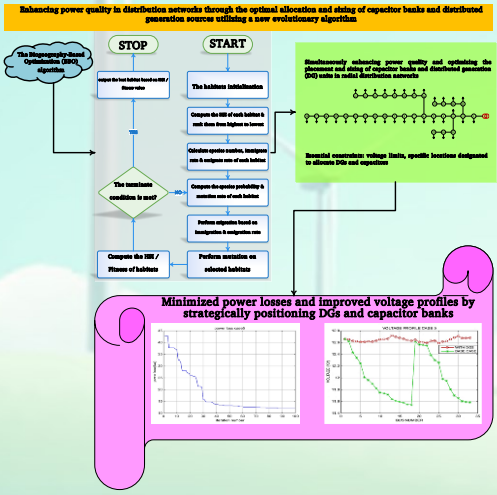

Use your device to scan and read the article online

Citation

L. Mohammadian," Enhancing Power Quality in Distribution Networks Through the Optimal Allocation and Sizing of Capacitor Banks and Distributed Generation Sources, Utilizing A New Evolutionary Algorithm," *Journal of Green Energy Research and Innovation*, vol. 2, no. 3, pp. 54-71, 2025.

https://doi.org/10.61882/jgeri.2.3.54

Journal of Green Energy Research and Innovation 2.3 (2025) 54-71

Online ISSN: 3041-9018

Journal of Green Energy Research and Innovation

Journal Homepage: www.jgeri.araku.ac.ir

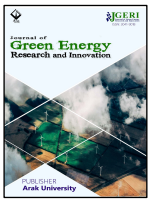

Enhancing Power Quality in Distribution Networks Through the Optimal Allocation and Sizing of Capacitor Banks and Distributed Generation Sources, Utilizing A New Evolutionary Algorithm

Leila Mohammadian *

Department of Electrical Engineering, Shabestar Branch, Islamic Azad University, Shabestar, Iran.

A R T I C L E I N F O

Keywords:
Biogeography-based optimization,
Capacitor Banks,
Distributed Generation,
Power Quality.

Article History:
Received: 22 February 2025;
Revised: 06 April 2025;
Accepted: 09 April 2025.

Article type:
Research Article

* ***Corresponding author***
E-mail address
lemohammadian@iau.ir (L. Mohammadian)

A B S T R A C T

This study presents a comprehensive framework for enhancing power quality in radial distribution networks by simultaneously optimizing the placement and size of capacitor banks and distributed generation (DG) units. Employing the biogeography-based optimization (BBO) algorithm, this research addresses key objectives, including minimizing power losses and improving voltage profiles. The methodology incorporates critical operational constraints, such as voltage limits and permissible installation locations for DG units and capacitors. The proposed approach is validated using the IEEE 33-bus radial distribution system, where numerical results demonstrate a reduction in power losses by 88.28% with the simultaneous placement of DGs and capacitors (Mode 4), compared to the base case. Voltage profiles improved significantly, with the lowest voltage rising from 0.9117 pu in the base mode to 0.9835 pu. Additionally, Mode 5, involving variable power factors, achieved a 94.4% reduction in losses, further enhancing system efficiency. These results highlight the BBO algorithm's superior performance and computational efficiency in addressing complex distribution system challenges. This study is particularly relevant for optimizing renewable energy integration and future power system resilience.

1. Introduction

Recent advancements in the integration of distributed generation (DG) and capacitor placement have provided crucial insights into power distribution network optimization. In [1] explored the optimal placement of capacitors in distribution networks impacted by harmonic pollution, especially in the presence of wind energy-based DG sources. Their study emphasizes the importance of harmonics control in maintaining power quality and highlights the challenges posed by renewable energy integration into distribution systems. The findings provide a basis for designing harmonic-resilient networks with efficient capacitor placement strategies. In [2], reactive power optimization for DG units using stochastic modeling techniques is investigated to minimize power system losses. This work underscores the role of advanced mathematical approaches in addressing uncertainty in DG operations. By focusing on the probabilistic behavior of DG units, this study enhances system reliability and reduces energy losses, making it particularly relevant for modern power networks integrating renewable sources. [3] proposed a robust control strategy using nonlinear methods for maintaining load voltage stability in islanded wind energy conversion systems. Their research illustrates how effective control mechanisms can ensure stability under varying operational conditions. The study is significant for its focus on isolated systems, a critical area in renewable energy deployment, and highlights the challenges in managing voltage fluctuations caused by intermittent wind energy sources.

Electric power distribution networks typically operate at low voltage levels. These networks are connected to high-voltage transmission systems, which transport electricity over long distances before delivering it to consumers at a low voltage suitable for everyday use. However, distribution networks experience significant power losses due to the combination of low voltage and high current, particularly in comparison to transmission networks. This situation increases power costs and results in a bad voltage profile along the feeder [4,21]. The power losses in distribution networks are divided into two categories: active power loss and reactive power loss. Among these, active power loss is critical as it reduces transmission power efficiency and adversely affects the voltage profile. Consequently, minimizing active power losses in distribution networks is of greater importance than in transmission networks. Addressing this issue is predominantly the responsibility of the electrical distribution system [5]. Current statistics indicate that approximately 13% of generated power is lost at the distribution level. Because of the capacity limitations of radial lines, it is important to find alternative methods to meet future load demands with improved quality and reliability. To achieve this, strategies must be developed to release the existing line capacity to support additional loads [6]. A notable challenge is that most elements within distribution networks, such as motors and transformers, exhibit inductive properties, leading to a lagging power factor. This condition decreases system capacity, increases system losses, and causes voltage reductions at various points within the system [7]. Parallel capacitors are widely employed to address these challenges by reducing power losses, improving voltage profiles, enhancing power factors, and stabilizing the system's voltage [8,19].

Despite advancements in power distribution systems, optimizing the placement of capacitors and DGs remains an active research area. Previous studies have explored various optimization techniques, but there remain gaps in achieving comprehensive solutions that balance computational efficiency, cost-effectiveness, and network performance under practical constraints.

Several prior works have tackled this issue using diverse methodologies. For instance, [9] proposed a multi-objective optimization approach for distribution feeder reconfiguration alongside capacitor placement, employing a modified gravitational search algorithm to enhance reliability and voltage security. [10] introduced a fuzzy framework for optimizing radial systems, addressing balanced and unbalanced networks with high precision and fast convergence. [11] formulated an integrated demand response program (DRP) combining DGs and shunt capacitors to optimize energy loss, operational cost, and network reliability, leveraging a shuffled frog-leaping algorithm. [12] investigated dynamic distribution feeder reconfiguration (DDFR), incorporating DGs, PV panels, and energy storage to optimize energy loss and operational costs via a modified particle swarm optimization algorithm [18].

Hybrid approaches have also gained attention for addressing multi-objective challenges in distribution systems. In [13,22-23], practical planning of distribution networks includes the optimal selection of conductor sizes and strategic capacitor placement to handle increasing load demands. This study explores a hybrid approach combining Genetic Algorithm (GA) and Particle Swarm Optimization (PSO), referred to as HGAPSO, to minimize power losses effectively. The method reduces overall costs associated with network planning and improves voltage profiles to achieve a semi-flat configuration under technical constraints such as voltage limits, conductor capacity, and reactive power injection [17]. This approach highlights the potential of combining optimization techniques to balance computational efficiency and system reliability.

Despite these efforts, challenges persist in efficiently integrating DG units and capacitor banks while considering real-world constraints such as voltage limits and operational costs. This study leverages the BBO algorithm to address these gaps by strategically placing DG units and capacitor banks to minimize power losses and improve voltage profiles in radial distribution networks.

This study builds upon the limitations of prior works and proposes the following contributions:

1. Development of a comprehensive optimization framework for capacitor and DG unit placement and sizing, leveraging advanced algorithms such as BBO.
2. Integration of renewable energy resources into distribution networks, addressing challenges related to voltage security and power quality, ensuring enhanced computational efficiency and practical applicability.
3. Presentation of practical scenarios, considering real-world network constraints, including voltage limits and permissible locations for DG units.

A graphical abstract summarizing the research workflow, key objectives, and contributions is provided in Figure 1.

2. The Theory of Biogeography

The BBO algorithm is a population-based optimization method inspired by the principles of biogeography. It was introduced by Dan Simon in 2008 and studies the distribution of species across different habitats over time. BBO mathematically models the migration and adaptation processes between habitats to solve complex optimization problems effectively. The algorithm draws on the natural dynamics of species migration and information exchange to enhance solutions iteratively.

BBO differs from other evolutionary algorithms in several key aspects. It requires fewer parameter settings, operates with low computational complexity, and demonstrates efficient memory usage—even when tackling high-dimensional numerical problems. These characteristics make it an attractive tool for solving engineering challenges, although its application in real-world engineering problems has been relatively limited, signifying untapped potential in diverse optimization contexts [24-26].

In the BBO framework, potential solutions to a problem are represented as individual habitats, each characterized by a Habitat Suitability Index (HSI). The HSI serves as a measure of the quality of a solution, analogous to the fitness function used in other population-based algorithms. Habitats with high HSI values represent effective solutions, whereas low HSI values indicate less optimal solutions. The algorithm improves solutions over successive generations by simulating migration and mutation processes.

In BBO, each element is likened to an island or habitat, where the exchange of traits among these elements is illustrated through migration and intra-migration. Figure 2 illustrates the migration of species and the emergence of a new island.

Each element in a solution is identified as a Suitability Index Variable (SIV). Regions classified as suitable habitats for a species correspond to a high HSI. A high HSI indicates effective performance in the optimization process, whereas a low HSI signifies inadequate performance.

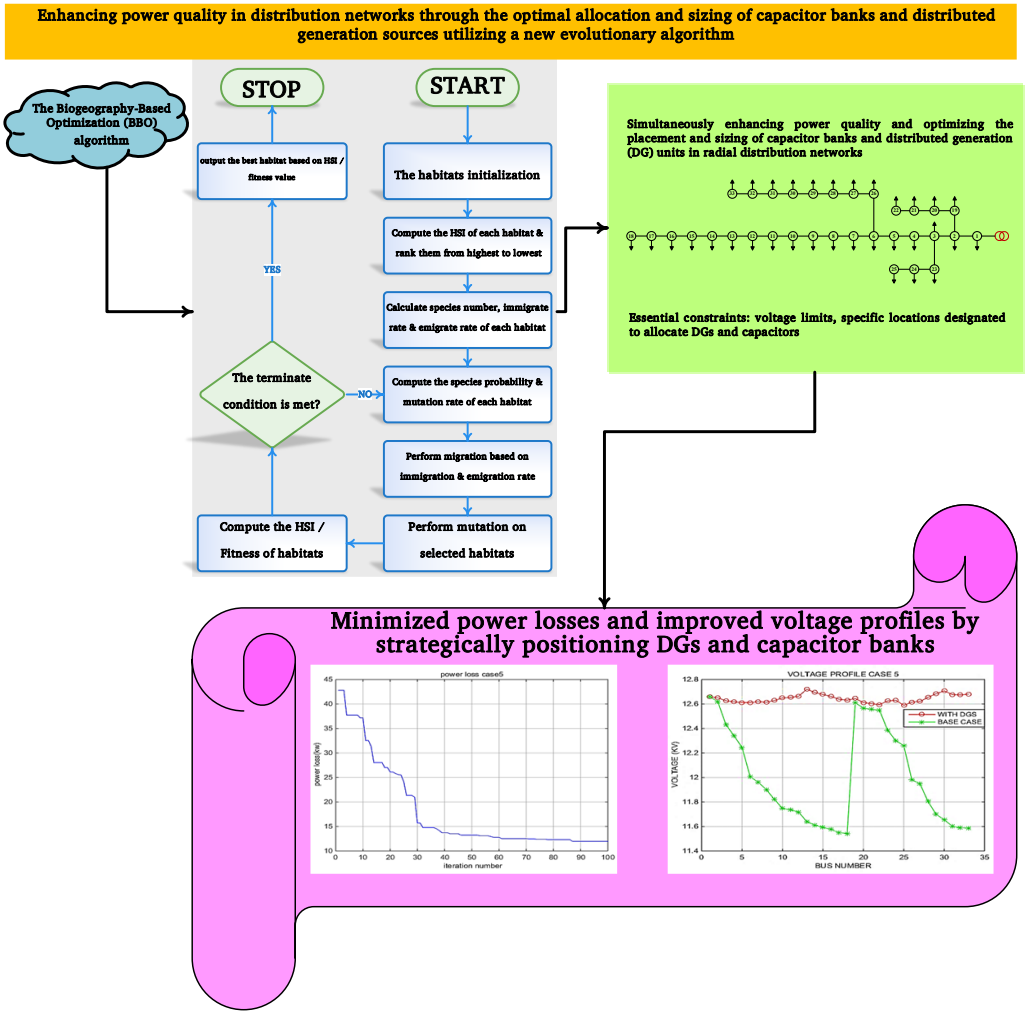

Figure 1. Graphical abstract.

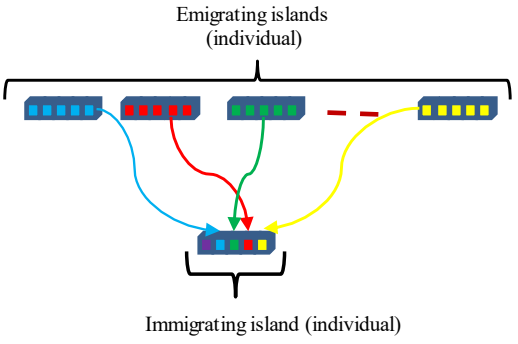

Figure 2. Migration of species and the formation of a new island.

Population growth serves as a strategy to address challenges within heuristic algorithms. In BBO, the subsequent generation is generated by migrating solution characteristics between islands and acquiring attributes from them. Additionally, mutation is introduced throughout the population in a manner akin to that found in genetic algorithms. Figure 3 illustrates the connection between the BBO algorithm and biogeography theory.

Migration Mechanism: Migration is a core concept in BBO, emulating the movement of species between habitats. Habitats with high HSI (strong solutions) can effectively share their desirable traits (solutions) with other habitats, enhancing the overall population quality. Each solution has an emigration (external migration rate) rate (μ) and an immigration (internal migration) rate (λ). Strong solutions typically have lower immigration rates and higher emigration rates, enabling them to share information without being disrupted by external influences. Conversely, weaker solutions have higher immigration rates, allowing them to acquire traits from stronger solutions.

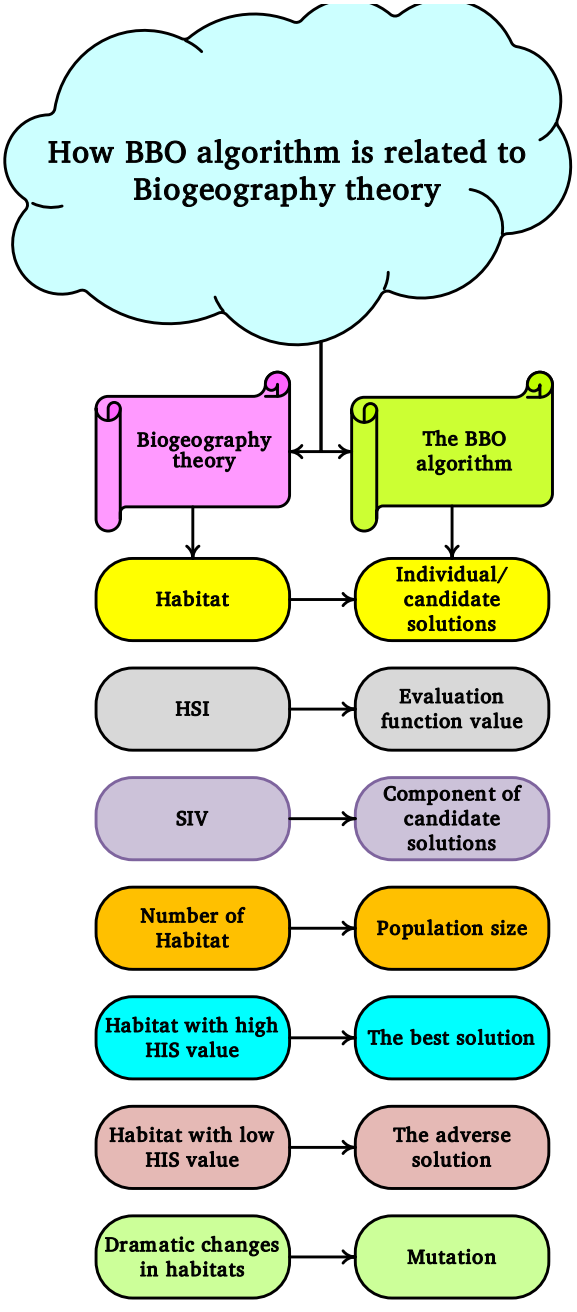

Figure 3. Relationship between the BBO algorithm with the Biogeography theory.

It's important to note that when an individual migrates to another island, the original island doesn't lose any traits in the procedure. Figure 4 shows the migration of species between habitats. The concepts of migration and intra-migration are mathematically modeled through a probabilistic framework. Furthermore, if the probability of a specific species, S, retaining its habitat at time t is considered as P_s, how this probability evolves from time t to time t + Δt will be described as follows:

$$P_s(t+\Delta t) = P_s(t)(1-\lambda_s\Delta t-\mu_s\Delta t) + P_{s-1}\lambda_{s-1}\Delta t + P_{s+1}\mu_{s+1}\Delta t \quad (1)$$

If the time (t) is small enough in Equation (1), then the following Equation (2) is obtained:

$$\dot{P}_s = \begin{cases} -(\lambda_s+\mu_s)P_s + \mu_{s+1}P_{s+1}S = 0 \\ -(\lambda_s+\mu_s)P_s + \lambda_{s-1}P_{s-1} + \mu_{s+1}P_{s+1}1 \le S \le S_{max} \\ -(\lambda_s+\mu_s)P_s + \lambda_{s-1}P_{s-1}S = S_{max} \end{cases} \quad (2)$$

The migration rates and internal migration values are as follows in Equations (4) to (5):

$$\mu k = EK/n \quad (3)$$

$$\lambda k = I(1-k/n) \quad (4)$$

Let's define the variables: I represents the highest possible internal migration rate, E is the highest possible displacement rate, K represents the count of member species (k), and n represents the total number of species. To explore a specific scenario where E is equivalent to I, it will proceed as follows in Equation (5):

$$\lambda\kappa + \mu\kappa = E \quad (5)$$

3. Biogeography-based optimization

Figure 5 presents a flowchart that shows the BBO process. Following other evolutionary algorithms, the initial phase of BBO entails the generation of a random population known as 'habitat.' To assess the quality of individual solutions, known as potential solutions, as well as the appropriateness of the habitats and regions, two essential parameters are established: HSI and SIV. The BBO framework fundamentally consists of two operations: migration and mutation. In this context, consider a defined problem where a set of potential solutions is represented as vectors coupled with a method for quality assessment. High-quality solutions can be compared to islands with a high Island Suitability Index (ISI), while those of lower quality are akin to islands characterized by a low ISI. It is crucial to note that the ISI aligns with the concept of "fitness" in other population-based optimization algorithms. The primary operations of BBO—migration and mutation of solutions—are depicted in Figures 6 and 7, respectively. Initially, potential solutions are adjusted to improve their quality. In this stage, an immigration rate (λ) is defined to assess the necessity of modifying the island. An emigration rate (μ) is implemented to select the solution that will probably migrate. It is crucial to emphasize that the algorithm is designed to avoid overfitting solutions to maintain quality. Natural hazards present a variety of threats to geographical regions, often resulting in abrupt fluctuations in HSI values. Consequently, the habitat may diverge from its equilibrium HSI during the mutation. At this stage, a probability factor is calculated for each individual within the population, as delineated in Equation (2), to assess the need for mutation.

Mutation ensures diversity within the population, preventing premature convergence to suboptimal solutions. Natural disturbances, such as environmental changes, are modeled as abrupt alterations in habitat conditions, which trigger mutations. The mutation rate for a habitat is proportional to the deviation of its HSI from equilibrium or the probabilities associated with the number of species, and it can be expressed as Equation (6):

$$m(s) = m_{max}\,((1-Ps)/P_{max}) \quad (6)$$

which is a parameter defined by the user.

The BBO algorithm iteratively applies these mechanisms to identify optimal solutions. The overall process can be summarized as follows:

1. **Initialization:** Generate a random initial population (habitats) and compute their HSIs.
2. **Migration:** Exchange solution traits between habitats based on immigration and emigration rates, enhancing solution diversity and quality.
3. **Mutation:** Apply probabilistic alterations to solutions to introduce diversity and avoid local optima.
4. **Evaluation:** Recalculate the HSI of each habitat after migration and mutation, and rank the solutions from best to worst.
5. **Convergence Check:** Repeat the process until a termination criterion, such as the maximum number of iterations or a satisfactory solution quality, is met.

The algorithm's ability to balance exploration and exploitation makes it a compelling choice for multi-objective optimization problems in engineering.

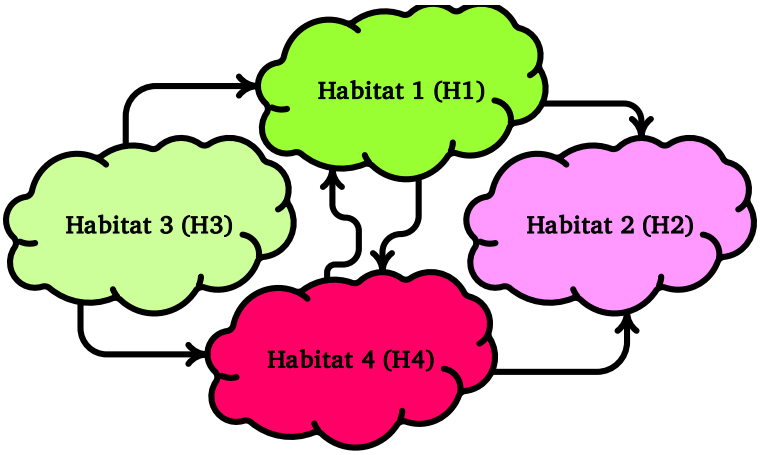

Figure 4. Species migration between habitats.

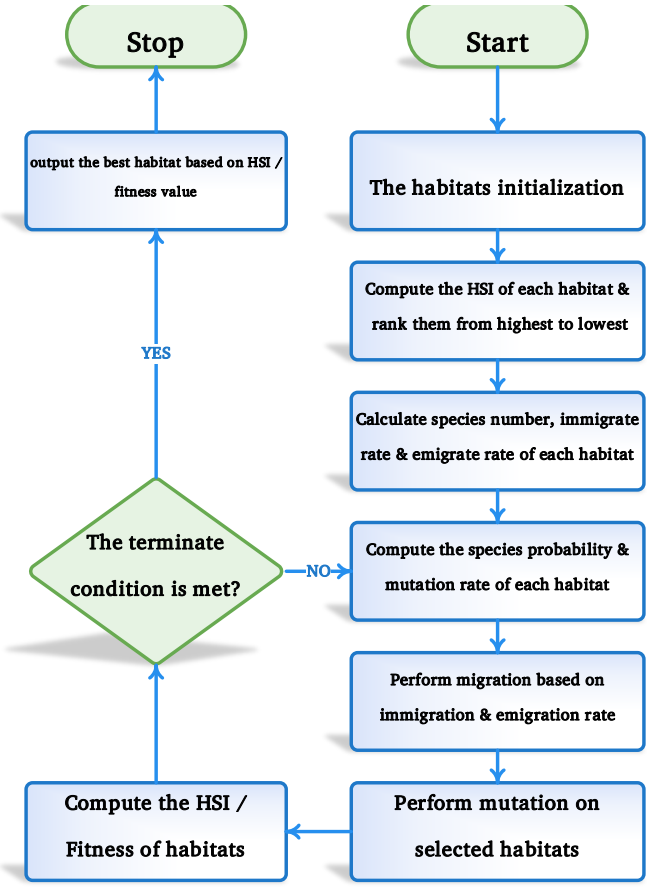

Figure 5. The flowchart of the BBO optimization method.

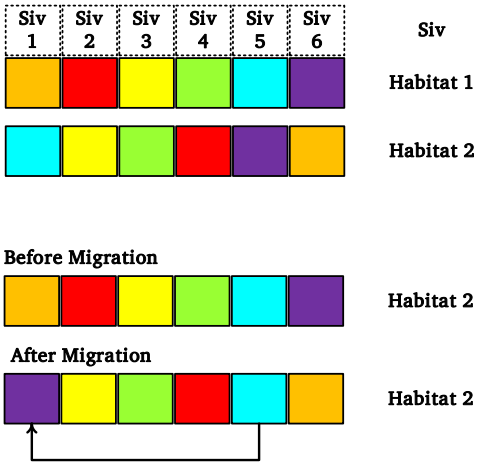

Figure 6. Migration process in BBO.

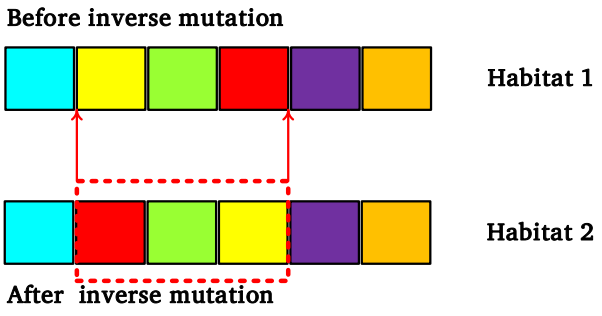

Figure 7. Mutation process in BBO.

4. Formulation of the problem

The optimization problem in this study aims to identify the optimal placement and sizing of DG units and capacitor banks within radial distribution systems. The objectives include minimizing active power losses, improving voltage profiles, and ensuring efficient resource utilization while adhering to predefined operational constraints. Some key considerations include:

- Achieving optimal load distribution to reduce system losses.
- Optimizing operational modes to enhance the overall power factor of the system.
- Refining generator parameters to improve efficiency.
- Reducing design costs while maximizing efficiency, among others.

Figure 8 illustrates the single-line diagram of the radial distribution system comprising 33 buses.

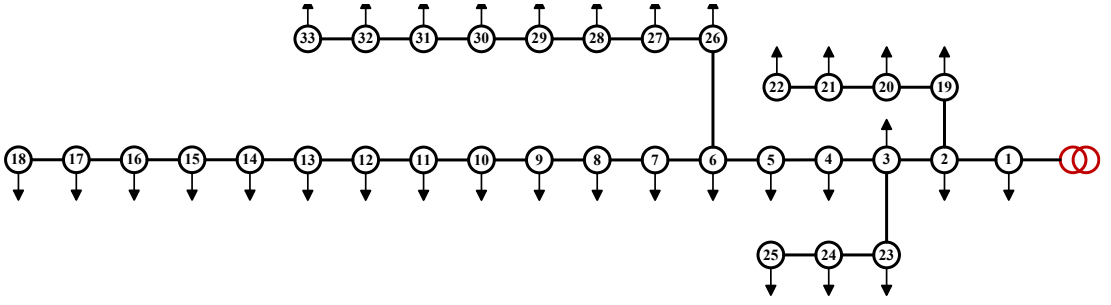

Figure 8. Single-line diagram of the radial distribution system of 33 buses [6].

Allocating and determining the optimal capacity of DGs is articulated as a nonlinear optimization problem. Each engineering system is represented by a collection of variables, manifesting features to be design or decision variables.

Variables $(x_i, i = 1,2, \dots, n())$provide a set of design variables for the design vector $X = \begin{bmatrix} x_1 \\ \vdots \\ x_n \end{bmatrix}$.

4.1. Objectives

The primary objectives are the minimization of real power losses and voltage profile improvement**,** ensuring the bus voltage magnitude is maintained within the permissible range, and enhancing voltage stability.

4.2. Design Variables

The optimization design variables include:
DG variables: DG location and DG active/reactive power output
Capacitor variables: Capacitor location and capacitor reactive power output.

4.3. Constraints

Voltage Constraints: Maintain voltage levels within acceptable operational limits for all buses:
Reactive Power Injection: Capacitor bank outputs must remain within their capacity:
Power Balance: Ensure system equilibrium between generation and demand.
Power Factor Constraints (for Variable Power Factor Modes): DGs must operate within the permissible power factor range:
Location Constraints: Only specified candidate buses are eligible for DGs and capacitors.

4.4. Optimization Modes

Five operational modes are analyzed:

1. **Mode 1:** Optimal placement of capacitors for reactive power compensation.
2. **Mode 2:** Allocating DGs with a unit power factor (active power injection).
3. **Mode 3:** Allocating DGs with a variable power factor (active and reactive power injection).
4. **Mode 4:** Simultaneous placement of capacitors and DGs with a unit power factor.
5. **Mode 5:** Simultaneous placement of capacitors and DGs with variable power factors.

4.4.1. First stage:

At this stage, the various parameters employed for optimization are quantified through the principles of biogeography. In this study, the initial population, represented as the number of habitats, is set at 100, with the number of iterations also established at 100. The selection index is designated as 10, while the maximum migration rate is set at E = 1, the maximum value for the intra-migration rate is I = 1, and the maximum mutation rate is $m_{max} = 0.005$ is selected.

4.4.2. The second stage:

The initial population is generated through a random process. This study examines five distinct configurations, which encompass the optimal placement of capacitor banks, the optimal placement of DGs operating at a unit power factor, the optimal placement of DGs with variable power factor, the simultaneous optimal placement of capacitors and DGs with unit power factor; and the simultaneous optimal placement of capacitors and DGs with variable power factor.

Mode 1: Optimal placement of capacitor banks for reactive power compensation can enhance the voltage profile and the system power factor. The initial population is defined in the following manner as in Equation (7).

$$X = [x_i] = \left[L_1 L_2 \dots L_{N_{Cap}} Q_1 Q_2 \dots Q_{N_{Cap}}\right]_{1\times(2\times N_{Cap})} \quad (7)$$

where N_{Cap} is the number of capacitors installed in $L_{N_{Cap}}$. Q is the reactive power provided by the capacitor bank. In this study, for example, for the number of capacitors, 3, according to the initial population number of 100, the dimensions of the initial population matrix are 6×100. The location of the capacitors is randomly selected between buses 2 and 33, and the reactive power value is randomly chosen between 0 and 1200 kVars.

Mode 2: Optimum placement of DGs with unit power factor: In this case, the DG unit only injects active power. The initial population is defined as follows in Equation (8).

$$X = [x_i] = \left[L_1 L_2 \dots L_{N_{DG}} P_1 P_2 \dots P_{N_{DG}}\right]_{1\times(2\times N_{DG})} \quad (8)$$

where N_{DG} is the number of DGs that are installed in $L_{N_{DG}}$. P is the active power produced by DGs. In this study, for instance, with three DGs, the dimensions of the initial population matrix are defined as 6×100, consistent with the size of the initial population. The locations of the DGs are randomly allocated between buses 2 and 33, while the active power values are randomly assigned within the range of 0 to 1000 kW for comparison with other references.

Mode 3: Optimum placement of DGs with variable power factor: In this mode, the placement of optimal DGs that can provide reactive power with variable power factor is done. The initial population is defined as follows in Equation (9).

$$X = [x_i] = \left[L_1 L_2 \dots L_{N_{DG}} P_1 P_2 \dots P_{N_{DG}} pf_1 pf_2 \dots pf_{N_{DG}}\right]_{1\times(3\times N_{DG})} \quad (9)$$

where N_{DG} is the number of DGs that are installed proportionally in $L_{N_{DG}}$ is the active power produced by DGs, and is the power factor of DGs. For the number of DG 3, according to the number of the initial population is 100, the dimensions of the initial population matrix are 100×9. The positions of the DGs are randomly determined within the interval between buses 2 and 33, while

the active power values are randomly selected from a range of 0 to 1200 kW. Additionally, the power factor for each unit is randomly assigned within the range of -0.9 to 0.9.

Mode 4: Optimal simultaneous placement of capacitor banks and DGs with a unit power factor: In this scenario, the locations of the capacitors and DGs are selected independently, assuming that the DGs are solely capable of supplying active power. The initial population is defined as follows in Equation (10):

$$X = [x_i] = \begin{bmatrix} L_1^{DG} L_2^{DG} .. L_{N_{DG}}^{DG} P_1 P_2 .. P_{N_{DG}} \\ .. L_1^{Cap} L_2^{Cap} .. L_{N_{Cap}}^{Cap} Q_1 Q_2 .. Q_{N_{Cap}} \end{bmatrix}_{1\times(2\times N_{DG}+2\times N_{Cap})} \quad (10)$$

where N_{DG} and N_{Cap} are the number of DGs and capacitors that are installed in the bus $L_{N_{DG}}^{DG}$ and $L_{N_{Cap}}^{Cap}$, respectively. DGs generate active power, while capacitor banks supply the reactive power. For the number of DG 3 and the number of capacitor 3, according to the initial population number of 100, the dimensions of the initial population matrix are 12×100. Of course, the number of capacitors and DGs can be chosen differently. The location of DGs and capacitors is randomly selected between buses 2 and 33, the active power value is randomly chosen between 0 and 500, and the reactive power value is randomly selected between 0 and 1200 kVars using Equation (11).

$$X = \begin{bmatrix} L_1^{DG} L_2^{DG} .. L_{N_{DG}}^{DG} P_1 P_2 .. P_{N_{DG}} pf_1 pf_2 . \\ . pf_{N_{DG}} L_1^{Cap} L_2^{Cap} .. L_{N_{Cap}}^{Cap} Q_1 Q_2 .. Q_{N_{Cap}} \end{bmatrix}_{1\times(3\times N_{DG}+2\times N_{Cap})} \quad (11)$$

where N_{DG} and N_{Cap} are the number of DGs and capacitors that are installed in the bus $L_{N_{DG}}^{DG}$and $L_{N_{Cap}}^{Cap}$, respectively. DGs generate active power, while capacitor banks supply the reactive power. For the number of DGs, 3, and the number of capacitors, 3, according to the number of the initial population, 100, the dimensions of the initial population matrix are 15×100. Of course, the number of capacitors and DGs can be chosen differently. The location of DGs and capacitors is randomly selected between buses 2 and 33, the amount of active power is randomly chosen between 0 and 1200 kW, and the amount of reactive power is selected between 0 and 1200 kW. The power factor of each unit is randomly chosen between 1 and -1.

4.5. The third step: calculating the values of the objective function

At this stage, first, the values of the objective function, i.e., losses, are calculated from Equation (12) using power flow for each vector of the initial population solution. Then, the order of the rows of the initial matrix is changed based on the values of the objective function in ascending order. Therefore, the first line is the best solution, having the least losses. The last line is the worst solution and has the highest losses.

$$P_{loss} = \sum_{i=1}^{n} R_i |I_i|^2 \quad (12)$$

where $P_{loss}$is the total loss of the distribution system, R_i the ohmic resistance of the branches, $|I_i|$ The magnitude of current passing through branches, and n is the number of branches in the distribution system.

4.6. Fourth step: applying the migration operator

In this step, we need to apply the migration operator. For this, we must first determine the number of species for each solution vector. In this way, the highest number of species is considered the best answer, i.e., the first line. No species is considered for the worst answer, i.e., the last line. This means that the number of species in the first row is 99, and in the last one is 0. Then, the values for each solution are calculated using the number of species and the relations of migration rate and intra-migration rate. To apply the migration operator, we calculate the criterion value for the internal migration rate from Equation (13):

$$\lambda_{scale} = \lambda_{lower} + (\lambda_{upper} - \lambda_{lower}) \times (\lambda(k) - \lambda_{min})/(\lambda_{max} - \lambda_{min}) \quad (13)$$

In this regard, λ_{lower} and λ_{upper} are the lower limit and the upper limit for the intra-migration rate, respectively, and λ_{min} and λ_{max} are the minimum and maximum values for the intra-migration rate, respectively. λ_{lower} and λ_{upper} are considered 0 and 1, respectively, in this study. The values of λ_{min} and λ_{max} are 0 and 1. Therefore, like the in-nomadic rate for a solution vector with k species, the criterion value for the in-nomadic rate is $\lambda(k)$. To apply the migration operator, first, the selection process is performed, and a number (10, in this study) that has a lower objective function value is removed from the solution vectors. Then, the migration operator is applied to the residuals of the solution as follows:

First, a random number between 0 and 1 for each variable in a solution vector is generated, that is, for each SIV in a solution vector. If this number is smaller than the criterion value of the inner migration rate for that vector, we perform migration on that variable. Because the solution vectors that have lower objective function values also have a small internal migration rate, the probability that migration is applied to them is low, and they are less changed at this stage, conversely, the solution vectors that have more objective function values and have a larger intra-migration rate, and therefore the probability that the migration operation is applied to them is high, and they are changed more at this stage. After a variable in one vector is selected for the migration operation, the migration rate values of the other vectors are used to find a replacement variable from another vector. This vector is

randomly chosen among other vectors so that the probability of selecting a vector is equal to the rate of change of that vector. In this way, considering that the solution vectors with lower objective function values have a larger migration rate, the probability that these vectors are selected is higher. After choosing the vector, the equivalent value of SIV chosen in the previous step is removed from this vector and replaced. After applying the migration operator, considering that the values of the vectors have changed, we recalculate the values of the objective function for each solution vector and change the order of the rows of the matrix based on the values of the new objective function in ascending order.

5. Results and Analysis

5.1. Simulation setup

The proposed BBO algorithm is applied to a 33-bus IEEE benchmark system, which operates at a voltage level of 12.66 kV and comprises 32 buses and four feeders. The parameters utilized for the BBO include a population size of 200, a habitat modification probability of 1, migration probability bounds in the gene range of [0,1], a step size for numerical integration probability of 1, a rate and maximum value of 1 for each island, and a mutation probability of 0.5. This study presents simulation analyses for three distinct scenarios. Case 1 performs the optimal placement and capacitor banks capacity determination; Case 2 addresses the optimal placement and capacity determination of DGs; and the final case investigates the simultaneous optimal placement and capacity determination of both capacitor banks and DGs. All harmonic sources are assumed to be in phase, with their corresponding data provided in Table 1 [20]. Figure 8 depicts the final radial configuration of the system following compensation, while Figure 9 illustrates the convergence characteristics of both the BBO and GA in terms of the loss objective function. The analysis demonstrates that capacitors and DGs can significantly reduce active power losses and enhance the voltage profile and Total Harmonic Distortion (THD) at each bus within the system, as evidenced by Figures 10 and 11.

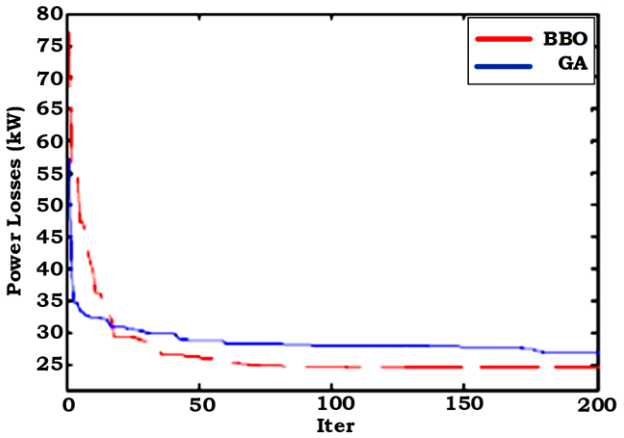

Figure 9. Convergence characteristic of BBO and GA.

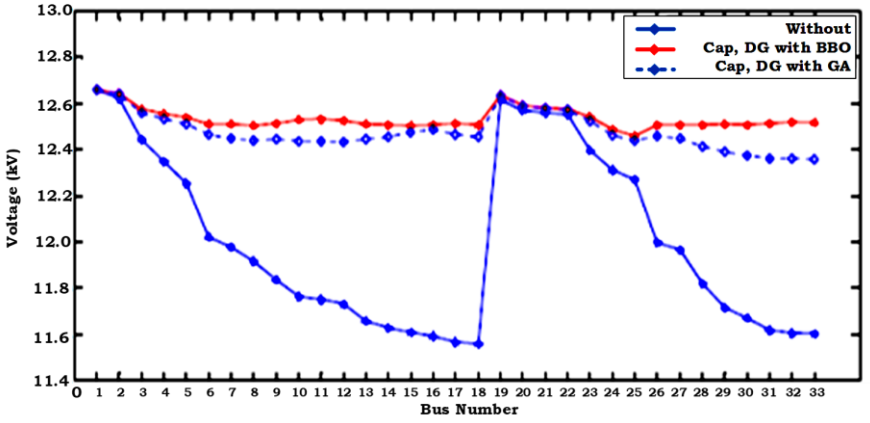

Figure 10. Voltage profile before and after installation of the capacitor and DG at each system bus.

The described method has been implemented along with the load distribution program of distribution systems using MATLAB software for the five mentioned modes. In this section, the obtained results are presented and analyzed. Then, they are compared with the results of some other sources.

5.2. The results obtained for the first case: Optimal placement of capacitor banks to provide reactive power

There are three capacitors in this mode, and their reactive power is between 0 and 1200 kVars. The obtained results are presented in Table 2 and compared with the base state [6].

Although the loss reduction percent of the simulation performed in this article is slightly lower than in [6], the results show that this loss reduction was achieved by installing capacitors with a total reactive power of 1972.8 kVars, while in [6], reducing the mentioned losses requires the installation of capacitors with a total reactive power of 2900 kW. Figure 12 presents convergence characteristics in terms of the number of iterations. This algorithm has a suitable convergence response.

Table 1. Harmonic information.

Harmonic order	5	7	11	13	17	19
W	0.03	0.02	0.01	0.004	0.003	0.001

Table 2. Results obtained for Mode 1.

	Location and reactive power of capacitors (kVars)		Power loss (kW)	Loss reduction %	The lowest voltage and its bus
Base mode	-		211.87	-	0.9117 bus 18
Result of the simulation	13 24 30	359.7 545.9 1067.2	139.57	34.1	0.9361 bus 18
Reference [6]			130.03	35.8	

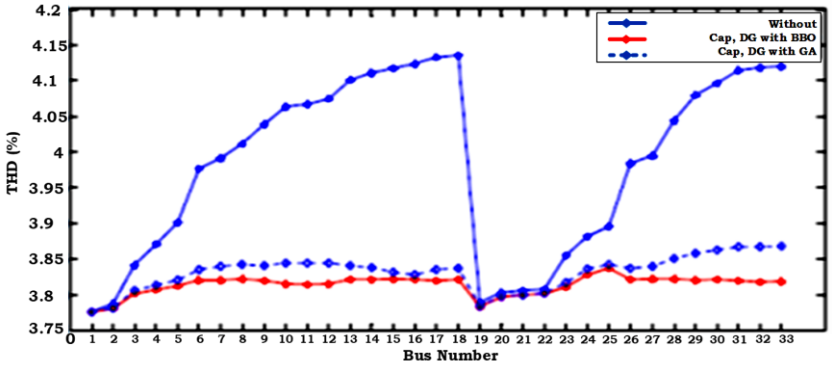

Figure 11. THD before and after installing capacitors and DG at each system bus.

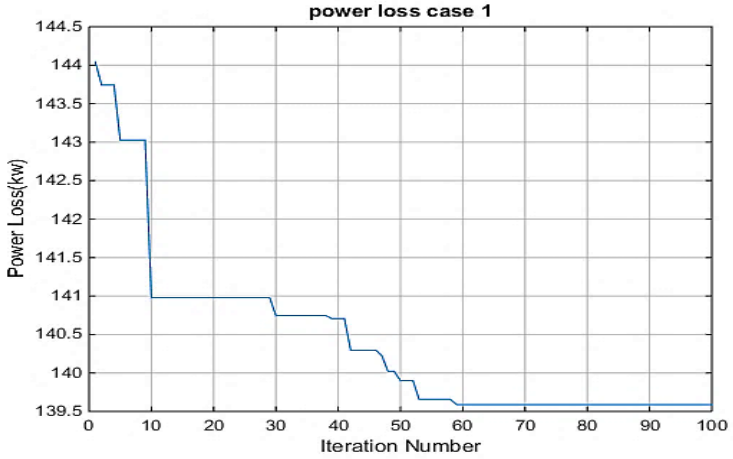

Figure 12. Characterization of the convergence of the first mode according to the number of iterations.

The voltage values of the buses in the basic state and after the capacitor are shown in Figure 13. It can be seen that the capacitors have improved the voltage profile of the distribution system.

So, in the first case, by placing and determining the optimal capacity of the capacitor banks, the reactive power passing through the branches of the distribution system is reduced, and this causes the real power loss of the system to be significantly reduced and the voltage profile improved.

5.3. The results obtained for the second case: Optimal placement of DGs with a single power factor

The number of DGs, in this case, is three, and their active production power is between 0 and 1000 kW. The obtained results are presented in Table 3 and compared with the base state and [15].

The convergence characteristic in terms of the number of iterations is presented in Figure 14. Bus voltage values in the basic state and after the addition of distributed generation units are shown in Figure 15. It can be seen that DGs affect voltages very well and have improved the voltage profile of the distribution system.

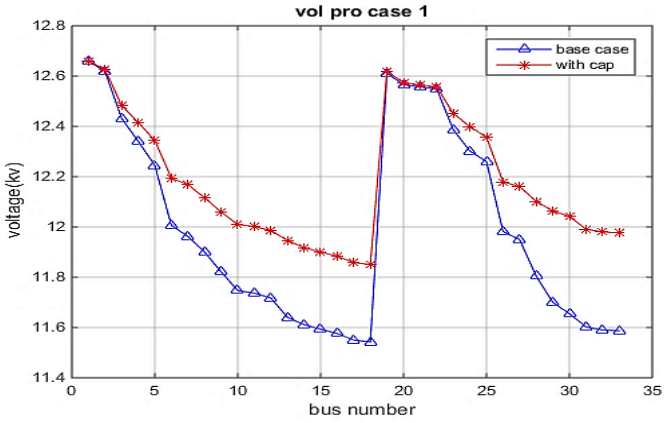

Figure 13. Bus voltage values in the basic state and after the capacitor for the first state.

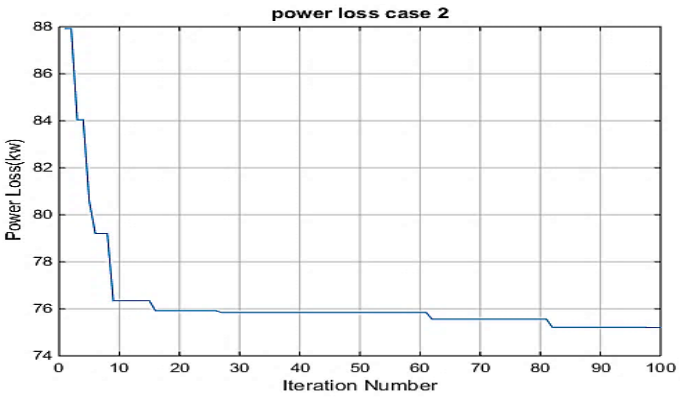

Figure 14. Convergence characteristic of the second mode according to the number of iterations.

Table 3. Results obtained for Mode 2.

	Location and active power of DGs (kW)		Power loss (kW)	Loss reduction percentage	The lowest voltage and corresponding bus
Base mode	-		211.87	-	0.9117 Bus18
Result of the simulation	12 24 30	940.6 977.6 944.6	75.27	64.4	0.9652 bus 18
Reference [15]	13 24 30	900 900 900	74.27	64.83	

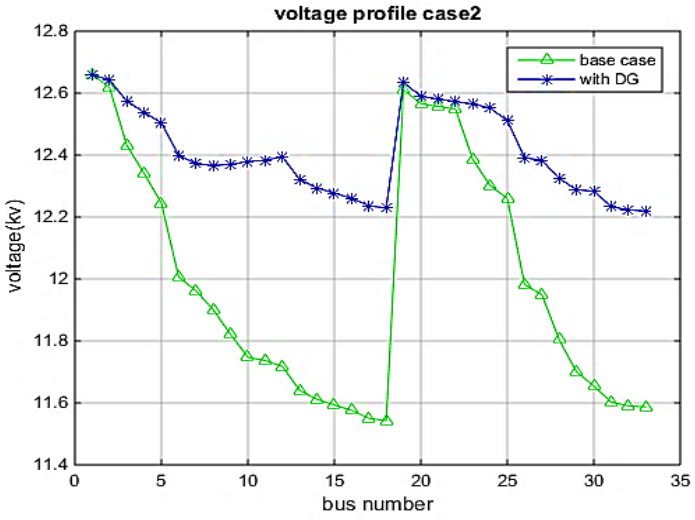

Figure 15. Bus voltage values in the basic state and after adding DGs for Mode 2.

In the second case, by locating and determining the optimal capacity of the DG system with a unit power factor, the active power passing through the branches of the distribution system is reduced. This causes the real power loss of the system to be significantly reduced. At the same time, the voltage profile of the distribution system improves. By locating and determining the optimal capacity of a distributed generation system with variable power factor, both active and reactive power passing through the branches of the distribution system are reduced, causing the real power loss of the system to be reduced more than in the previous two cases, and the system voltage profile improvement is more than the base state.

5.4. The results obtained for the third case: Optimal placement of DGs with variable power factor

For this case, the number of DGs is 3. Their active power output is between 0 and 1200 kW, and the power factor is between 0.9 and -0.9. The results are presented in Table 4 and compared with the base case and [3]. As can be seen, the results obtained from the simulation have a better loss reduction compared to [6].

The convergence characteristic in terms of the number of iterations is presented in Figure 16. The voltage values of the buses in the basic state and after the addition of DGs are shown in Figure 17. It can be seen that DGs, in this case, affect the voltages strongly and have improved the voltage profile of the distribution system.

So, in Mode 3, by placing and determining the optimal capacity of capacitor banks and the distributed generation system with a single power factor, the capacitor banks reduce the reactive power passing through the branches of the distribution system. The DG system with a single power factor reduces the active power passing through the branches of the distribution system, causing the real power loss of the system to decrease more than the previous three conditions, and the voltage profile of the distribution system is also improved more than the basic condition.

Table 4. The results obtained for Mode 3.

	Location and active power of DGs (kW)			Power loss (kW)	Loss reduction percentage	The lowest voltage and corresponding bus
Base mode	-		Power factor	211.87	-	0.9117 bus 18
Result of the simulation	6	510	0.8887	21.24	90	0.982 bus 25
	14	655	0.8976			
	30	877	0.7483			
Reference [6]	17	300	0.89	39.99	80.3	
	30	500	0.55			
	12	500	0.89			
	32	300	0.89			
	29	293	0.39			

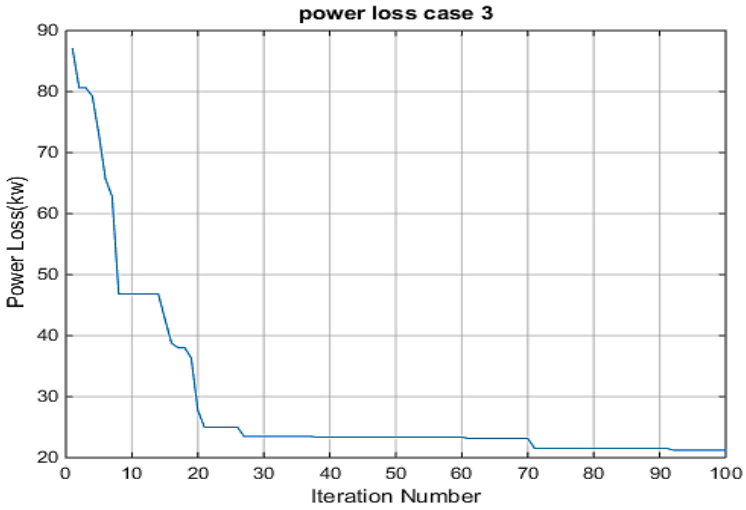

Figure 16. The convergence characteristic of Mode 3.

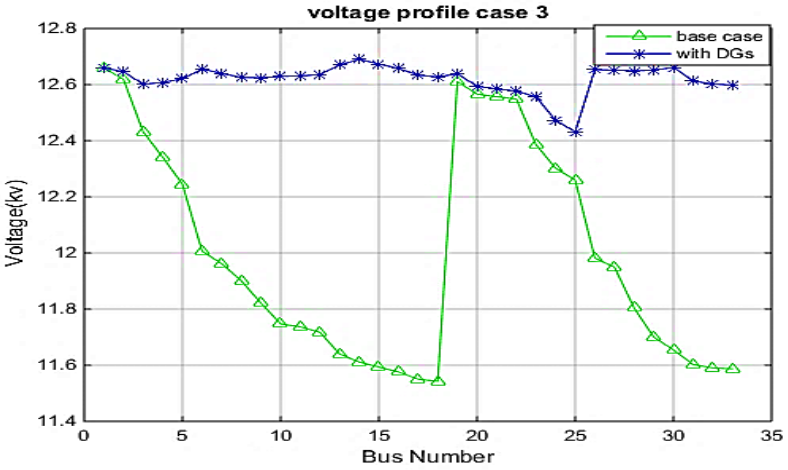

Figure 17. Bus voltage values in the basic state and after adding DGs for Mode 3.

Table 5. Results obtained for Mode 4.

	Location and active power of DGs (kW) and location and reactive power of the capacitor (kVAR)				Power loss (kW)	Loss reduction percentage	The lowest voltage and corresponding bus
Base mode	-				211.87	-	0.9117 bus 18
Result of the simulation	6	473	12	474	24.82	88.28	0.9835 bus 18
	15	498	24	513			
	32	493	30	965			
Reference [3]					24.45	87.9	

5.5. The results obtained for the fourth case: Simultaneous optimal placement of the capacitor bank and DGs with a single power factor

For this mode, the number of DGs is three, and the number of capacitors is also 3. The active power of DGs is between 0 and 500 kW. The power factor is between 0.9 and -0.9. The injected reactive power of capacitors is considered between 0 and 1200 kW. The results are presented in Table 5 and compared with the base state and [3]. The obtained results are close to the results of [3], but in this reference, 2581 kW of a capacitor and 1892 kW of DG have been used to reduce losses. The obtained results used 1951 kW of a capacitor and 1464 kW of DG for the same amount of loss reduction.

The convergence characteristic in terms of the number of iterations is presented in Figure 18. Bus voltage values in the basic state and after adding capacitors and DGs are shown in Figure 19 It can be seen that DGs and capacitors, in this case, affect the voltages strongly and have improved the voltage profile of the distribution system.

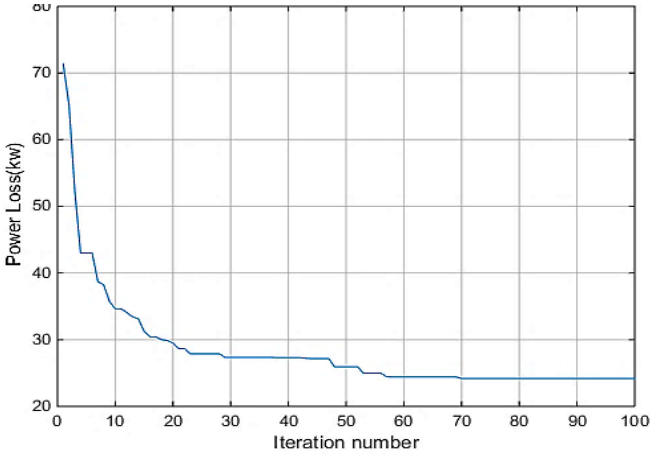

Figure 18. Convergence characteristic of Mode 4 according to the number of iterations.

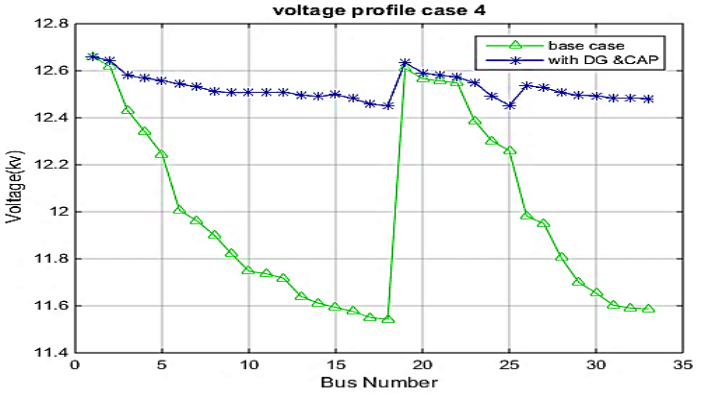

Figure 19. Bus voltage values in the basic state and after adding DGs and capacitors for Mode 4.

Table 6. Results obtained for Mode 5.

	Location and active power of DGs (kW) and their power factor, and location and reactive power of the capacitor (kVar)					Power loss (kW)	Loss reduction percentage	The lowest voltage and corresponding bus
Base mode	-					211.87	-	0.9117 bus 18
Result of the simulation	13	753	0.9	7	176	11.85	94.4	0.9923 Bus 18
	24	1112	0.94	19	232			
	30	1065	0.82	33	199			
Reference [13]	13	795	0.91	8	150	11.71	94.47	
	24	1069	0.9	18	150			
	30	1029	0.81	30	300			

So, in Mode 4, by placing and determining the optimal capacity of capacitor banks and a DG with variable power factor, capacitor banks reduce the reactive power passing through the branches of the distribution system. The distributed generation system with variable power factor reduces both active and reactive power crossing of the branches of the distribution system, and this causes the real power loss of the system to be reduced more than in the previous cases, and the voltage profile of the distribution system is also improved more than the base case.

5.6. The results obtained for the fifth case: Simultaneous optimal placement of the capacitor bank and DGs with variable power factor

For this mode, the number of DGs is three, and the number of capacitors is also 3. The active power of DGs is between 0 and 1200 kW. The power factor is between 1 and -1. The injected reactive power of capacitors is considered between 0 and 1200 kW. The results are presented in Table 6 and compared with the base state and [16]. The convergence characteristic in terms of the number of iterations is presented in Figure 20. Bus voltage values in the basic state and after adding capacitors and distributed generation units are shown in Figure 21. It can be seen that DGs and capacitors, in this case, affect the voltages strongly and have improved the voltage profile of the distribution system.

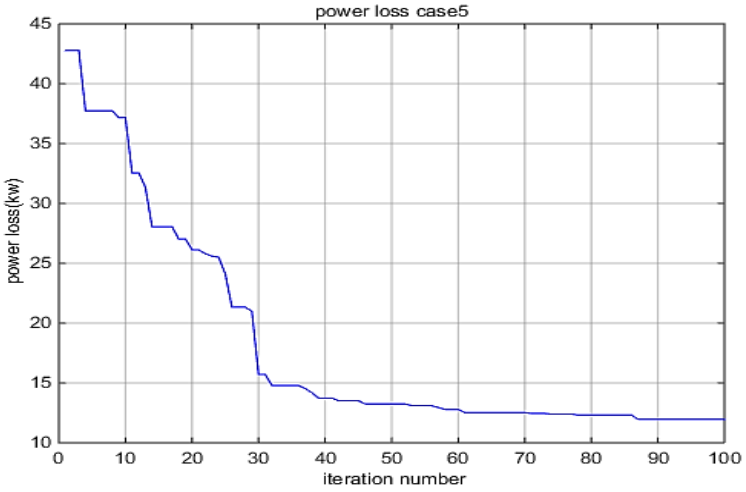

Figure 20. Convergence characteristic of Mode 5.

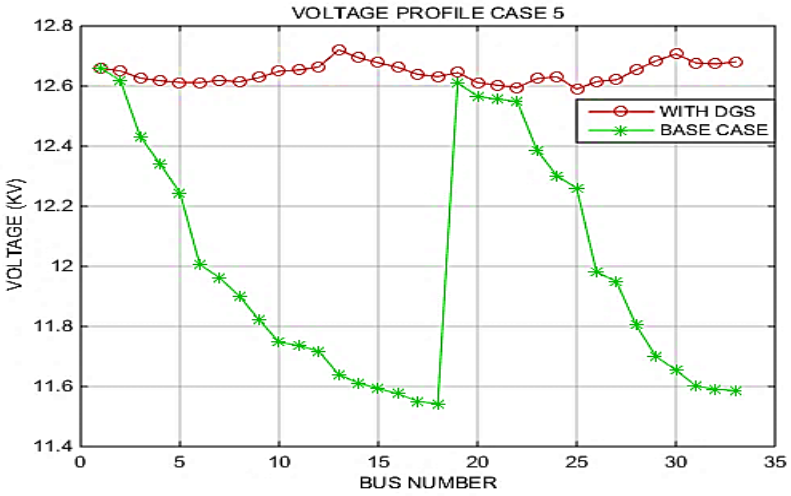

Figure 21. Bus voltage values in the basic state and after adding DGs and capacitors for Mode 5.

5.7. Optimization results

1. Mode 1- Capacitor Placement: Optimally allocating three capacitors, total power loss decreased from 211.87 kW to 139.57 kW, achieving a 34.1% reduction. The lowest bus voltage increased from 0.9117 pu to 0.9361 pu.
2. Mode 2 - DG Placement (Unit Power Factor): Optimally placing three DGs reduced power losses to 75.27 kW, achieving a 64.4% reduction. Voltage profile improvements raised the lowest bus voltage to 0.9652 pu.
3. Mode 3 - DG Placement (Variable Power Factor): Incorporating variable power factors resulted in losses as low as 21.24 kW, with a 90% reduction. Bus voltages improved significantly, with the lowest increasing to 0.982 pu.
4. Mode 4- Combined Placement with Unit Power Factor: Simultaneously allocating three DGs and three capacitors reduced power losses to 24.82 kW (an 88.28% reduction). The lowest voltage reached 0.9835 pu.
5. Mode 5 - Combined Placement with Variable Power Factor: This mode yielded the best results. Power losses were minimized to 11.85 kW (a 94.4% reduction). Voltage profiles improved significantly, with the lowest bus voltage rising to 0.9923 pu.

The results highlight the effectiveness of the proposed BBO-based optimization approach. In all five modes, significant reductions in power losses and enhancements in voltage profiles were achieved. The allocation of DGs with variable power factors demonstrated superior performance, particularly in Mode 5, where a combination of capacitors and DGs produced the most efficient results. These findings underscore the potential of BBO for addressing complex, multi-objective optimization problems in distribution systems.

6. Conclusion

This study proposed a biogeography-based optimization framework for the optimal placement and sizing of DG units and capacitor banks in radial distribution systems. As a result, power loss was minimized and the voltage profile improved simultaneously. The methodology demonstrated significant performance improvements across all 5 operational modes. Mode 5, combining capacitors and DGs with variable power factors, emerged as the most effective approach, reducing losses by 94.4% and improving the lowest bus voltage to 0.9923 pu.

Future research may explore the involvement of economic factors, such as installation and operational costs, and expand the model to accommodate higher-order harmonics and stochastic load variations.

References

[1] N. Bagheri, M. A. Bahramian, and A. A. Ghadimi, "Optimal Capacitor Placement in Distributed Networks Polluted with Harmonics in the Presence of Wind Energy-Based Distributed Generation Sources," *Journal of Green Energy Research and Innovation*, vol. 1, no. 4, pp. 1–16, 2024.

[2] M. Najjarpour, B. Tousi, and A. H. Karamali, "Optimizing Reactive Power for DG Units to Minimize Power System Losses Using Stochastic Modeling," *Journal of Green Energy Research and Innovation*, vol. 1, no. 4, pp. 35–46, 2024.

[3] A. Sotoudeh, M. M. Rezaei, and M. Moradian, "Robust Control of Load Voltage in an Islanded Wind Energy Conversion System Using Nonlinear Methods," *Journal of Green Energy Research and Innovation*, vol. 1, no. 4, pp. 17–34, 2024.

[4] S. A. Taher, M. Hasani, and A. Karimian, "A Novel Method for Optimal Capacitor Placement and Sizing in Distribution Systems with Nonlinear Loads and DG Using GA," *Communications in Nonlinear Science and Numerical Simulation*, vol. 16, no. 2, pp. 851–862, 2011.

[5] K. Kasturi, C. K. Nayak, S. Patnaik, and M. R. Nayak, "Strategic Integration of Photovoltaic, Battery Energy Storage and Switchable Capacitor for Multi-Objective Optimization of Low Voltage Electricity Grid: Assessing Grid Benefits," *Renewable Energy Focus*, vol. 41, pp. 104–117, 2022.

[6] K. Valipour, E. Dehghan, and M. H. Shariatkhah, "Optimal Placement of Capacitor Banks and Distributed Generation for Losses Reduction and Voltage THD Improvement in Distribution Networks Based on BBO Algorithm," *International Research Journal of Applied and Basic Sciences*, vol. 4, no. 7, pp. 1663–1670, 2013.

[7] L. Mohammadian, M. T. Hagh, E. Babaei, and S. Khani, "Using PSO for Optimal Planning and Reducing Loss of Distribution Networks," *in Proceedings of 17th Conference on Electrical Power Distribution*, pp. 1–6, 2012.

[8] Z. Wu, "Optimal Choice of Fixed and Switched Capacitors in Radial Distributors with Distorted Substation Voltage," *IEE Proceedings - Generation, Transmission and Distribution*, vol. 142, no. 1, 24, 1995.

[9] H. Lotfi, A. Azizivahed, A. A. Shojaei, S. Seyedi, and M. F. B. Othman, "Multi-Objective Distribution Feeder Reconfiguration Along with Optimal Sizing of Capacitors and Distributed Generators Regarding Network Voltage Security," *Electric Power Components and Systems*, vol. 49, no. 6-7, pp. 652–668, 2021.

[10] M. Sedighizadeh, and R. Bakhtiary, "Optimal Multi-Objective Reconfiguration and Capacitor Placement of Distribution Systems with the Hybrid Big Bang–Big Crunch Algorithm in the Fuzzy Framework," *Ain Shams Engineering Journal*, vol. 7, no. 1, pp. 113–129, 2016.

[11] H. Shareef, A. Ibrahim, N. Salman, A. Mohamed, and W. Ling Ai, "Power Quality and Reliability Enhancement in Distribution Systems Via Optimum Network Reconfiguration by Using Quantum Firefly Algorithm," *International Journal of Electrical Power & Energy Systems*, vol. 58, pp. 160–169, 2014.

[12] H. Lotfi, "Optimal Sizing of Distributed Generation Units and Shunt Capacitors in the Distribution System Considering Uncertainty Resources by the Modified Evolutionary Algorithm," *Journal of Ambient Intelligence and Humanized Computing*, vol. 13, no. 10, pp. 4739–4758, 2021.

[13] H. Lotfi, "Multi-objective Energy Management Approach in Distribution Grid Integrated with Energy Storage Units Considering the Demand Response Program," *International Journal of Energy Research*, vol. 44, no. 13, pp. 10662–10681, 2020.

[14] L. Mohammadian, A. Mohammadian, S. Khani, M. T. Hagh, and E. Babaei, "Using a Hybrid Evolutionary Method for Optimal Planning and Reducing Loss of Distribution Networks," *in Proceedings of the 16th Electrical Power Distribution Conference*, 2011, pp. 1–9.

[15] D. Simon, "Biogeography-Based Optimization," *IEEE Transactions on Evolutionary Computation*, vol. 12, no. 6, pp. 702–713, 2008.

[16] L. D. Pereira, I. Yahyaoui, et al., "Optimal Allocation of Distributed Generation and Capacitor Banks Using Probabilistic Generation Models with Correlations," *Applied Energy*, vol. 307, 118097, 2022.

[17] M. H. Moradi, A. Zeinalzadeh, Y. Mohammadi, and M. Abedini, "An Efficient Hybrid Method for Solving the Optimal Sitting and Sizing Problem of DG and Shunt Capacitor Banks Simultaneously Based on Imperialist Competitive Algorithm and Genetic Algorithm," *International Journal of Electrical Power & Energy Systems*, vol. 54, pp. 101–111, 2014.

[18] M. T. Mouwafi, R. A. El-Sehiemy, and A. A. A. El-Ela, "A Two-Stage Method for Optimal Placement of Distributed Generation Units and Capacitors in Distribution Systems," *Applied Energy*, vol. 307, 118188, 2022.

[19] E. Ali, S. Abd Elazim, and A. Abdelaziz, "Improved Harmony Algorithm and Power Loss Index for Optimal Locations and Sizing of Capacitors in Radial Distribution Systems," *International Journal of Electrical Power & Energy Systems*, vol. 80, pp. 252–263, 2016.

[20] C. Duffey, and R. Stratford, "Update of Harmonic Standard IEEE-519-IEEE Recommended Practices and Requirements for Harmonic Control in Electric Power Systems," *Conference Record of the IEEE Industry Applications Society Annual Meeting*, vol. 2, pp. 1618–1624, 1989.

[21] M. Ladjavardi, and M. A. S. Masoum, "Genetically Optimized Fuzzy Placement and Sizing of Capacitor Banks in Distorted Distribution Networks," *IEEE Transactions on Power Delivery*, vol. 23, no. 1, pp. 449–456, 2008.
[22] M. Aman, G. Jasmon, A. Bakar, and H. Mokhlis, "A New Approach for Optimum Simultaneous Multi-DG Distributed Generation Units Placement and Sizing Based on Maximization of System Loadability Using HPSO (hybrid Particle Swarm Optimization) Algorithm," *Energy*, vol. 66, pp. 202–215, 2014.
[23] A. Zeinalzadeh, Y. Mohammadi, and M. H. Moradi, "Optimal Multi Objective Placement and Sizing of Multiple DGs and Shunt Capacitor Banks Simultaneously Considering Load Uncertainty Via MOPSO Approach," *International Journal of Electrical Power & Energy Systems*, vol. 67, pp. 336–349, 2015.
[24] M. Demirtas, and F. Ahmad, "Fractional Fuzzy PI Controller Using Particle Swarm Optimization to Improve Power Factor by Boost Converter," *An International Journal of Optimization and Control: Theories & Applications (IJOCTA)*, vol. 13, no. 2, pp. 205–213, 2023.
[25] A. A. Ahmad, K. M. Saffer, M. Sari, and H. Uslu, "Prediction of Anemia with a Particle Swarm Optimization-Based Approach," *An International Journal of Optimization and Control: Theories & Applications (IJOCTA)*, vol. 13, no. 2, pp. 214–223, 2023.
[26] G. Bektur, and H. K. Aslan, "Artificial Bee Colony Algorithm for Operating Room Scheduling Problem with Dedicated/Flexible Resources and Cooperative Operations," *An International Journal of Optimization and Control: Theories & Applications (IJOCTA)*, vol. 14, no. 3, pp. 193–207, 2024.

Declaration of competing interest

The author declares that there are no known competing financial interests or personal relationships that could have appeared to influence the work reported in this paper. All ethical standards, including avoidance of plagiarism, informed consent, research misconduct, data fabrication or falsification, duplicate publication or submission, and redundancy, have been fully observed by the author.

Bibliography

Leila Mohammadian was born in Tabriz, Iran, in 1984. She received her B.S., M.S., and Ph.D. degrees in Electrical Engineering from the Department of Electrical and Computer Engineering, University of Tabriz, Tabriz, Iran, in 2007, 2011, and 2015, respectively. She has been with the Department of Electrical Engineering, Shab.C., Islamic Azad University, Shabestar, Iran, since 2011. She has been an Assistant Professor since 2015. She is the author of more than 60 journal and conference papers. Her current research interests include the analysis and control of power electronic converters and their applications, power quality enhancement and FACTS devices, application of control systems and theory in power engineering, and power system dynamics, renewable energy sources, and energy storage systems.
Email: le.mohammadian@iau.ac.ir
ORCID: 0000-0001-5202-1397
Contribution Statement: Conceptualization, Methodology, Project administration, Resources, Supervision, Writing-review & editing.

Journal of Green Energy Research and Innovation

A Cutting-Edge Reliability Assessment of MPPT-Driven Photovoltaic Systems Enhanced by Recursive Least Squares Adaptive Identification

Peyman Bayat, Pezhman Bayat

Highlights

- **RLS-driven dynamic parameter identification for MPPT reliability assessment.**
- **Hierarchical MPPT categorization framework for reliability benchmarking.**
- **Irradiation set-point isolation methodology.**
- **Direct correlation between MPPT dynamics and grid reliability.**

Graphical Abstract

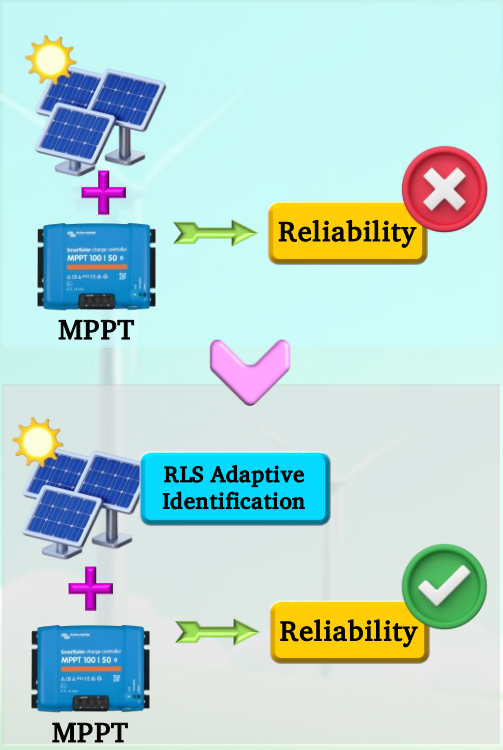

Use your device to scan and read the article online

Citation
P. Bayat, and P. Bayat," A Cutting-Edge Reliability Assessment of MPPT-Driven Photovoltaic Systems Enhanced by Recursive Least Squares Adaptive Identification," *Journal of Green Energy Research and Innovation*, vol. 2, no. 3, pp. 72-93, 2025.

https://doi.org/10.61882/jgeri.2.3.72

JGERI Journal of Green Energy Research and Innovation

Journal of Green Energy Research and Innovation 2.3 (2025) 72-93

Online ISSN: 3041-9018

Journal of Green Energy Research and Innovation

Journal Homepage: www.jgeri.araku.ac.ir

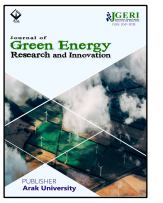

A Cutting-Edge Reliability Assessment of MPPT-Driven Photovoltaic Systems Enhanced by Recursive Least Squares Adaptive Identification

Peyman Bayat [*] , Pezhman Bayat

Department of Electrical Engineering, Hamedan University of Technology, Hamedan, Iran.

ARTICLE INFO

Keywords:
Solar energy
Reliability metrics,
System identifications,
Maximum power point tracking.

Article History:
Received: 12 March 2025;
Revised: 04 May 2025;
Accepted: 12 May 2025.

Article type:
Research Article

[*] ***Corresponding author***
E-mail address
peyman.bayat@hut.ac.ir (P.Bayat)

ABSTRACT

Solar energy has become an important global energy research topic, recognized for its potential to address sustainability challenges. While photovoltaic (PV) technology offers clean energy generation, its broader adoption is constrained by limitations such as suboptimal conversion efficiency and high perceived initial costs. This study explores the influence of various maximum power point tracking (MPPT) methods on the reliable performance of PV systems that operate in network-connected mode. It investigates how these power optimization strategies impact overall operational reliability, emphasizing the role of MPPT in achieving stable and efficient grid integration. By categorizing MPPT techniques into offline, online, and hybrid groups, the research assesses their impact on reliability metrics within a standardized distribution network. Using the recursive least squares (RLS) method, localized solar cell parameters are dynamically estimated under different MPPT configurations. To isolate the effects of methodologies, irradiation fluctuations are treated as controlled set-point adjustments. Simulation results conducted with MATLAB/Simulink reveal statistically significant correlations between MPPT selection and system reliability, providing actionable insights for enhancing PV grid integration.

1. Introduction

The intensifying global energy crisis, together with the worsening impacts of climate change, has driven a remarkable increase in the adoption of renewable energy and sustainable fuel technologies. This shift represents a critical departure from our prolonged reliance on finite fossil fuel resources, while actively aiming to mitigate additional environmental damage. To explain further, with energy supplies becoming scarcer and environmental challenges mounting, societies worldwide are driven to seek cleaner and more sustainable energy solutions [1]. This increasing focus on renewable energy signifies not only an essential shift towards sustainable energy sources but also highlights the pressing need to safeguard our planet against the harmful consequences of excessive fossil fuel usage. Renewable energy sources, including wind, ocean waves, tidal forces, solar radiation, biomass, biofuels, and geothermal heat, act as potential energies for electricity generation. The conversion of these resources into electrical energy occurs through both direct and indirect methods, depending on the technology employed. For instance, solar thermal power plants utilize concentrated solar energy to heat fluids, which drive turbines to generate electricity indirectly. In contrast, photovoltaic (PV) cells bypass intermediate steps by directly converting sunlight into direct current (DC) electricity through the photovoltaic effect, a quantum mechanical phenomenon that liberates electrons when photons strike semiconductor materials [2]. The integration of renewable energy into modern infrastructure involves two primary pathways: grid-connected systems, where electricity is fed into centralized power networks, and off-grid applications, which provide decentralized energy access to remote or underserved regions. This dual approach underscores the adaptability of renewable technologies to diverse energy needs [1,2]. One objective of advancing renewable energy systems is reliability modeling, a technique aimed at identifying unforeseen outages, forecasting potential failures, and quantifying performance metrics such as failure rates and mean time to failure (MTTF) [2].

By analyzing potential faults and component failures, engineers can refine system designs to meet strict reliability standards. To achieve this, methodologies like failure modes and effects analysis (FMEA) systematically list failure scenarios and their impacts, while fault tree analysis (FTA) illustrates the relationships between component failures and system-wide malfunctions [2,3]. Markov analysis (MA) employs probabilistic models to forecast system behavior over time, and probabilistic risk assessment (PRA) quantifies the probability and consequences of adverse events [4]. Reliability block diagrams (RBD) complement these tools by visually representing the interdependencies of system components, enabling engineers to accurately identify critical failure points [4-7].

Despite these methodologies, developing renewable energy systems with reliability comparable to conventional power grids presents significant challenges. A significant challenge lies in the inherent instability of renewable energy sources, especially solar PV systems. These systems exhibit output fluctuations due to their dependence on weather conditions, such as cloud cover, temperature shifts, and variations in solar irradiation. For example, abrupt weather changes can cause rapid swings in solar irradiance, leading to sudden spikes or drops in power generation. This variability complicates grid stability, as traditional energy storage solutions like batteries often lack the capacity or response time to buffer such transient power changes effectively [8].

To address these challenges, researchers have focused on fine-tuning the maximum power point (MPP) of photovoltaic modules. The MPP is the specific operating condition where a PV system produces its highest possible power output given the current environmental factors. Advanced maximum power point tracking (MPPT) techniques are essential for dynamically adjusting system parameters to maintain operation at or near the MPP [8]. These techniques are broadly categorized into three groups:

- **Offline Methods:** Offline techniques depend basically on detailed solar cell models to estimate the MPP. In these approaches, the characteristics of the PV module, such as its voltage and current behavior under varying irradiance and temperature, are known in advance, and specific model parameters are used to compute the optimum operating point. Commonly, methods such as the short circuit current (SCC) approach, open circuit voltage (OCV) approach, and artificial intelligence-based methods such as artificial neural networks (ANN) are suggested as popular methods [8]. In practical implementations, these methods aim to identify essential electrical parameters, particularly the V_{OC}, which denotes the voltage in an open-circuit condition, and the I_{SC}, which signifies the current in a short-circuit condition. These approaches achieve their goals by employing two primary strategies; one approach involves actively forcing the system into an open or short circuit state so that the parameter can be measured directly. Alternatively, the values of V_{OC} or I_{SC} can be estimated indirectly by using temperature and irradiance measurements to calculate these parameters. The accuracy of these indirect calculations depends on the accuracy of the characteristic data supplied by the manufacturer; however, an advantage of this computed approach is that it avoids the power interruption that direct measurements may require. Once V_{OC} or I_{SC} is determined, these values are transformed into control signals that continuously direct the PV system toward its MPP. Provided that environmental conditions remain stable, these signals do not change, maintaining a constant operating point.

- **Online Methods:** Contrary to offline strategies, online methods do not require a prior model of the solar cell. Instead, they dynamically track the MPP using real-time measurements of PV voltage and current. These methods introduce a small, systematic perturbation, be it in voltage, current, or duty cycle, to induce a variation in the output power. By analyzing how the output power responds to each perturbation, the system determines whether to increase or decrease the control signal, thereby progressively guiding the operating point toward the MPP. This real-time adjustment leads to a continuously changing control signal and, consequently, introduces slight oscillations about the optimum point. Techniques such as perturbation and observation method (P&O), extremum seeking control method (ESC), and incremental conductance method (IncCond) fall under this category [9,10]. One clear benefit of the P&O approach is that it does not rely on detailed knowledge of the panel's specific characteristics. However, when conditions change rapidly (as under fluctuating irradiance), the P&O method often faces challenges due to the inherent delays in sampling and adjustments, leading researchers to develop numerous improvements to enhance its performance in dynamic conditions [10].

- **Hybrid Methods:** Hybrid methods merge the strengths of both offline and online approaches to achieve a more robust MPPT strategy. Typically, these methods are executed in three phases. First, the system establishes an initial operating point based on offline computations, using predetermined parameters to set a system MPP. Next, this initial value is refined through iterative online fine-tuning loops that continuously adjust the control signal as real-time measurements are acquired. For example, one study [11] integrates the system's impedance and efficiency factors by coupling a DC-DC boost converter with a battery load, which serves as a substitute for the standard load. In this particular hybrid implementation, the control process is structured into two loops: the first loop estimates the MPP from the open circuit voltage under steady temperature conditions, and the second loop employs the P&O method to fine-tune the positioning of the MPP by determining the accurate maximum output power. To ensure that the system responds quickly to changes while also maintaining stable performance, the amplitude and frequency of the perturbations in the online loop are minimized. Graphically, as depicted in Figure 1, the overall control signal is constructed from an offline component that sets the initial target and an online component that continuously refines the target.

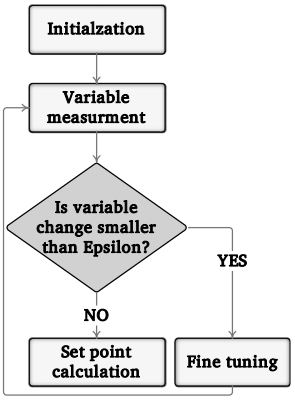

Figure 1. General flowchart used in hybrid MPPT methods.

This study thoroughly examines the impact of various MPPT methods on the reliability of PV systems operating in grid-connected modes and classifies MPPT methods into three main categories to encompass their diverse mechanisms and operational complexities, e.g., offline, online, and hybrid approaches. For a comprehensive analysis, simulations were conducted using three distinct offline methods, which include ANN, OCV, and SCC, alongside two online techniques, P&O and ESC, as well as two hybrid configurations (labeled as hybrid [11] and hybrid [12]). Each of these techniques represents a unique way of tracking the MPP, and by simulating them, the study can compare their performance in a consistent framework. A critical component of the analysis is the dynamic identification of PV system parameters. To achieve this, the RLS algorithm is employed, ensuring that the local PV system model is accurately updated under the influence of each MPPT approach. This allows for an accurate assessment of the PV system's performance across different tracking strategies, capturing real-time variations in operating conditions. To isolate the impact of various MPPT techniques, variations in solar irradiation, an inherently fluctuating factor, are modeled as changes in the set point. This approach ensures that any shifts in the operating conditions, due to irradiance variability, are directly incorporated into the analysis, allowing each MPPT technique to be evaluated on a level playing field. The simulations, carried out within the MATLAB/Simulink environment, yielded clear results that demonstrate direct correlations between the MPPT technique employed and the overall system reliability. These findings highlight the main influence of MPPT strategies on the performance and reliability of PV systems operating in grid-connected mode.

1.1. Innovative Contributions

To highlight and discuss the innovative contributions of this paper, the key points can be summarized as follows**:**

- **RLS-driven dynamic parameter identification for MPPT reliability assessment:** This research introduces the innovative application of the RLS algorithm in combination with varying MPPT techniques to dynamically identify and model localized PV system parameters (e.g., series resistance, shunt impedance). By enabling real-time adaptation of reliability models to changing environmental and operational conditions, it bridges the gap between theoretical MPPT performance and practical system robustness.
- **Hierarchical MPPT categorization framework for reliability benchmarking:** The paper presents an organized classification system for MPPT methods, categorized into offline, online, and hybrid approaches, and benchmarks their reliability impacts through seven distinct algorithms, including recent hybrid techniques. This represents the first comparative analysis connecting MPPT categories to reliability metrics, offering practical guidelines for selecting optimal MPPT strategies based on grid resilience needs.
- **Irradiation set-point isolation methodology:** This innovative approach treats irradiation variations as controlled set-point adjustments rather than stochastic disturbances, effectively isolating the influence of MPPT dynamics on system reliability. By eliminating confounding variables, the methodology precisely attributes reliability fluctuations to specific MPPT behaviors, such as the fluctuations characteristic of P&O methods compared to the more stable transitions achieved by hybrid approaches.
- **Direct correlation between MPPT dynamics and grid reliability:** This study provides conclusive results demonstrating that hybrid MPPT methods (e.g., [11], [12]) reduce grid-side total harmonic distortion compared to conventional online methods like P&O. However, offline methods such as ANN and OCV are shown to compromise transient stability during rapid irradiation shifts. Quantifiable metrics are provided to inform the design of fail-safe PV systems for critical grid applications.

1.2. Paper Organization

This research is presented through the following step-by-step structure to achieve its objectives. Section 2 establishes the context for the present research by describing the architecture of the grid-connected PV system under study. It analyzes the operational principles of selected MPPT algorithms and develops mathematical models for critical system components. A dedicated subsection examines PV system parameter identification, comparing how different MPPT strategies affect the accuracy of these estimations. For example, it evaluates the influence of voltage ripple patterns in perturbative MPPT methods on parameter estimation under dynamic

weather conditions. Section 3 presents a detailed comparative analysis of simulation results, assessing the impact of various MPPT techniques, from conventional P&O to hybrid ANN-based methods, on long-term system reliability metrics. These metrics include component degradation rates, inverter stress profiles, and grid synchronization stability during irradiance transients. The section also employs quantitative benchmarking to link MPPT-induced electrical oscillations with failure probabilities. Section 4 extends the analysis to explore distribution network impacts, investigating how MPPT-driven power fluctuations affect grid infrastructure. This includes harmonic distortion analysis, voltage regulation challenges during partial shading events, and protection coordination requirements for varying levels of PV penetration. Case studies are included to demonstrate how adaptive MPPT configurations can mitigate cascading reliability risks in weak grid conditions. Section 5 integrates empirical and theoretical findings into actionable insights, highlighting the relationship between MPPT algorithm complexity and measurable improvements in both energy yield and system lifespan. The conclusion proposes updated cost-benefit paradigms that reflect the reliability gains associated with advanced MPPT strategies, offering new perspectives on PV system affordability based on lifecycle performance.

2. System Under Investigation

To thoroughly analyze the influence of MPPT techniques on the reliability of PV systems operating in grid-connected mode, it is essential to create a robust and detailed PV model that appropriately represents the complex interdependencies among key system parameters, including solar irradiation, temperature, and electrical properties. This detailed model serves as the foundation for understanding how fluctuations in these factors influence the overall performance and stability of the system. The system model under investigation, exemplifying an integrated PV power system, is depicted in Figure 2, providing a clear visual framework for subsequent analyses of different MPPT strategies.

2.1. Modeling of PV Cells

Accurate modeling of PV cells serves as a foundational requirement for both software simulations and data analysis, enabling the evaluation and verification of the operational performance of PV power generation systems [13]. Central to this modeling effort is the accurate prediction of the voltage-current (*V-I*) characteristic curve, which defines the electrical output profile of the PV cell. Notably, environmental variables, primarily solar irradiance and temperature, exert substantial influence on the cell's output voltage and current, as demonstrated by the comparative analyses in Figures 3 and 4. These fluctuations necessitate the use of adaptive modeling strategies to replicate real-world performance. To address this, researchers have developed diverse electrical circuit configurations that emulate PV module dynamics under shifting environmental parameters [14]. For instance, circuit models are designed to account for irradiance-dependent current generation and temperature-induced variations in semiconductor properties, enabling precise simulation of how modules respond to real-world operational stresses. By integrating these topological variations, models can better approximate the nonlinear relationships between environmental inputs and electrical outputs, ensuring reliable system evaluation across diverse climatic scenarios.

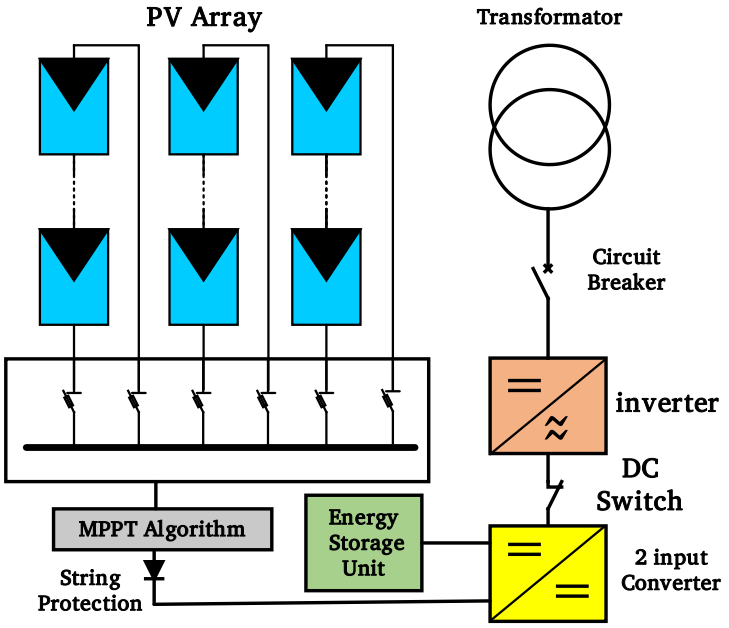

Figure 2. The configuration of the investigated PV system.

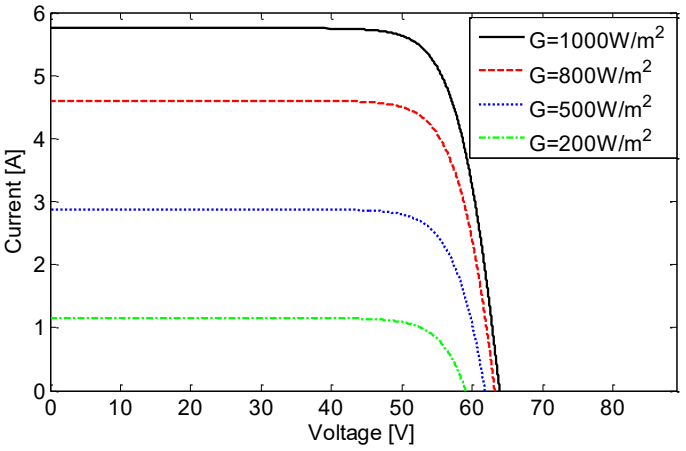

Figure 3. The influence of changes in ambient irradiation levels on the current-voltage (I–V) characteristics.

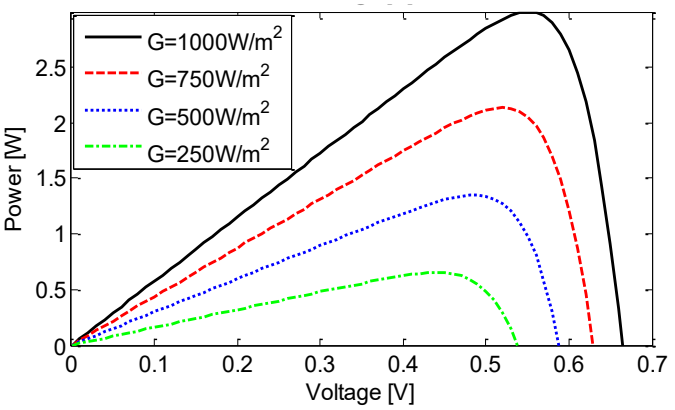

Figure 4. The effect of varying ambient irradiation levels on the characteristics of power-voltage (P–V) curve profiles.

Figure 5 illustrates the single-diode PV cell model, which utilizes an equivalent electrical circuit consisting of a light-sensitive current source, a diode, and two resistances, one in series and the other in shunt. This framework is mathematically defined by an adaptation of the Shockley diode equation [15], which accounts for resistive losses inherent to real-world PV cells. In this configuration: I_{ph} (photocurrent) quantifies the current generated by photon absorption in the semiconductor material. I_d (diode reverse saturation current) characterizes the leakage current under reverse bias, influenced by temperature and material properties. R_s (series resistance) represents resistive losses in metal contacts, busbars, and semiconductor bulk regions. R_{Sh} (shunt resistance) models leakage pathways across the cell's p-n junction, often caused by manufacturing defects. The interplay of these components governs the nonlinear voltage-current (*V-I*) relationship of the PV cell, formally expressed in Equation (1) [16]. This equation modifies the ideal diode law by incorporating voltage drops across R_s and current through R_{Sh}, enabling precise simulation of real-world cell behavior. For instance, R_s reduces the effective output voltage under high current loads, while R_{Sh} introduces parasitic losses at low irradiance levels. The accuracy of the model in reproducing empirical *V-I* curves (as shown in Figure 5) makes it indispensable for predicting performance degradation, optimizing MPPT algorithms, and evaluating efficiency losses under partial shading or aging effects.

$$I = N_P I_{Ph} - N_P I_d \left[exp\left(\frac{qV}{kTAN_S} - 1\right)\right] \quad (1)$$

Within PV system modeling, I (measured in amperes) defines the operational current produced by the PV array under load conditions, while V (in volts) represents the terminal voltage generated across the array's output. The architectural design of the PV system is shaped by two key parameters: 1) N_s: the count of solar cells connected in series, which scales the system's output voltage proportionally; and 2) N_p: the number of parallel-connected cell strings, which enhances current-carrying capacity to mitigate shading or mismatch losses. Fundamental physical constants embedded in the model include q (electron charge, $\sim 1.602 \times 10^{-19}$ C), governing charge carrier dynamics, and k (Boltzmann constant, $\sim 1.381 \times 10^{-23}$ J/K), linking thermal energy to semiconductor behavior. The dimensionless parameter A (ideality factor) quantifies deviations from ideal diode characteristics, reflecting recombination losses in the p-n junction. Values between 1 (ideal diode) and 5 (highly non-ideal) correlate with material defects, doping irregularities, or operating temperature extremes [17]. The reverse saturation current (I_d), representing leakage current under reverse bias, is temperature-dependent and influenced by minority carrier concentrations. It is derived analytically through Equation (2) [18], which incorporates material bandgap energy, intrinsic carrier density, and junction geometry.

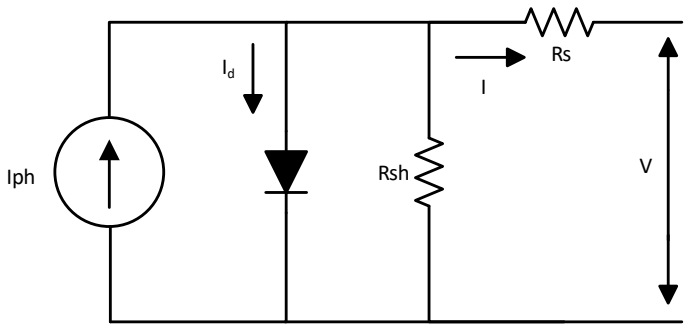

Figure 5. The single-diode equivalent circuit model for a PV cell.

Meanwhile, T (cell temperature in Kelvin) critically modulates both I_d and the thermal voltage (kT/q), with elevated temperatures reducing open-circuit voltage (V_{OC}) while marginally increasing short-circuit current (I_{SC}). This interdependence highlights the need for temperature-compensated MPPT algorithms in practical applications.

$$I_d = I_c[T/T_c]^3 exp\left[\left(q\frac{E_g}{KA}\right)\left(\frac{1}{T_c}-\frac{1}{T}\right)\right] \quad (2)$$

Within the PV cell's operational model, three critical parameters control temperature-dependent performance characteristics: T_C (reference temperature), I_c (reference saturation current) and E_g (band gap energy). These variables collectively determine the temperature-dependent behavior of the Shockley diode equation. For instance, E_g directly affects the temperature coefficient of I_c, as narrower bandgap materials exhibit stronger thermal degradation of V_{OC}. Meanwhile, deviations from T_C require recalibration of I_c to account for thermally accelerated carrier recombination, a process modeled in Equation (2). The interdependence of these parameters underscores their role in predicting efficiency losses under real-world thermal cycling conditions.

Equation (3) introduces a refined analytical framework for calculating the I_d in PV cells, explicitly addressing temperature-dependent carrier dynamics [19]. This enhanced formulation integrates three critical thermal effects: I) thermally activated carrier generation, which accounts for increased electron-hole pair generation at elevated temperatures, amplifying I_d through enhanced minority carrier concentrations; II) bandgap narrowing: models the temperature-induced reduction in semiconductor bandgap energy (E_g), which reduces the potential barrier for carrier recombination, directly influencing I_d exponential dependence on T, and III) non-ideal junction behavior: Incorporates temperature-dependent deviations from ideal diode characteristics via adjustments to the ideality factor (A), particularly under high-injection conditions. The equation resolves limitations in conventional I_d models by coupling these mechanisms through a multiplicative correction factor. For instance, it quantifies how a 10°C temperature rise in crystalline silicon cells increases I_d by approximately 7–9%, critically impacting MPP and maximum power (P_{max}) stability. By embedding these relationships, the model enables precise prediction of efficiency losses during thermal transients, such as midday irradiance spikes or partial shading-induced hot-spot heating. This advancement supports the design of temperature-resilient MPPT algorithms, particularly for grid-connected systems operating in climates with wide daily temperature variations.

$$I_d = \frac{q\left(I_{SC,T_c} + K_I\Delta T\right)}{exp\left[\left(V_{OC,T_c} + K_V\Delta T\right)/AKT\right] - 1} \quad (3)$$

Within this framework, the symbols I_{SC,T_c} and V_{OC,T_c} designate the short-circuit current and open-circuit voltage measured at a specific reference temperature, T_C. Here, K_I serves as the coefficient that characterizes how the short-circuit current adjusts with temperature changes, while K_V is the corresponding coefficient for the open-circuit voltage. The term ΔT, defined as $T - T_C$, quantifies the deviation between the current cell temperature, T, and the reference temperature, T_C. Additionally, the photocurrent (I_{ph}) mentioned in Equation (1) is sensitive to variations in both solar irradiation and the cell's temperature. Its variation with these factors is mathematically captured by the formula provided, which delineates the interplay between environmental conditions and the cell's electrical output. This formulation is critical for understanding and accurately modeling the behavior of photovoltaic cells under diverse operating conditions as in Equation (4).

$$I_{ph} = [I_{scr} + K_i(T - T_c)][S/100] \quad (4)$$

In this equation, I_{scr} represents the cell's short-circuit current measured at the reference temperature and a standard radiation level. K_i is the temperature coefficient that quantifies how the I_{scr} changes with variations of temperature, and S denotes the solar irradiation, expressed in mW/cm^2. Using these parameters, the total output power of the PV array can be calculated with the subsequent equation as in Equation (5).

$$P = V \times I \quad (5)$$

To determine the MPP of the array, the process begins by analyzing the variation in output power (P) in response to changes in voltage (V). The MPP is achieved when the rate of change of power with respect to voltage is zero, which we mathematically express as: $(dP/dV) = 0$. At this specific point, any infinitesimal change in voltage does not cause a corresponding change in power, indicating that the system is operating at its optimal condition. Deriving this zero-slope condition gives rise to the following equation that defines the MPP precisely in mathematical terms.

$$exp\left(\frac{qV_{max}}{KTAN_s}\right)\left[\left(\frac{qV_{max}}{KTAN_s}\right)+1\right]=\left(I_{ph}+I_d\right)/I_d \quad (6)$$

By rearranging Equation (5) algebraically, we derive V_{max}, representing the voltage at which the array achieves its peak power output. The output voltage generated by a PV cell is not an isolated phenomenon; it is inherently linked to the photocurrent produced within the cell. This photocurrent is primarily dictated by both the load current and the level of solar irradiation that the cell experiences during operation (refer to [15,20] for further details). The following equation presents this interdependent relationship, providing a clear mathematical framework for how these parameters work together to determine V_{max}.

$$V=\left(\frac{AKT}{a}\right)ln\left[\left(I_{ph}+I_d-I\right)/I_d\right]-R_sI \quad (7)$$

Adjusting solar radiation (S) and cell temperature (T) within Equations (1) to (6) enables the simulation of the $I-V$ and $P-V$ characteristics of a PV array [21]. A similar MATLAB-based simulation procedure for PV arrays, accounting for diverse shadow patterns and temperature conditions, was proposed in [22].

At the V_{OC}, the predictions of the single-diode model start to deviate significantly from experimental observations, particularly in scenarios with low irradiance levels [23]. This divergence highlights a significant limitation of the model, which is founded on the premise that recombination losses within the depletion region are negligible and can be disregarded. In reality, however, recombination plays a significant role as a source of loss in actual solar cells, its effect being particularly pronounced at lower voltage levels. Consequently, by disregarding these recombination losses, the single-diode model fails to accurately depict the cell's behavior when operating near V_{OC}, highlighting its inadequacy for precise modeling under such conditions [24].

2.2. PV Array Efficiency

The performance of a solar cell is determined by the complex interaction of key parameters such as solar irradiance, temperature, and overall resistance. This intricate relationship results in a non-linear dependency between the operating conditions and the efficiency of the cell. A primary method to analyze this behavior is through the current–voltage (I-V) characteristic curve, which captures how variations in these parameters affect the cell's performance. For instance, as demonstrated in Figures 3 and 4, an increase in solar irradiance leads to a significant boost in the short-circuit current, while the open-circuit voltage remains almost unchanged. In practical terms, because the peak power output is closely related to the short-circuit current, higher irradiation levels directly translate into increased power generation. Conversely, when the temperature elevates, the short-circuit current shows a modest increase; however, this is counterbalanced by a slight decline in the open-circuit voltage. Hence, the optimal power generation occurs at the precise intersection of the current source behavior and the voltage source behavior, a condition defined as the MPP. To ensure that the PV cells consistently operate at this optimal point, MPPT algorithms are employed. Despite these measures, PV systems encounter two primary challenges. The first challenge is that the conversion efficiency of generating electrical power remains relatively low, typically in the range of 9–25%, a situation that worsens under conditions of low irradiance. The second challenge is that the power output is inherently variable, as it continuously fluctuates with the changing patterns in the weather.

Analyzing MPPT behavior involves evaluating performance in both static and dynamic scenarios. In static conditions, MPPT efficiency specifically refers to the algorithm's ability to accurately detect and sustain the MPP when environmental factors, such as solar irradiance and temperature, are constant. Under these conditions, efficiency ($\eta_{inst}(t)$) is computed as an average over a predefined time interval once the system has reached a stable steady state. This stabilization period, or transient phase, may last several seconds, depending on the prevailing operating conditions. In contrast, dynamic MPPT efficiency considers the capability of the algorithm to continuously track the shifting MPP as environmental conditions vary. Here, the system's response is monitored in real time, and instantaneous efficiency is determined by comparing the actual measured power output against the ideal power output, theoretically calculated for the current level of irradiation. This calculation follows the formula provided in [25].

$$\eta_{inst}=\frac{P_{pv-meas}}{P_{MPP-ideal}}*100 \rightarrow for\ k\ \ number\ of\ samples: \frac{1}{k}\sum_{i=0}^{k}\frac{P_{pv-meas}}{P_{MPP-ideal}}*100 \quad (8)$$

In this framework, the symbol η_{inst} denotes the steady-state efficiency, which quantifies the PV system's performance under constant operating conditions. Meanwhile, $P_{pv-meas}$ refers to the actual power output produced by the solar panel, reflecting its real-world performance under the given circumstances. In contrast, $P_{MPP-ideal}$ represents the theoretical maximum power that the solar panel is capable of generating under ideal, controlled conditions. By recording the values of $P_{PV-meas-mean}$ and $P_{MPP-ideal-mean}$ during these dynamic tests, an equivalent efficiency can be exactly computed using the formula provided in [26].

$$\eta_{dynamic}=\frac{P_{pv-meas-mean}}{P_{MPP-ideal-mean}}*100 \quad 9)$$

In the given expression, the dynamic efficiency $\eta_{dynamic}$ is determined by comparing two averaged power values over the entire duration of the test. The first value is the mean of the measured power output $P_{PV-mean-mean}$ is obtained by recording the instantaneous power throughout the entire testing duration. The second value represents the average of the maximum power, $P_{MPP-ideal-mean}$, predicted by the PV model over the same period.

2.3. Comparative Evaluation of Set Point Tracking Across Various MPPT Techniques

A set point refers to a predefined target value that a control system aims to maintain or reach. When the controller employs set point tracking, it continuously adapts to align the target value with the current process value. In this paper, "set point tracking"

specifically refers to the process of continuously monitoring and maintaining the MPP as irradiation conditions change. For the offline evaluation, various techniques, namely OCV, SCC, and ANN, were simulated under dynamic irradiance conditions (see Figure 6 for the irradiance profiles). The corresponding outcomes of these simulations are displayed in Figure 7. The results clearly show that the ANN method is exceptionally precise in tracking the MPP when irradiance is variable. On the other hand, both the OCV and SCC approaches produce estimates of the MPP; however, the accuracy of them is compromised by interruptions in power supply. These disruptions can be attributed to the inherent need of the OCV and SCC approaches to measure the V_{OC} and I_{SC}, respectively. Among these, the SCC method offers better tracking performance compared to the OCV method. In addition to the offline techniques, the study also examined online methods, specifically, P&O and ESC, as well as hybrid strategies described in [11,12]. The simulation results presented in Figures 8 and 9 highlight notable variations in performance; while the P&O algorithm struggles to reliably follow the MPP during sudden shifts in irradiance, the ESC method, along with the hybrid techniques, demonstrates a considerably stronger ability to uphold the MPP under such dynamic conditions.

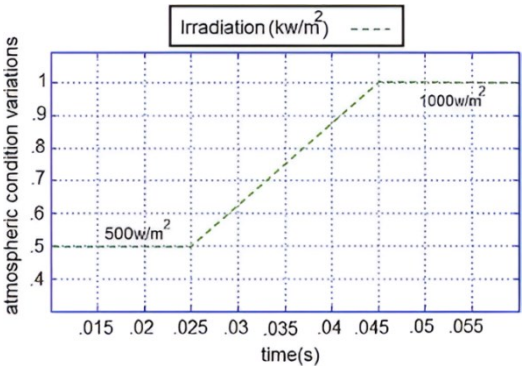

Figure 6. The dynamic patterns of solar irradiation over time.

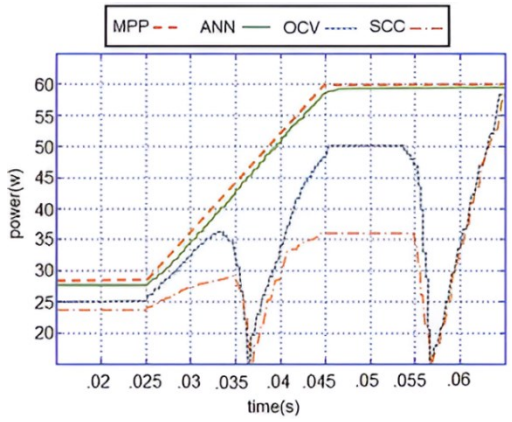

Figure 7. PV system output power under the offline MPPT method during dynamic irradiance conditions.

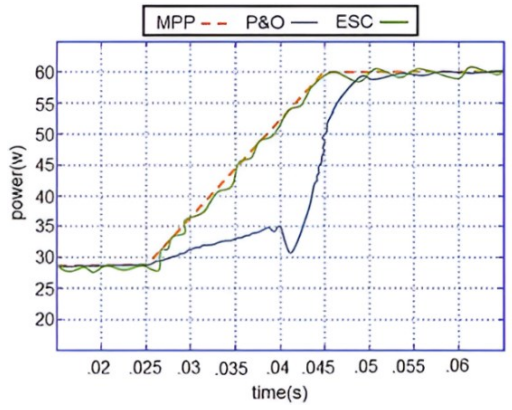

Figure 8. PV output power using online MPPT method under varying irradiance conditions.

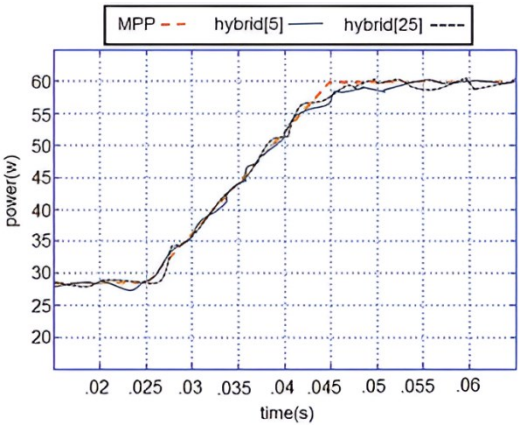

Figure 9. PV output power using a hybrid MPPT technique under fluctuating irradiance conditions.

Stability indices for the voltage output of PV systems are crucial in evaluating performance under varying conditions. Here are some notable indices used in assessing PV voltage stability: 1) Total voltage deviation index (TVDI): Measures fluctuations in the DC output voltage of PV systems. It helps assess system stability under dynamic conditions; voltage deviation refers to the variation between the output voltage of the PV system and the voltage at the MPP. A smaller deviation indicates improved voltage stability within the system. As expressed in Equation (10), the TVDI quantifies this deviation by summing the squared absolute differences between the PV output voltage and the MPP voltage across all PV arrays in the system. and 2) Dynamic voltage stability index (DVSI): Evaluates the ability of the PV system to maintain stable voltage under transient events such as sudden load changes or shading. A voltage recovery issue arises when the deviation in voltage exceeds 0.2, indicating instability in the system. The DVSI is computed based on Equation (11). In doing so, the voltage deviation for each PV panel is determined based on the steady-state voltage at the MPP condition. Based on the extracted shape of the TVDI, the graph corresponding to method hybrid [25] demonstrates excellent performance and maintains strong stability (see Figure 10). Additionally, methods hybrid [5], ESC, and ANN follow in terms of stability ranking. Furthermore, the results illustrated in Figure 11 for the (DVSI fully support this assessment.

$$TVDI = \sum_{i=1}^{N} |V_{PV-meas} - V_{MPP}|^2 \tag{10}$$

$$DVSI = \frac{V_{St}^{i} - V_{PV-meas}^{i}}{V_{c_t}^{i}} \tag{11}$$

Where N is the total number of PV panels, $V_{PV-meas}$ is the actual output voltage produced by the PV panels, V_{MPP} is the theoretical maximum voltage that the solar panel is capable of generating under MPP condition, and V_{St}^{i} is the actual steady-state voltage at the MPP condition.

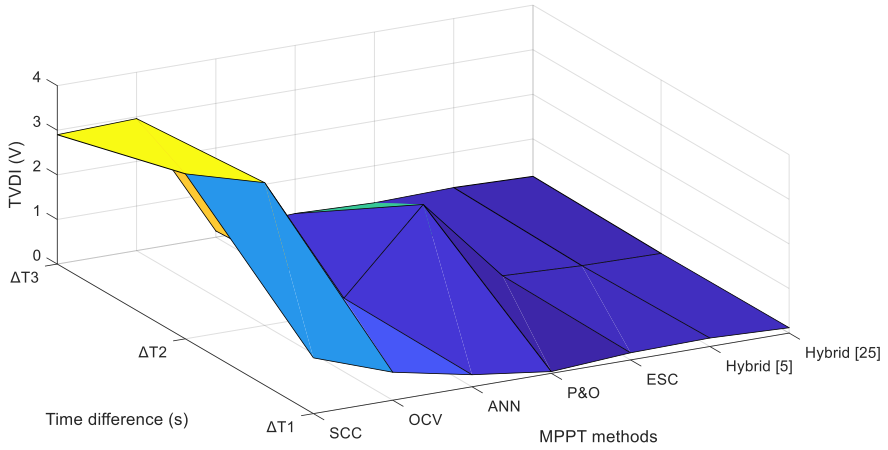

Figure 10. TVDI for a PV system utilizing various MPPT techniques under fluctuating irradiance conditions; $\Delta \boldsymbol{T_1} = \boldsymbol{0} < \boldsymbol{T} \leq \boldsymbol{0.025s}, \Delta \boldsymbol{T_2} = \boldsymbol{0.025s} < \boldsymbol{T} \leq \boldsymbol{0.045s}, \boldsymbol{T} > \boldsymbol{0.045s}$.

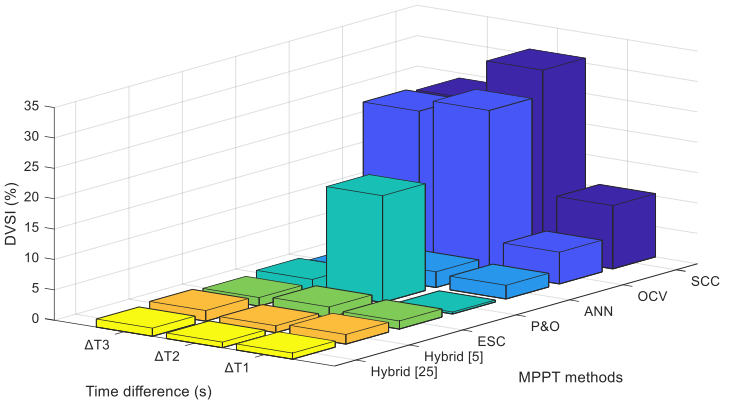

Figure 11. DVSI for a PV system utilizing various MPPT techniques under fluctuating irradiance conditions; $\Delta T_1 = 0 < T \leq 0.025s, \Delta T_2 = 0.025s < T \leq 0.045s, T > 0.045s$.

2.4. System Identification

We appreciate the respected referee's opinion and thank you for this question. System identification involves constructing empirical models of dynamic systems when their exact parameters or physical foundations are uncertain. This method generally implies that system dynamics can be estimated with high precision, eliminating the necessity for modeling. Hence, the primary objective of this method is to implement numerical optimization methods for model parameterization, enabling accurate prediction of nonlinear system behavior and stability analysis. Indeed, one of the key contributions of this article is the introduction of a comprehensive method that removes the necessity for dynamic modeling of the methods being analyzed. Without this innovation, it would be required to model the converter and then carry out dynamic modeling for each MPPT method under investigation. Consequently, system identification focuses on constructing mathematical models that reflect the inherent dynamics of a system by examining its input–output data. This process is crucial as it facilitates the creation of accurate models, which serve as a foundation for effective control strategies and reliable predictive analyses. So, to evaluate the dependability of the system, it is essential to identify its key parameters across a variety of atmospheric conditions. The RLS algorithm operates as an adaptive filter, adjusting its coefficients iteratively to reduce a weighted error based on the linear least squares principle associated with the input signals. In real-time applications, both the input and output data are processed sequentially at predetermined sampling intervals. Adaptive or self-adjusting control systems depend on continuously revising parameter estimates whenever new data samples are acquired. This continuous updating is typically achieved through online recursive strategies, which allow engineers to monitor and adjust parameter values as they evolve in real time. Owing to their computational efficiency, these recursive techniques are especially advantageous for implementation in microprocessor-based environments [27]. Furthermore, the dynamics of the transfer functions obtained in Equation (12) can be described by a linear difference equation that represents the relationship between the system's input and output.

$$G(Z^{-1}) = \frac{Y(Z^{-1})}{U(Z^{-1})} = \frac{b_1 + b_2 z^{-2} + b_3 z^{-3} + b_4 z^{-4} + \cdots + b_n z^{-n}}{1 + a_1 Z^{-1} + a_2 Z^{-2} + a_3 Z^{-3} + a_4 Z^{-4} + \cdots a_m Z^{-m}} \quad (12)$$

There are various approaches available to derive Equation (12); however, this work employs the relatively straightforward autoregressive exogenous (ARX) technique [28]. An ARX model integrates an autoregressive component with an exogenous input component to characterize and simulate the dynamic behavior of a system. By applying this method, the corresponding difference equation for the system's inputs and outputs can be formulated (see Equations (13) to (16)).

$$y(k) = -a_1 y(k-1) - a_2 y(k-2) - a_3 y(k-3) - \cdots - a_m y(k-m) + b_1 u(k-1) + b_2 u(k-2) + b_3 u(k-3) + \cdots + b_n u(k-n) + \lambda(k) \quad (13)$$

Within this framework, the notation y(k) represents the output signal, which corresponds to the power generated by the PV module. Conversely, u(k) denotes the input signal that captures the fluctuations in irradiance.

The sequence of parameters [a_1, a_2, …, a_n, b_1, b_2, …, b_n] comprises the coefficients that must be determined through estimation. In addition, the term $\lambda(k)$ is introduced as a white noise process with a normal distribution, characterized by a zero mean and a variance of 0.05, representing the random disturbances in the system.

$$\hat{\theta}(k) = \hat{\theta}(k+1) + \frac{P(k+1)\varphi(k)}{1 + \varphi^T(k)P(k-1)\varphi(k)} \times \varepsilon(k) \quad (14)$$

$$\varepsilon(k) = y(k) - \theta^T(k-1)\varphi(k) \quad (15)$$

$$P(k) = P(k-1) - \frac{P(k+1)\varphi(k)}{1 + \varphi^T(k)P(k-1)\varphi(k)} \times \varphi^T(k)P(k-1) \quad (16)$$

Within this framework, $y(k)$ is defined as the output power of the PV module. The regression vector $\varphi(k)$ encapsulates past and current input data, the estimated parameter vector $\hat{\theta}(k)$ contains the system's coefficients, and the prediction error $\varepsilon(k)$ quantifies

the difference between the model's output and the measured output. Moreover, $P(k)$ represents the covariance matrix associated with the estimation process.

To thoroughly analyze PV performance, output power data were collected over 730 hours from simulations using four distinct MPPT methods: ANN (typifying offline methods), P&O (representing online approaches), and two hybrid techniques as detailed in [11] and [12]. This comprehensive dataset was then utilized to build an ARX time series model, which has been determined to be the most effective for capturing the dynamic behavior of PV power. The parameters for each MPPT method, as derived from the ARX model, are presented as follows in Equations (17) to (20):

$$W_1(k) = 1.9874W_1(k-1) + 0.354W_1(k-2) - 0.5412W_1(k-3) + 0.4071u(k-1) + 0.987u(k-2) - 0.1004u(k-3) + \lambda(k) \quad (17)$$

$$W_2(k) = 1.305W_2(k-1) + 0.447W_2(k-2) - 0.369W_2(k-3) + 0.49811u(k-1) + 0.505u(k-2) - 0.0924u(k-3) + \lambda(k) \quad (18)$$

$$W_3(k) = 1.237W_3(k-1) - 0.0127W_3(k-2) + 0.347W_3(k-3) + 0.7151u(k-1) + 0.834u(k-2) - 0.121u(k-3) + \lambda(k) \quad (19)$$

$$W_4(k) = 0.924W_4(k-1) + 0.455W_4(k-2) - 0.612W_4(k-3) + 0.55051u(k-1) + 0.699u(k-2) - 0.1214u(k-3) + \lambda(k) \quad (20)$$

Here, $W_1(k)$, $W_2(k)$, $W_3(k)$, $W_4(k)$ represent the output power of the PV module, measured under each of the four MPPT strategies: the ANN method, the P&O method, and the two hybrid approaches as detailed in [11] and [12].

2.5. Reliability

This study utilizes the loss of load probability (LOLP) as a key metric to evaluate the reliability of the entire system. The LOLP serves as a measure to determine the probability that, during a defined timeframe (such as one month), the total energy demand will exceed the amount of power generated by the system. Leveraging this measure, the loss of load expectation (LOLE) can be derived. The LOLE estimates the average number of hours in a month during which an imbalance, caused by demand exceeding generation, is expected to occur. The calculation of LOLE is carried out using the formula provided in Equations (21) to (23).

$$LOLE = \sum_{i=1}^{730} [(W_t(i) + W_{batt}(i)) - P_l(i) < 0] \quad (21)$$

$$W_t(i) = W(k) - W_l \quad (22)$$

$$W(k) = -a_1W(k-1) - a_2W(k-2) - a_3W(k-3) - \cdots - a_mW(k-m) + b_1u(k-1) + b_2u(k-2) + b_3u(k-3) + \cdots + b_nu(k-n) + \lambda(k) \quad (23)$$

In this formula, the first parameter $W_t(i)$ denotes the validity coefficient of the PV module capacity, a factor that quantifies the effective capacity of the PV module under its operating conditions. Next, the term $W(k)$, representing actual power generation, refers to the real-time output of the entire PV module, fully accounting for the effects of irradiance variations throughout the statistical period for each MPPT method. Another parameter W_l in the formula corresponds to the power generation loss incurred due to PV module outages, capturing the impacts of any interruptions on energy yield. Additionally, W_{batt} defines the total power available from the battery pack when operating in discharge mode. Finally, $P_l(i)$ indicates the effective load power, which accounts for the gap between the demanded load and the losses in power generation that are influenced by the power grid.

3. Analysis of Simulation Outcomes and Interpretation

This section details the methodology employed to evaluate the performance of the PV system, focusing on its reliability and operational efficiency. The evaluation was carried out using four unique MPPT strategies, namely ANN, P&O, and two hybrid techniques as described in the studies cited in [11,12]. All the simulations were executed within the MATLAB software environment. A critical aspect of assessing the impact of the different MPPT strategies on the PV system's reliability is the precise modeling of solar irradiation. Since irradiation exhibits continuous fluctuations and varies with geographic location, capturing these dynamics accurately is essential.

To achieve this, an irradiance model is implemented, precisely simulating the temporal variations of solar energy over a predetermined period. For the specific PV system under analysis, the model generated simulations of daily solar irradiation patterns, as depicted in Figure 12. Based on these data, Figure 13 provides a detailed comparison of the evaluated efficiency as a function of PV output power for the various MPPT techniques under study. The performance of a PV system in generating electricity is heavily influenced by weather conditions. While maximum power is generated on sunny days, sudden cloud-induced shading diminishes both efficiency and output.

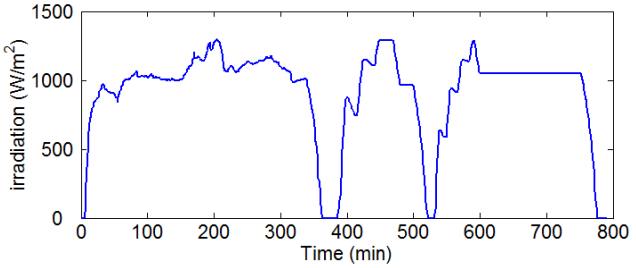

Figure 12. Variation of solar irradiation.

Shading refers to any obstruction that prevents sunlight from reaching the PV panels and can also result from accumulated dust, which gradually reduces system efficiency. Additionally, the efficiency and output of a PV system are influenced by various factors, such as increased temperatures and abrupt changes in irradiance. Therefore, an effective MPPT algorithm is essential to enhance system performance, ensuring maximum power tracking and addressing these issues.

In this illustration, each curve shown in Figure 13 represents the efficiency performance of its respective MPPT method as the output power from the PV module changes. It is important to note that this efficiency diagram is derived under idealized conditions, excluding any losses attributed to secondary power stage components. Specifically, the diagram omits reductions due to power semiconductor device losses, the inherent losses in the output inductor, and the power consumption attributed to both the control circuit and its associated driver circuit. This exclusion allows for a focused evaluation of the intrinsic performance of the MPPT strategies, isolating the impact of the MPPT algorithm on the PV system's efficiency without interference from losses in the main power conversion components. Tables 1 to 4 present the operating performance and key metrics of a PV power generation system when the different MPPT approach is applied.

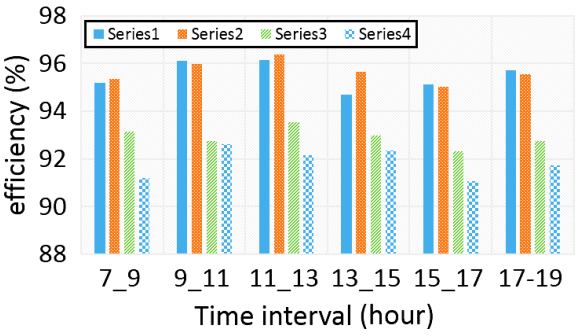

Figure 13. The measured conversion efficiency of the PV system as a function of its output power. Series 1 represents the hybrid method [11], series 2 represents the hybrid method [12], series 3 corresponds to the P&O method, and series 4 corresponds to the ANN method.

Table 1. Operating performance and key metrics of a PV module when applying the ANN MPPT approach.

Solar irradiance (W/m^2)	The PV power capacity (W)	
	in	out
900-1000	10100	900
800-900	9780	1200
700-800	9150	1850
600-700	8340	2660
500-600	7260	3740
400-500	7015	3985
300-400	6740	4260
200-300	6420	4580
100-200	6229	4771

Table 2. Operating performance and key metrics of a PV module when applying the P&O MPPT approach.

Solar irradiance (W/m2)	The PV power capacity (W)	
	in	out
900-1000	10350	650
800-900	10020	980
700-800	9089	1911
600-700	8979	2021
500-600	8445	2555
400-500	7565	3435
300-400	6730	4270
200-300	6659	4341
100-200	6467	4533

Table 3. Operating performance and key metrics of a PV module when applying the hybrid [11] MPPT approach.

Solar irradiance (W/m2)	The PV power capacity (W)	
	in	out
900-1000	10778	212
800-900	10410	590
700-800	9961	1039
600-700	9473	1527
500-600	9156	1844
400-500	8567	2433
300-400	8008	2992
200-300	7352	3648
100-200	7011	3989

The comparative analysis illustrated in Figure 14 reveals that incorporating hybrid MPPT strategies into the PV system consistently improves the LOLE metric. This finding highlights that hybrid approaches effectively reduce load loss, thereby enhancing the system's overall reliability. A detailed examination of these indices indicates that applying hybrid MPPT methods, rather than solely relying on offline or online techniques, leads to significant changes in the average duration of annual outages. However, the analysis also reveals that as hybrid methods are increasingly adopted, the degree of improvement in the load point's LOLE under PV power conditions gradually diminishes.

4. Distribution System Studies

The primary objective of electrical power systems is to supply electricity to consumers in a manner that is both reliable and cost-effective. Simply put, the reliability of the system reflects its ability to consistently meet energy demands by delivering the required electricity. To evaluate performance, a set of metrics known as electric power distribution reliability indices [29] is utilized to assess the behavior of electrical distribution networks. Central to reliability assessments of electrical distribution systems are parameters that quantify their operational performance over time. These parameters include the average failure rate (denoted as λ), which represents the frequency at which system components fail within a specified time frame. It provides critical insight into the overall reliability of the network's infrastructure. Another significant parameter is the typical outage duration (denoted as r), which reflects the average amount of time required to restore functionality after a failure occurs. This metric is pivotal for evaluating the efficiency of maintenance and repair processes. Additionally, the average annual outage time (denoted as U) measures the cumulative time over a year during which the system is unavailable or not meeting energy demands. This value is essential for assessing the long-term performance and impact of outages on consumers and operations.

These variables are typically derived by employing statistical models, such as exponential distribution models, which are widely used in reliability engineering. These models estimate the likelihood of failure and repair times by analyzing the time intervals between successive failures and the durations needed for repairs. The exponential distribution assumes that events occur at a constant rate, making it well-suited for scenarios where failure and repair events are random but follow predictable patterns. This methodology is detailed mathematically in Equations (24) to (26), where the relationships between failure rates, outage durations, and cumulative outage times are formulated to ensure accurate and comprehensive evaluations of system reliability.

Among the critical indices utilized in utility systems to assess reliability are the system average interruption frequency Index (SAIFI) and the system average interruption duration index (SAIDI). SAIFI provides a measure of the frequency of service interruptions by calculating the average number of outages experienced by individual customers within a given time frame. This index is essential for determining the regularity of disruptions and identifying areas where infrastructure improvements may be needed. In contrast, SAIDI evaluates the cumulative duration of these interruptions, representing the average time customers are without electricity during outages. This metric is pivotal for understanding the impact of service disruptions in solar systems on customer satisfaction and operational efficiency. Table 5 offers a comprehensive summary of the primary indices applied in assessing the performance of electrical power systems considering solar power generation.

Table 4. Operating performance and key metrics of a PV module when applying the hybrid [12] MPPT approach.

Solar irradiance (W/m2)	The PV power capacity (W)	
	in	out
900-1000	10533	467
800-900	10256	744
700-800	10002	998
600-700	9467	1533
500-600	9139	1861
400-500	8733	2267
300-400	8144	2856
200-300	7466	3534
100-200	7109	3891

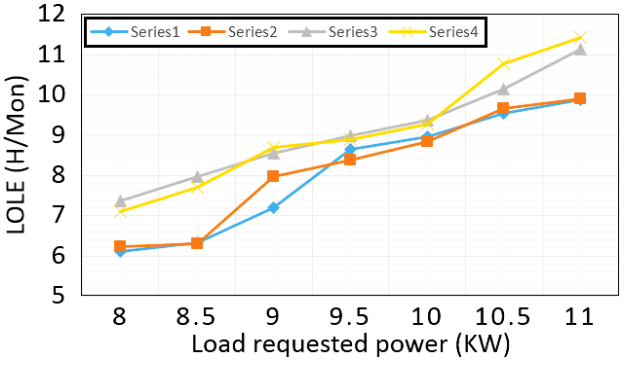

Figure 14. The LOLE, expressed in hours per month, for a PV module under different load requirements. The graph is divided into four series corresponding to the different MPPT methods. Series 1 to 4 represent the same methods as described in Figure 11.

These indices serve as valuable tools for utility providers to monitor, evaluate, and enhance the reliability and efficiency of their networks, ensuring consistent and dependable power delivery to consumers.

$$\lambda_s = \sum_{i=1} \lambda_j \tag{24}$$

$$U_s = \sum_{i=1} \lambda_j r_j \tag{25}$$

$$r_s = \frac{U_s}{\lambda_s} = \frac{\sum_{j=1} \lambda_j r_j}{\sum_{i=1} \lambda_i} \tag{26}$$

As shown in Figure 15, the distribution system used to analyze the impact of MPPT methods on reliability indices consists of 4 main feeders, 31 primary lines, 73 lateral lines, and 54 load points. A total of 3,080 customers are connected across all feeders. Each feeder includes a variety of components, such as lines, breakers, disconnect switches, and fuses. The primary system components are distribution lines or a combination of lines with disconnect switches, while lateral system parts typically include lines, fuses, or their combinations. Additional system specifications are detailed in Table 6.

The process of repair and switching within the system is characterized using log-normal distributions to reflect the inherent variability in response times. Specifically, the repair duration for power lines follows a log-normal distribution with a standard deviation of 4 hours, capturing the fluctuations in maintenance efforts due to varying conditions such as weather, accessibility, and resource availability. Likewise, the switching times associated with system elements are modeled using the same statistical distribution, but with a much lower standard deviation of 0.4 hours, highlighting the relatively swift nature of reconfiguration actions.

In terms of failure rates, the probability of faults occurring in lines and cables is largely dependent on their physical lengths (L), as longer segments are exposed to greater environmental stresses and potential points of failure. The primary feeder sections, those responsible for transmitting electricity along the main network pathways, are subject to failure rates quantified by the formula ($L \times 0.075$) faults per kilometer per year ($f/km-yr$). In contrast, lateral distribution lines, which typically branch off to supply individual sectors or consumers, experience a slightly higher failure rate of ($L \times 0.097$) faults per kilometer per year, likely due to their exposure to more complex operational conditions and external disturbances.

To provide a comprehensive overview of system reliability and performance, the fundamental indices for each load point are systematically documented in Table 7. This table presents key reliability metrics, such as outage frequencies and durations, enabling a detailed assessment of service continuity across different segments of the network. Additionally, Table 8 outlines the respective line lengths, which serve as crucial parameters for evaluating the maintenance requirements within the system.

Table 5. Distribution system reliability indices [29]

System Average Interruption Frequency (SAIFI)	$SAIFI = \frac{\sum \lambda_j N_j}{\sum N_i}$
System Average Interruption Duration Index (SAIDI)	$SAIDI = \frac{\sum U_j N_j}{\sum N_i}$
Customer Average Interruption Duration Index (CAIDI)	$CAIDI = \frac{\sum U_j N_j}{\sum \lambda_i N_i}$
Average Service Availability Index (ASAI)	$ASAI = \frac{\sum N_j \times 8760 - \sum U_j N_j}{\sum N_i \times 8760}$
Average Energy Not Supplied (AENS)	$AENS = \frac{\sum L_a(j) U_j}{N_i}$
* 8760 is the number of hours in a calendar year	

Table 6. Specification for the test distribution system of Figure 13.

Load Points	Load Level per Load Point (MW)		Number of Customers
	Peak	Average	
1, 3, 5, 7, 37, 41	0.74114	0.56369	15
8, 35, 36, 48, 52	0.48712	0.39647	130
9-12, 38-40	0.74651	0.61279	25
2, 4, 6, 44, 46, 49, 53	1.10459	0.96781	10
13, 15, 29-31	0.84562	0.63647	55
17-20, 27, 28	0.60073	0.41136	30
14, 16, 42, 50, 51	1.23349	1.00127	25
21, 22, 32-34, 54	0.47126	0.37719	45
24, 26, 43	0.54557	0.41879	210
23, 25, 45, 47	0.73267	0.55264	160

Table 7. Line types and lengths.

Line numbers	Type	Length (km)
1, 3, 5, 7, 9, 11	main	0.85
13, 24, 26, 28, 30, 40, 42	main	0.9
45, 51, 53, 55, 67, 69	main	0.7
72, 74, 76, 78, 80, 82	main	0.95
93, 95, 97, 99, 101, 103	main	0.75
0, 2, 4, 6, 8, 10, 12, 83, 85	lateral	0.35
15, 17, 19, 21, 23, 94, 98, 102	lateral	0.5
14, 31, 33, 46, 56, 62	lateral	0.45
25, 27, 29, 41, 43, 44, 52, 54, 68, 70, 92, 96, 100, 104	lateral	0.6
32, 34-39, 47, 49, 57, 59, 61, 63, 65, 84, 86-91	lateral	0.4
16, 18, 20, 22, 48, 50, 58, 60, 64, 66	lateral	0.65
71, 73, 75, 77, 79, 81	lateral	0.5

To assess the impact of MPPT techniques on the reliability of grid-connected PV systems, consider a scenario in which the PV unit serves as a load transfer mechanism. This means that the PV system dynamically adjusts its power output based on the MPPT algorithm it employs, thereby influencing how effectively it compensates for load fluctuations and contributes to overall grid stability.

In this context, the outage duration following a failure event is directly influenced by the ability of the PV unit to sustain or exceed the required load demand. Specifically, if the MPPT algorithm enables the PV unit to generate adequate power to meet the load requirement during the failure period, the outage time is limited to the isolation time, the duration needed to disconnect the affected component from the network and stabilize operations. This scenario assumes that the PV system continues to supply uninterrupted power to the load, preventing an extended outage.

Conversely, if the PV unit fails to deliver sufficient power due to either inefficiencies in MPPT tracking or unfavorable operating conditions (such as shading, temperature fluctuations, or transient changes in irradiance), the outage time is determined by the required repair duration. In this case, the affected component remains out of service until restoration efforts are completed.

To quantify the reliability impact of different MPPT techniques, the average outage time can be estimated using the expectation concept as Equation (27), integrating the probabilities of each scenario. Mathematically, this expectation-based approach captures the likelihood-weighted contributions of both isolation and repair times, allowing for a comparative evaluation of various MPPT algorithms in terms of system resilience and service continuity.

$$Outage\ time = (outage\ time \mid PV\ unit\ can\ generate\ enough\ power) \times P(generate) + (outage\ time \mid PV\ unit\ cannot\ generate\ enough\ power) \times Q(generate) \quad (27)$$

It is important to note that $P(generate)$ is significantly influenced by the performance of the PV unit (output power based on the applied MPPT methods) and the extent of the outage, particularly the number of customers impacted by the feeder outages.The comprehensive evaluation of reliability indices for the distribution PV-grid, as depicted in Figure 13, presents a comparative analysis across various MPPT algorithms. These indices, derived through analytical methodologies, provide critical insights into how different MPPT strategies influence the operational stability and dependability of the grid-integrated PV system.

One of the key observations from Table 9 is that all examined scenarios maintain an identical SAIFI. This consistency indicates that regardless of the MPPT algorithm employed, the frequency of interruptions remains uniform across the system. However, while the occurrence of interruptions remains unchanged, significant variations are observed in reliability indices related to interruption duration, highlighting the role MPPT strategies play in determining the length of outages.

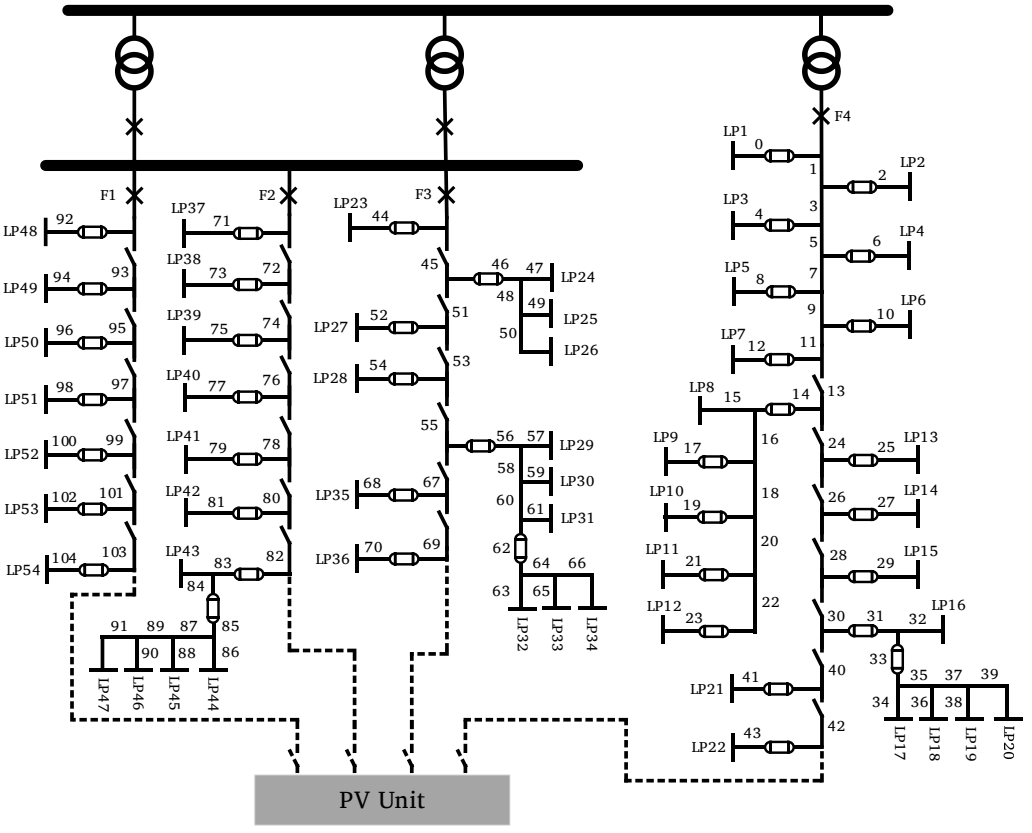

Figure 15. Test distribution system.

Table 8. The basic system indices for the distribution systems for each load point in different modes of MPPT algorithms for PV units (for load points 37-47, the calculation is set as given in the Appendix)

MPPT Method	ANN			P&O			Hybrid method [11]			Hybrid method [12]		
Load Point	λ	r	U	λ	r	U	λ	r	U	λ	r	U
1	1.2375	3.3342	4.1261	1.2375	3.2657	4.0413	1.2375	3.1014	3.8379	1.2375	3.1665	3.9185
2	1.2375	3.3342	4.1261	1.2375	3.2657	4.0413	1.2375	3.1014	3.8379	1.2375	3.1665	3.9185
3	1.2375	3.3342	4.1261	1.2375	3.2657	4.0413	1.2375	3.1014	3.8379	1.2375	3.1665	3.9185
4	1.2375	3.3342	4.1261	1.2375	3.2657	4.0413	1.2375	3.1014	3.8379	1.2375	3.1665	3.9185
5	1.2375	3.3342	4.1261	1.2375	3.2657	4.0413	1.2375	3.1014	3.8379	1.2375	3.1665	3.9185
6	1.2375	3.3342	4.1261	1.2375	3.2657	4.0413	1.2375	3.1014	3.8379	1.2375	3.1665	3.9185
7	1.2375	3.3342	4.1261	1.2375	3.2657	4.0413	1.2375	3.1014	3.8379	1.2375	3.1665	3.9185
8	1.3079	2.9567	3.8671	1.3079	2.8114	3.6770	1.3079	2.7994	3.6613	1.3079	2.8002	3.6623
9	1.3214	2.9634	3.9158	1.3214	2.8746	3.7984	1.3214	2.8201	3.7264	1.3214	2.8255	3.7336
10	1.3214	3.1219	4.1252	1.3214	3.0989	4.0948	1.3214	3.0149	3.9839	1.3214	3.0154	3.9845
11	1.3214	3.1978	4.2256	1.3214	3.0012	3.9657	1.3214	2.9872	3.9472	1.3214	2.9901	3.9511
12	1.3214	3.2416	4.2834	1.3214	3.1137	4.1144	1.3214	3.0134	3.9819	1.3214	3.0123	3.9804
13	1.3299	2.1827	2.9027	1.3299	2.0999	2.7926	1.3299	2.0057	2.6673	1.3299	2.0061	2.6679
14	1.3299	2.2789	3.0307	1.3299	2.1213	2.8211	1.3299	2.0639	2.7447	1.3299	2.0657	2.7471
15	1.3299	2.2999	3.0586	1.3299	2.1997	2.9253	1.3299	2.1482	2.8569	1.3299	2.1493	2.8583
16	1.3357	3.1149	4.1605	1.3357	3.0112	4.0220	1.3357	2.9901	3.9938	1.3357	2.9976	4.0039
17	1.3368	3.1477	4.2078	1.3368	3.1009	4.1452	1.3368	2.9842	3.9892	1.3368	2.9912	3.9986
18	1.3368	3.2007	4.2786	1.3368	3.1145	4.1634	1.3368	3.0997	4.1437	1.3368	3.1006	4.1449
19	1.3368	3.2034	4.2823	1.3368	3.1553	4.2180	1.3368	3.1005	4.1447	1.3368	3.1094	4.1566
20	1.3368	3.2101	4.2912	1.3368	3.1412	4.1991	1.3368	3.1497	4.2105	1.3368	3.1572	4.2205
21	1.3401	3.4141	4.5752	1.3401	3.2998	4.4220	1.3401	3.2012	4.2899	1.3401	3.2106	4.3025
22	1.3401	3.4141	4.5752	1.3401	3.2998	4.4220	1.3401	3.2012	4.2899	1.3401	3.2106	4.3025
23	0.7354	1.9746	1.4521	0.7354	1.8544	1.3637	0.7354	1.7433	1.2820	0.7354	1.7591	1.2936
24	0.7397	2.1211	1.5690	0.7397	2.1002	1.5535	0.7397	1.9819	1.4660	0.7397	1.9893	1.4714
25	0.7401	2.2723	1.6817	0.7401	2.2521	1.6667	0.7401	2.1464	1.5885	0.7401	2.1401	1.5839
26	0.7397	2.3009	1.7019	0.7397	2.2808	1.6871	0.7397	2.2017	1.6286	0.7397	2.2135	1.6373
27	0.7412	2.0017	1.4836	0.7412	1.9869	1.4727	0.7412	1.9832	1.4699	0.7412	1.9907	1.4755
28	0.7445	2.0179	1.5023	0.7445	1.9912	1.4824	0.7445	1.9517	1.4530	0.7445	1.9635	1.4767
29	0.7509	2.4712	1.8556	0.7509	2.3712	1.7805	0.7509	2.3113	1.7356	0.7509	2.3214	1.7431
30	0.7512	2.3625	1.7747	0.7512	2.3417	1.7591	0.7512	2.3146	1.7387	0.7512	2.3264	1.7476
31	0.7509	2.2525	1.6914	0.7509	2.2405	1.6824	0.7509	2.2135	1.6621	0.7509	2.2247	1.6705
32	0.7526	2.6839	2.0199	0.7526	2.6151	1.9681	0.7526	2.5146	1.8925	0.7526	2.5207	1.8970
33	0.7533	2.7494	2.0711	0.7533	2.7295	2.0561	0.7533	2.6319	1.9826	0.7533	2.6392	1.9881
34	0.7526	2.7506	2.0701	0.7526	2.7351	2.0584	0.7526	2.7019	2.0334	0.7526	2.7084	2.0376
35	0.7412	2.1468	1.5912	0.7412	2.1255	1.5754	0.7412	2.0197	1.4970	0.7412	2.0236	1.4998
36	0.7412	2.1468	1.5912	0.7412	2.1255	1.5724	0.7412	2.0197	1.4970	0.7412	2.0236	1.4998
37	0.47600	0.7668	0.36499	0.4760	0.7573	0.3604	0.4760	0.7211	0.3432	0.4760	0.7305	0.3477
38	0.47600	1.3057	0.62150	0.4760	1.2996	0.6186	0.4760	1.2514	0.5956	0.4760	1.2584	0.5989
39	0.47600	1.4868	0.70771	0.4760	1.47117	0.7003	0.4760	1.4312	0.6812	0.4760	1.4398	0.6853
40	0.47600	1.6679	0.79392	0.4760	1.65979	0.7901	0.4760	1.6113	0.7669	0.4760	1.6183	0.7703
41	0.47600	1.8490	0.88012	0.4760	1.8490	0.8801	0.4760	1.8112	0.8621	0.4760	1.8187	0.8657
42	0.47600	2.0301	0.96635	0.4760	2.0219	0.9624	0.4760	1.9963	0.9502	0.4760	1.9989	0.9514
43	0.50025	2.2979	1.14956	0.50025	2.2817	1.1414	0.50025	2.2317	1.1164	0.50025	2.2384	1.1197
44	0.76700	2.8899	2.21656	0.7670	2.8703	2.2015	0.7670	2.8243	2.1662	0.7670	2.8305	2.1710
45	0.76700	2.8899	2.21656	0.7670	2.8703	2.2015	0.7670	2.8243	2.1662	0.7670	2.8305	2.1710
46	0.76700	2.8899	2.21656	0.7670	2.8703	2.2015	0.7670	2.8243	2.1662	0.7670	2.8305	2.1710
47	0.76700	2.8899	2.21656	0.7670	2.8703	2.2015	0.7670	2.8243	2.1662	0.7670	2.8305	2.1710
48	0.39571	1.44127	0.57032	0.39571	1.4319	0.5666	0.39571	1.4011	0.5544	0.39571	1.4094	0.5577
49	0.38600	1.01261	0.39086	0.38600	1.00556	0.3881	0.38600	0.9964	0.3846	0.38600	1.0003	0.3861
50	0.39571	1.59762	0.63219	0.39571	1.59001	0.6291	0.39571	1.5517	0.6140	0.39571	1.5582	0.6166
51	0.38600	1.69753	0.65524	0.38600	1.68775	0.6514	0.38600	1.6429	0.6341	0.38600	1.6504	0.6370
52	0.39375	1.89998	0.74812	0.39375	1.89067	0.7444	0.39375	1.8732	0.7376	0.39375	1.8806	0.7404
53	0.38600	2.01813	0.77900	0.38600	2.00311	0.7732	0.38600	1.9864	0.7667	0.38600	1.9913	0.7686
54	0.39570	2.22307	0.87967	0.39570	2.21547	0.8766	0.39570	2.1468	0.8495	0.39570	2.1355	0.8450

These differences are further illustrated in Figure 16, which visually demonstrates how each MPPT algorithm affects the system's reliability metrics. The results suggest that selecting the most efficient MPPT technique can substantially influence unavailability indices, a crucial factor in assessing the continuous availability of power supply at load points. Furthermore, an optimal MPPT approach has a direct impact on the expected energy not supplied (EENS), which quantifies the amount of energy that remains unavailable due to system disruptions. This metric is especially relevant for grid planners and operators seeking to minimize the adverse effects of power shortages.

Given these findings, the development and refinement of an optimized MPPT methodology becomes imperative, not only for enhancing system reliability but also for facilitating a thorough cost-benefit analysis of PV unit deployment. A well-calibrated MPPT technique can lead to improved energy extraction efficiency, reduced outage durations, and an overall increase in power system resilience. Thus, further research into adaptive MPPT strategies and predictive control mechanisms may prove instrumental in maximizing the performance of grid-connected PV systems while ensuring their economic viability.

The cost of a PV system is closely linked to the number of sensors required for monitoring and control. Sensors play a crucial role in ensuring the accurate tracking of electrical parameters, but their quantity and type directly influence the overall expense of the system. In general, voltage measurement is considered simpler, more reliable, and less costly compared to current measurement. This distinction arises due to the inherent complexities in current sensing technologies, which often involve precision components such as Hall-effect sensors or shunt resistors. These components can be relatively expensive and may introduce additional calibration and maintenance requirements.

This cost consideration becomes particularly significant in multi-array PV systems, where each PV array is equipped with its own MPP tracker [30]. In such configurations, the need to monitor individual current outputs from multiple arrays can dramatically increase the total number of required sensors, further inflating system costs. The complexity of implementing multiple current sensors, along with the associated data acquisition and processing requirements, can pose logistical and financial challenges. To mitigate these concerns, an alternative approach involves adopting MPPT methods that either minimize sensor dependency or rely on voltage-based estimations to infer current behavior. Certain advanced MPPT strategies, as demonstrated in [31], leverage mathematical models and algorithmic approximations to estimate current from voltage measurements, reducing the necessity for direct current sensing. These techniques optimize system performance while maintaining cost efficiency, making them particularly advantageous for large-scale PV deployments.

By implementing sensor-efficient MPPT methodologies, system designers can achieve a balance between performance, reliability, and cost-effectiveness, ensuring that photovoltaic arrays operate efficiently without unnecessary expenses linked to excessive sensor integration. Continued research in this domain may lead to further refinements in MPPT algorithms, enabling even more precise estimations of electrical parameters with minimal hardware requirements.

High-cost applications like solar vehicles, industrial systems, and large-scale residential setups typically prioritize accuracy and fast response times, necessitating advanced and complex circuit designs. On the other hand, simpler and more affordable MPPT techniques are suitable for applications such as small residential systems or water pumping for irrigation. Given these considerations, it is challenging to determine the exact monetary cost of each MPPT technique without actual implementation. However, in general, analog implementations are more cost-effective than digital ones, which often require a microcontroller and related programming.

Addressing cost challenges in PV distribution systems requires the integration of advanced reliability cost/worth evaluation techniques into both system design and operational frameworks. These evaluation methods aim to balance economic feasibility with system performance, ensuring that PV installations maintain high efficiency while minimizing unnecessary expenditures. By incorporating cost-benefit analysis approaches, decision-makers can effectively determine the most suitable MPPT strategies based on reliability, implementation complexity, and return on investment. Based on overall implementation considerations, MPPT methods can be ranked as follows: 1) P&O; 2) hybrid methods; and 3) ANN.

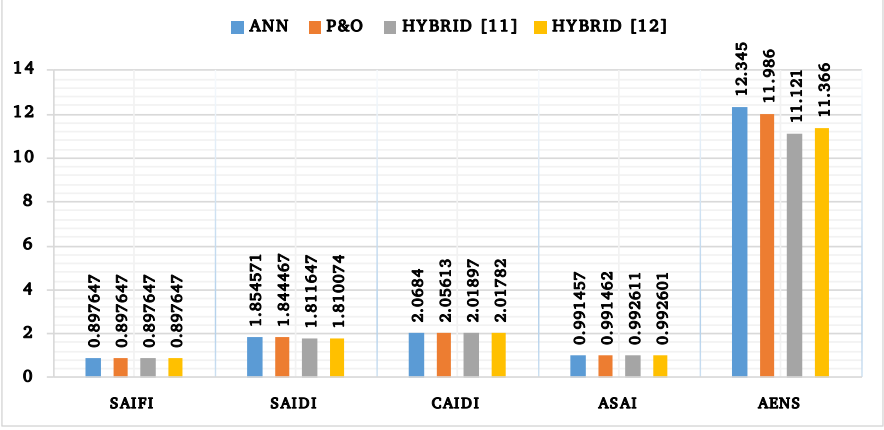

Figure 16. The differences in the reliability indices for each MPPT algorithm.

Table 9. The differences in the reliability indices.

Reliability Indices	MPPT Method			
	ANN	P&O	Hybrid method [11]	Hybrid method [12]
(SAIFI)	0.897647	0.897647	0.897647	0.897647
(SAIDI)	1.854571	1.844467	1.811647	1.810074
(CAIDI)	2.0684	2.05613	2.01897	2.01782
(ASAI)	0.991457	0.991462	0.992611	0.992601
(AENS)	12.345	11.986	11.121	11.366

5. Conclusion and Future Works

This study investigated the impact of various MPPT methods on the operational reliability of PV systems operating in grid-connected mode. The analysis classified MPPT methods into three distinct categories: offline, online, and hybrid methods, enabling a comprehensive assessment of their performance characteristics. To comprehensively assess system performance, a series of simulations was conducted to evaluate three critical metrics: reliability, efficiency, and set-point tracking. These factors play a pivotal role in determining the operational robustness and effectiveness of the implemented methodologies. Specifically, various offline, online, and hybrid methods were compared under similar implementation conditions. This rigorous analysis provided valuable insights into the practical performance of each strategy. The results demonstrated that hybrid methods significantly outperformed both standalone offline and online techniques. A key factor behind their superior performance is the reliance of online methods on real-time output sampling, which tracks the MPP by monitoring electrical parameters without requiring predefined system parameters, allowing for rapid adaptation to changes. By integrating these fast-response online techniques within a hybrid framework, the stability and robustness of offline strategies are combined, resulting in enhanced overall performance. These findings indicate that further optimization and adoption of hybrid MPPT strategies could substantially improve the performance and reliability of grid-connected PV systems, positioning them as a promising avenue for advancing renewable energy technologies. However, the practical implementation of the proposed method is crucial for validating simulation results and identifying potential challenges in real-world applications. This aspect has been assigned as a focus for future studies of the present research.

The results demonstrate that building geometry, floor configuration, and block arrangement significantly influence both energy consumption and thermal comfort. High-rise buildings with fewer shared walls and larger exposed surfaces tend to exhibit higher heating and cooling loads, whereas designs incorporating shared walls and optimized block layouts reduce energy demand while maintaining occupant comfort. These findings underscore the importance of integrating energy-efficient design strategies with climate-responsive planning to achieve sustainable and comfortable residential developments across diverse urban contexts.

The results demonstrated that the number of shared walls has a more significant influence on energy performance than the number of floors. Specifically, single-story buildings without shared walls exhibited up to 58.9% higher heating loads and 67.1% higher cooling loads compared to scenarios with greater wall adjacency. On average, the difference in energy consumption between the buildings with the maximum and minimum number of common walls was approximately 60%. Moreover, heat loss through the roof of a one-story building was found to be nearly 30 times greater than that of high-rise buildings with multiple units (Figure 9).

Additionally, exterior façade simulations were performed and analyzed to further assess their impact on energy performance. Future research will focus on examining the potential of phase change materials in reducing energy consumption in both high-rise and low-rise buildings.

Nomenclature

G	Ambient irradiation (W/m^2)
I_{ph}	Photocurrent (A)
I_d	Diode reverse saturation current (A)
R_s	Series resistance
R_{sh}	Shunt resistance
N_S	The count of solar cells connected in series
N_P	The number of parallel-connected cell strings
q	Electron charge, $\sim 1.602 \times 10^{-19}\ C$
k	Boltzmann constant, $\sim 1.381 \times 10^{-23}\ J/K$
A	Ideality factor
V_{oc}	Open-circuit voltage
I_{SC}	Short-circuit current
T_C	Reference temperature
I_C	Reference saturation current
E_g	Band gap energy
P_{max}	Maximum power point
$I_{sc,Tc}$	Designate the short-circuit current measured at a specific reference temperature
$V_{oc,Tc}$	Designate the open-circuit voltage measured at a specific reference temperature
ΔT	Defined as $T - Tc$, quantifies the deviation between the current cell temperature (T), and the reference temperature (T_C)
K_i	The temperature coefficient that quantifies how the short-circuit current changes with temperature variations
S	Denotes the solar irradiation, expressed in mW/cm^2
P	Total output power of the PV array
η_{inst}	The steady-state efficiency
$P_{pv-meas}$	The actual power output produced by the solar panel
$P_{MPP-ideal}$	The theoretical maximum power that the solar panel is capable of generating under ideal conditions
$\eta_{dynamic}$	The dynamic efficiency
$V_{pv-meas}$	The actual output voltage produced by the solar panel
V_{MPP}	The theoretical maximum voltage that the solar panel is capable of generating under MPP conditions
y(k)	The output signal
u(k)	The input signal
$\varphi(k)$	The past and current input data
$\hat{\theta}(k)$	Estimated parameter vector
$\varepsilon(k)$	Prediction error
a_i, b_i	The coefficients that must be determined through estimation
$W_t(i)$	The PV module capacity validity coefficient
W_{batt}	The total power available from the battery pack when operating in discharge mode
$P_t(i)$	The effective load power
N_j	Number of consumers at load point j
λ_j	Average failure rate at load point j
U_j	Average annual outage time at load point j
$L_a(j)$	Average load connected to load point i

Appendix

For load points 37-47 the calculations of basic system indices are shown in table A_1.

Table A_1. Calculation of basic system indices for load points 37-47.

	Load point																							
	37		38		39		40		41		42		43		44		45		46		47			
Line	λ	r	λ	r	λ	r	λ	r	λ	r	λ	r	λ	r	λ	r	λ	r	λ	r	λ	r		
71	0.0485	4	0	0	0	0	0	0	0	0	0	0	0	0	0	0	0	0	0	0	0	0		
72	0.07125	0.4	0.07125	4	0.07125	1.61	0.07125	1.61	0.07125	1.61	0.07125	1.61	0.07125	1.61	0.07125	1.61	0.07125	1.61	0.07125	1.61	0.07125	1.61		
73	0	0	0.0485	4	0	0	0	0	0	0	0	0	0	0	0	0	0	0	0	0	0	0		
74	0.07125	0.4	0.07125	0.4	0.07125	4	0.07125	1.61	0.07125	1.61	0.07125	1.61	0.07125	1.61	0.07125	1.61	0.07125	1.61	0.07125	1.61	0.07125	1.61		
75	0	0	0	0	0.0485	4	0	0	0	0	0	0	0	0	0	0	0	0	0	0	0	0		
76	0.07125	0.4	0.07125	0.4	0.07125	0.4	0.07125	4	0.07125	1.61	0.07125	1.61	0.07125	1.61	0.07125	1.61	0.07125	1.61	0.07125	1.61	0.07125	1.61		
77	0	0	0	0	0	0	0.0485	4	0	0	0	0	0	0	0	0	0	0	0	0	0	0		
78	0.07125	0.4	0.07125	0.4	0.07215	0.4	0.07125	0.4	0.07125	4	0.07125	1.61	0.07125	1.61	0.07125	1.61	0.07125	1.61	0.07125	1.61	0.07125	1.61		
79	0	0	0	0	0	0	0	0	0.0485	4	0	0	0	0	0	0	0	0	0	0	0	0		
80	0.07125	0.4	0.07125	0.4	0.07125	0.4	0.07125	0.4	0.07125	0.4	0.07125	4	0.07125	1.61	0.07125	1.61	0.07125	1.61	0.07125	1.61	0.07125	1.61		
81	0	0	0	0	0	0	0	0	0	0	0.0485	4	0	0	0	0	0	0	0	0	0	0		
82	0.07125	0.4	0.07125	0.4	0.07125	0.4	0.07125	0.4	0.07125	0.4	0.07125	0.4	0.07125	4	0.07125	4	0.07125	4	0.07125	4	0.07125	4		
83	0	0	0	0	0	0	0	0	0	0	0	0	0.03395	4	0.03395	4	0.03395	4	0.03395	4	0.03395	4		
84	0	0	0	0	0	0	0	0	0	0	0	0	0.0388	4	0.0388	4	0.0388	4	0.0388	4	0.0388	4		
85	0	0	0	0	0	0	0	0	0	0	0	0	0	0	0.03395	4	0.03395	4	0.03395	4	0.03395	4		
86	0	0	0	0	0	0	0	0	0	0	0	0	0	0	0.0388	4	0.0388	4	0.0388	4	0.0388	4		
87	0	0	0	0	0	0	0	0	0	0	0	0	0	0	0.0388	4	0.0388	4	0.0388	4	0.0388	4		
88	0	0	0	0	0	0	0	0	0	0	0	0	0	0	0.0388	4	0.0388	4	0.0388	4	0.0388	4		
89	0	0	0	0	0	0	0	0	0	0	0	0	0	0	0.0388	4	0.0388	4	0.0388	4	0.0388	4		
90	0	0	0	0	0	0	0	0	0	0	0	0	0	0	0.0388	4	0.0388	4	0.0388	4	0.0388	4		
91	0	0	0	0	0	0	0	0	0	0	0	0	0	0	0.0388	4	0.0388	4	0.0388	4	0.0388	4		
	0.476	0.7668	0.476	1.3057	0.476	1.4868	0.476	1.6679	0.476	1.849	0.476	2.0301	0.50025	2.2979	0.767	2.8899	0.767	2.8899	0.767	2.8899	0.767	2.8899		
	U=0.365		U=0.6215		U=0.7077125		U=0.793925		U=0.880137		U=0.96635		U=1.14956		U=2.21656		U=2.21656		U=2.21656		U=2.21656			

References

[1] Q. Bi, G. Zhou, L. Deng, and N. Xue, "Target Voltage Iterations Based Global Flexible Power Point Tracking Algorithm Under Partial Shading Photovoltaic Systems," *IEEE Transactions on Sustainable Energy*, vol. 15, no. 1, pp. 236–248, 2024.

[2] B. Mandal, and P. S. Bhowmik, "A Deep Neural Network-Based Highly Simplified Intelligent Approach for Maximum Power Point Tracking of Dye-Sensitized Solar Panel System," *IEEE Journal of Emerging and Selected Topics in Industrial Electronics*, vol. 6, no. 1, pp. 196–203, 2025.

[3] A. Motovilov, and S. Lutchenko, "Calculation of Mean Time to Failure of Infocommunication System Wich Failure Rate Is Cycle Changed," *2022 Dynamics of Systems, Mechanisms and Machines (Dynamics)*, pp. 1–4, 2022.

[4] L. T. Ostrom and C. A. Wilhelmsen, “Probabilistic Risk Assessment,” in *Risk Assessment: Tools, Techniques, and their Applications*, John Wiley & Sons, ch. 15, pp. 223-230, 2012.

[5] H. E. Moumen, N. E. Akchioui, and A. Toukmati, "Continuous-Time Markov Processes for Reliability Analysis: A Comprehensive Study," *2024 4th International Conference on Innovative Research in Applied Science, Engineering and Technology (IRASET)*, pp. 1–8, 2024.

[6] I. Mehdi, E. M. Boudi, and M. A. Mehdi, "Reliability, Availability, and Maintainability Assessment of a Mechatronic System Based on Timed Colored Petri Nets," *Applied Sciences*, vol. 14, no. 11, 4852, 2024.

[7] M. Čepin, "Reliability Block Diagram," *Assessment of Power System Reliability*, pp. 119–123, 2011.

[8] A. Reza Reisi, M. Hassan Moradi, and S. Jamasb, "Classification and Comparison of Maximum Power Point Tracking Techniques for Photovoltaic System: A Review," *Renewable and Sustainable Energy Reviews*, vol. 19, pp. 433–443, 2013.

[9] Z. Chen, X. Sun, et al., "Maximum Efficiency Tracking Control for Omnidirectional Wireless Power Transfer System Based on AdamW Algorithm," *IEEE Transactions on Power Electronics*, vol. 40, no. 3, pp. 4602–4612, 2025.

[10] M. A. G. de Brito, L. Galotto, L. P. Sampaio, G. d. A. e Melo, and C. A. Canesin, "Evaluation of the Main MPPT Techniques for Photovoltaic Applications," *IEEE Transactions on Industrial Electronics*, vol. 60, no. 3, pp. 1156–1167, 2013.

[11] M. H. Moradi, and A. R. Reisi, "A Hybrid Maximum Power Point Tracking Method for Photovoltaic Systems," *Solar Energy*, vol. 85, no. 11, pp. 2965–2976, 2011.

[12] J. Jiang, Y. Su, et al., "On Application of a New Hybrid Maximum Power Point Tracking (MPPT) Based Photovoltaic System to the Closed Plant Factory," *Applied Energy*, vol. 124, pp. 309–324, 2014.

[13] H. Park, and H. Kim, "PV Cell Modeling on Single-Diode Equivalent Circuit," *IECON 2013 - 39th Annual Conference of the IEEE Industrial Electronics Society*, pp. 1845–1849, 2013.

[14] N. M. A. Alrahim Shannan, N. Z. Yahaya, and B. Singh, "Single-Diode Model and Two-Diode Model of PV Modules: A Comparison," *2013 IEEE International Conference on Control System, Computing and Engineering*, pp. 210–214, 2013.

[15] A. Sakhare, and S. Mikkili, "Enhancing Photovoltaic Array Performance Through the Integration of Perturb and Observe MPPT and Novel Ladder Configuration," *e-Prime - Advances in Electrical Engineering, Electronics and Energy*, vol. 11, 100943, 2025.

[16] D. Sharma, M. F. Jalil, M. S. Ansari, and R. C. Bansal, "A Review of Maximum Power Point Tracking (MPPT) Techniques for Photovoltaic Array Under Mismatch Conditions," *Photovoltaic Systems Technology*, pp. 85–102, 2024.

[17] S. Hassan Hakmi, H. Alnami, A. Ginidi, A. Shaheen, and T. A. Alghamdi, "A Fractional Order-Kepler Optimization Algorithm (FO-KOA) for Single and Double-Diode Parameters PV Cell Extraction," *Heliyon*, vol. 10, no. 16, e35771, 2024.

[18] A. O. Salau, S. K. Maitra, A. Kumar, A. Mane, and R. W. Dumicho, "Design, Modeling, and Simulation of a PV/Diesel/Battery Hybrid Energy System for an Off-Grid Hospital in Ethiopia," *e-Prime - Advances in Electrical Engineering, Electronics and Energy*, vol. 8, 100607, 2024.

[19] K. Ishaque, Z. Salam, and H. Taheri, "Simple, Fast and Accurate Two-Diode Model for Photovoltaic Modules," *Solar Energy Materials and Solar Cells*, vol. 95, no. 2, pp. 586–594, 2011.

[20] I. H. Altas, and A. Sharaf, "A Photovoltaic Array Simulation Model for Matlab-Simulink GUI Environment," *2007 International Conference on Clean Electrical Power*, pp. 341–345, 2007.

[21] G. Singh, "Solar Power Generation by PV (photovoltaic) Technology: A Review," *Energy*, vol. 53, pp. 1–13, 2013.

[22] H. Patel, and V. Agarwal, "MATLAB-Based Modeling to Study the Effects of Partial Shading on PV Array Characteristics," *IEEE Transactions on Energy Conversion*, vol. 23, no. 1, pp. 302–310, 2008.

[23] K. Ishaque, Z. Salam, H. Taheri, and Syafaruddin, "Modeling and Simulation of Photovoltaic (PV) System During Partial Shading Based on a Two-Diode Model," *Simulation Modelling Practice and Theory*, vol. 19, no. 7, pp. 1613–1626, 2011.

[24] N. A. Meineri, I. Santana, and I. G. Zurbriggen, "Ultra-Fast MPPT for Residential PV Systems with Low DC-Link Capacitance and Differential Power Processing," *IEEE Transactions on Power Electronics*, vol. 40, no. 2, pp. 2736–2745, 2025.

[25] D. Sera, T. Kerekes, R. Teodorescu, and F. Blaabjerg, "Improved MPPT Algorithms for Rapidly Changing Environmental Conditions," *2006 12th International Power Electronics and Motion Control Conference*, pp. 1614–1619, 2006.

[26] W. Marańda and M. Piotrowicz, "Static and Dynamic MPP-Tracking Efficiency of PV-Inverter Using Recorded Irradiance," *International Journal of Microelectronics and Computer Science*, vol. 4, no. 4, pp. 181–185, 2013.

[27] V. Bobál, J. Böhm, J. Fessl, and J. Macháček, *Digital self-tuning controllers: algorithms, implementation and applications*. London: Springer London, 2005.

[28] H. Qiang, S. Qiao, H. Huang, P. Cheng, and Y. Sun, "Nonlinear Adaptive Control of Maglev System Based on Parameter Identification," *Actuators*, vol. 14, no. 3, 115, 2025.

[29] R. N. Allan, *Reliability Evaluation of Power Systems*. Springer Science & Business Media, 2013.

[30] T. Esram, and P. L. Chapman, "Comparison of Photovoltaic Array Maximum Power Point Tracking Techniques," *IEEE Transactions on Energy Conversion*, vol. 22, no. 2, pp. 439–449, 2007.

[31] N. Kasa, T. Iida, and L. Chen, "Flyback Inverter Controlled by Sensorless Current MPPT for Photovoltaic Power System," *IEEE Transactions on Industrial Electronics*, vol. 52, no. 4, pp. 1145–1152, 2005.

Declaration of competing interest

The authors declare that they have no known competing financial interests or personal relationships that could have appeared to influence the work reported in this paper. The ethical issues, including plagiarism, informed consent, misconduct, data fabrication and/or falsification, double publication and/or submission, redundancy, have been completely observed by the authors.

Bibliography

Peyman Bayat received the bachelor's and master's degrees from Hamedan University of Technology and Bu-Ali Sina University, respectively, and the Ph.D. degree from University of Guilan. Since 2018, he has been with Hamadan University of Technology, where he is currently an Assistant Professor in electrical engineering. His research area includes microgrids, power electronics, electric vehicles, smart grids, sustainable energy, artificial intelligence etc. He is a reviewer of several IEEE and Elsevier journals, such as sustainable cities and society, applied energy, energy storage and many others.
Email: peyman.bayat@hut.ac.ir
ORCID: 0000-0001-7289-825X
Contribution Statement: Conceptualization, Data curation, Formal analysis, Funding acquisition, Investigation, Methodology, Project administration, Resources, Software, Supervision, Validation, Visualization, Roles/Writing - original draft, Writing-review & editing.

Pezhman Bayat is currently working as an Assistant Professor (7 + Years Exp.) in the Department of Electrical Engineering at Hamedan University of Technology. He has completed his Ph.D. from University of Guilan. He has over 12 years research experience in power electronics, machines and drives. His research interests include electric vehicles, renewable energy systems, power electronics etc. He has published over 30 papers and supervised over 20 students to completion. Dr. Bayat is a reviewer of several journals, such as Elsevier journals, IEEE transactions on power electronics, IEEE transactions on industrial electronics, Taylor & Francis international Journal of Electronics, and many others.
Email: pezhman.bayat@hut.ac.ir
ORCID: 0000-0003-0598-841X
Contribution Statement: Conceptualization, Data curation, Formal analysis, Funding acquisition, Investigation, Methodology, Project administration, Resources, Software, Supervision, Validation, Visualization, Roles/Writing-original draft, Writing-review & editing.